Delft University of Technology

Hydraulic Engineering MSc Thesis

Supporting Decision Making under Deep Uncertainty techniques with hydraulic modeling

---

Author:
Xander Smits

Supervision:
Dr.ir. R.J. Labeur
Prof. dr. ir. M. Kok
J.A. Álvarez Antolínez
April 16, 2024

Acknowledgements

Writing this thesis was a collaborative process, while at times a lonely one. I want to thank both my supervisors for Civil and for EPA, both of which helped me finish this thesis, including Matthijs Kok en José Álvarez Antolínez. Special thanks to Robert Jan Labeur for each feedback session after reading earlier iterations of this thesis, it really helped to give me some much needed direction. Special thanks also to Jan Kwakkel for helping further my understanding of best modeling practices. I would also like to thank Otti, for all her gentle reminders.

Thanks also to Sophie, Jim, Bart, and Sebastiaan, all of whom had to endure me for some of the more stressful moments at one point or another. Thanks also to both my parents for helping with digesting some of the life lessons that came with a thesis process such as this.

Abstract

Infrastructure is at risk to climate uncertainty due to a combination of long life spans, complexity of the systems it is embedded in, and the high investment costs often necessary. Current infrastructure planning approaches lose efficacy under deep uncertainty, necessitating new approaches that function better under conditions where the future cannot be predicted. The approaches that attempt to deal with this are also called Decision Making under Deep Uncertainty (DMDU). Bangladesh, the Netherlands, and New Zealand have all already adopted the use of these DMDU approaches in their delta protection guidance. One popular DMDU technique is Robust Decision Making (RDM). RDM can be seen as a computational extension of scenario planning, where proposed plans are tested against every potential combination of uncertainties.

The Deep South Challenge (DSC), a New Zealand based research institute is looking into using RDM on a regional scale to discover vulnerabilities and identify robust strategies based on them. One of the test cases is in Helensville, where a Wastewater Treatment Plant (WTP) serving a small community is located in the middle of a floodplain. The WTP discharges its effluent into a strongly tidally influenced river, which drains the entire watershed and flows past large tidal flats into a dynamic estuarine environment.

In order to identify potential vulnerabilities in the system, robust decision making uses a vulnerability analysis. This consists of a scenario discovery and global sensitivity analysis which sample through every combination of uncertainties to characterize the vulnerabilities of the system. In order to facilitate this, usually simple conceptual models are used due to the high number of runs necessary. However, these types of models can oversimplify complex physical processes and topography. These complicating factors are all present at the current case site selected by the DSC. This research investigates whether the added computational demand of a complex model is worth it compared to a simple conceptual model. To do this, two models are selected and forced for the same event. They are then compared on predicted system behavior, identified vulnerabilities, and potential policy advice.

From a larger selection, the FLORES and SFINCS models were chosen. FLORES uses a simple hydrological balance to calculate the water level in the subbasins for each timestep. SFINCS is a reduced physics solver which only uses the Local Inertial Equations (LIE). Both models are forced by a compound rainfall and storm-tide event for a storm with a 24 hour duration, for which they were calibrated and validated using the results of previous modeling efforts in the region. After the calibration and validation, a sensitivity analysis and scenario discovery were run for both models.

The results of the sensitivity analysis show similar model behavior between FLORES and SFINCS. The upstream part of the model domain is only sensitive to rainfall, while the downstream part is mostly sensitive to storm surge and mean sea level, and to a lesser degree to tidal amplitude. This downstream part includes the wastewater treatment plant. Compared to SFINCS, the outcomes for FLORES on average overestimated water levels at the WTP. This is most likely due to the lack of flood attenuation taken into account by FLORES compared to SFINCS.

The scenario discovery showed similar results for each model's box describing 73% of the outcomes where failure occurs. Both models had the same three thresholds: storm surge, mean sea level, and tidal amplitude. The main difference between the boxes was the storm surge threshold being 21 centimeters lower for FLORES compared to SFINCS, indicating FLORES overestimates the water level at the WTP. The results of the scenario discovery also showed a linear relationship between these three factors. From this relationship, it is possible to see that, keeping all else similar, and with the same high tidal amplitude and storm surge, for SFINCS the plant only starts flooding when a mean sea level of at least 0.4 meters is reached, while for FLORES this is 0.25 meters. Using a RCP4.5 emissions scenario, a mean sea level of 0.25 meters will be reached in 20-30 years, and a mean sea level of 0.4 meters in 50 years.

The proposed policy options for both SFINCS and FLORES would be to mitigate storm surge as long as possible, since the water level at the WTP is most sensitive to this factor. Once this is no longer possible, the WTP should be relocated. The results of SFINCS indicate this relocation is necessary later than for FLORES.

These results show that while the behaviors exhibited by both models is relatively similar, the small differences in accuracy affect which are most likely due to the lack of flood attenuation taken into account for FLORES lead to a different timing of proposed adaptations. This leads to reason that while a conceptual model such as FLORES works well to identify important factors within the system, a more accurate model such as SFINCS can be more helpful once timing of adaptation becomes important. Further recommendations are to repeat this research for more models, further calibrate and validate the models, and to include scenario discovery methods that better deal with the found linear relation.

Contents

List of Figures

Chapter 1

Introduction

1.1 Infrastructure planning and modeling complexity in a changing climate

1.1.1 The effects of climate change on infrastructure

Infrastructure is the backbone of society. It connects people, provides them with services, and keeps them safe. Current infrastructure is at risk from climate change and its associated effects, however. The Organisation for Economic Co-operation and Development (OECD) has estimated that in order to adapt current infrastructure to the effects associated to climate change, over 6.3 trillion US dollars should be invested worldwide per year between 2016 and 2030 (Mullan, 2018). Consequences of climate change will most likely disproportionately affect poor and coastal regions, which will be the first to feel the effects.

The Intergovernmental Panel on Climate Change (IPCC) has predicted that the current risks affecting coastal regions will increase by at least one order of magnitude by the year 2100 due to climate change (Arias et al., 2021). This means populations living in coastal areas will most likely have to accept a managed retreat inland at some point in the future (WMO, 2019). For water infrastructure, the most serious effects of climate change and global warming are sea level rise, extreme precipitation as well as periods of drought, and increased frequency and intensity of storms. The magnitude and extent of these effects is still largely uncertain.

Infrastructure is especially vulnerable to the uncertainty related to climate change, since it is often embedded in complex systems. This means it is hard for infrastructure to adapt to changes within the system due to the lock-in of any choice made, which is caused by its long life-span as well as the different rules and regulations. These risks are exacerbated by the high up-front investment costs necessary for infrastructure (Stanton & Roelich, 2021). This raises the need for planning approaches that perform well under uncertain conditions.

1.1.2 Planning approaches for different levels of uncertainty

Different levels of uncertainty warrant different planning approaches. Marchau et al. (2019) has divided the degree of uncertainty into four different levels, which can be seen in Figure 1.1, limited by complete determinism on one side to total ignorance on the other side. The level of uncertainty encountered is dependent on the external factors, system model, and system outcomes.

Probabilistic approaches and scenario planning

Probabilistic approaches are the most widely used planning method. These approaches assume that external factors, the system model, and its outputs can be described in a probabilistic manner. Projections of the future are made, after which planning is based on these projections. These approaches work well on a shorter time scale, when the system is clear, or when external forces on the system are well-defined.

For cases where probabilities cannot be ascribed to the external factors, system model, or to the outcomes, scenario planning is used. Scenario planning examines a few mutually exclusive plausible scenarios in order to make "robust" decisions: those that lead to a satisfactory outcome in multiple different futures. By exploring various scenarios, decision-makers can better prepare for uncertainties and make strategic choices that are adaptable across a range of possible futures. Compared to the probabilistic approaches, choices are not made based on a prediction of what will likely happen, but rather on what could potentially happen. This works well when there are only a few plausible scenarios.

	Complete determinism	Level 1	Level 2	Level 3	Level 4 (deep uncertainty)		Total ignorance
					Level 4a	Level 4b	
Context (X)		A clear enough future	Alternate futures (with probabilities)	A few plausible futures	Many plausible futures	Unknown future	
System model (R)		A single (deterministic) system model	A single (stochastic) system model	A few alternative system models	Many alternative system models	Unknown system model; know we don't know	
System outcomes (O)		A point estimate for each outcome	A confidence interval for each outcome	A limited range of outcomes	A wide range of outcomes	Unknown outcomes; know we don't know	
Weights (W)		A single set of weights	Several sets of weights, with a probability attached to each set	A limited range weights	A wide range of weights	Unknown weights; know we don't know	
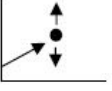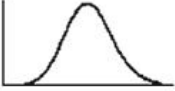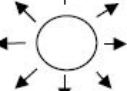
Figure 1.1: The progressive levels of uncertainty ranging from complete determinism on the left to total ignorance on the right. Context encompasses all external forces on the system, and weights denotes the preference of system outcomes by stakeholders. Probabilistic predictive approaches work well for levels 1 and 2, and scenario planning works well for level 3. Decision making under deep uncertainty techniques attempt to deal with level 4a and 4b uncertainty (Marchau et al., 2019).

Decision Making under Deep Uncertainty (DMDU)

In cases where uncertainty is even more profound, also sometimes called deep uncertainty, scenario planning can lose efficacy as well. Decision making under deep uncertainty is the collection name of techniques that attempt to deal with this level of uncertainty. These techniques recognize that the future is inherently uncertain, and attempt to make decisions that are not only robust against uncertainty but also flexible enough to adapt to evolving circumstances.

There are multiple DMDU techniques, each with their own strengths and weaknesses. One popular DMDU technique that is already widely adopted is Robust Decision Making (RDM) (Haasnoot et al., 2019; Kwakkel & Haasnoot, 2019; Kwakkel et al., 2016a; Lempert, 2019). RDM can be seen as an extension of scenario planning. Rather than making a selection of just a few mutually exclusive plausible scenarios as done for scenario planning, RDM samples through every combination of possible uncertainties. The two main benefits of this search are the ability to discover the conditions under which the system is vulnerable, as well as the ability to iteratively develop robust strategies by adapting to these discovered vulnerabilities.

1.1.3   Modeling support for different levels of uncertainty

Probabilistic methods often use complex models to best predict the future. As an example, to deal with climate change, integrated assessment models are used to attempt to predict carbon emission pathways (Arias et al., 2021). These models are complex and require a great deal of computational power.

Robust decision making samples through every combination of external uncertainties, meaning a large number of runs is necessary. In order to keep the analysis computationally feasible, often simple conceptual models are used that mimic the behavior of more complex models. A problem occurs, however, when reducing the complexity of a model oversimplifies system behavior. For hydraulic modeling, locations with complex topography and physical processes such as estuaries, flood plains and tidal rivers are especially vulnerable

to this oversimplification (Herdman et al., 2018; H. McGrath et al., 2018; Ngo et al., 2020; O'Neill et al., 2017; Teng et al., 2017).

1.2　Decision making under deep uncertainty in New Zealand

1.2.1　Risks in New Zealand and the Deep South Challenge

New Zealand will be among the first nations to feel the effects of climate change. Currently over 240,000 people here are living within 2 meters of the mean high tide line (level, 2021). Additionally, New Zealand's public infrastructure is greatly at risk from rising sea levels and increased storm frequency and intensity. At 0.5 meters sea level rise, more than $2.7 billion is at risk, which balloons to $13.4 billion for a rise of 3.0 meters (LGNZ, 2019). The area that is the most at risk the quickest is the Auckland region, where $620 million worth of infrastructure is already at risk with a sea level rise of 0.5 meters (LGNZ, 2019).

In order to help adapt infrastructure, and to help New Zealanders mitigate the most important effects of climate change, the Deep South Challenge initiative has been set up. The New Zealand government has already promoted the use of decision making under deep uncertainty concepts in the national guidance for adapting to coastal hazards and sea level rise (Lawrence et al., 2018; Stephens et al., 2021). One of the main goals of the Deep South Challenge is to bring these concepts to a more regional scale.

1.2.2　The Helensville wastewater treatment plant: a case study

The Helensville study is one of the adaptation planning case studies part of the Deep South Challenge (Stephens et al., 2018, 2021). Helensville is a small, low-lying town near Auckland which is expected to increase in population in the coming years. This community is currently being served by a wastewater treatment plant, the location of which can be seen in Figure 1.2a. Wastewater treatment plants are especially exposed to the effects of climate change, since they are often placed in low-lying areas near open bodies of water, and are affected by the effects of droughts and storms (Friedrich & Kretzinger, 2011; Hummel et al., 2018; Woetzel et al., 2020). The treatment plant in Helensville will also have to adapt to these effects, and most likely retreat inland at some point in the future if the sea level rises too high.

The Deep South Challenge wants to use robust decision making to identify vulnerabilities for the wastewater treatment plant, and identify robust policy options in order to keep the plant at the same location for as long as possible. However, using a simple model to represent the behavior at the case site could be oversimplified. The compound flooding the plant is at risk to, as well as the failure methods can be found in Figure 1.2b. The plant in Helensville is located in the middle of a coastal floodplain, with large intertidal flats at the downstream end protecting the from storm-tide. The plant discharges its effluent into the small Kaipara river. The water level in this river varies based on tides and rainfall, since it drains most of the upstream watershed.
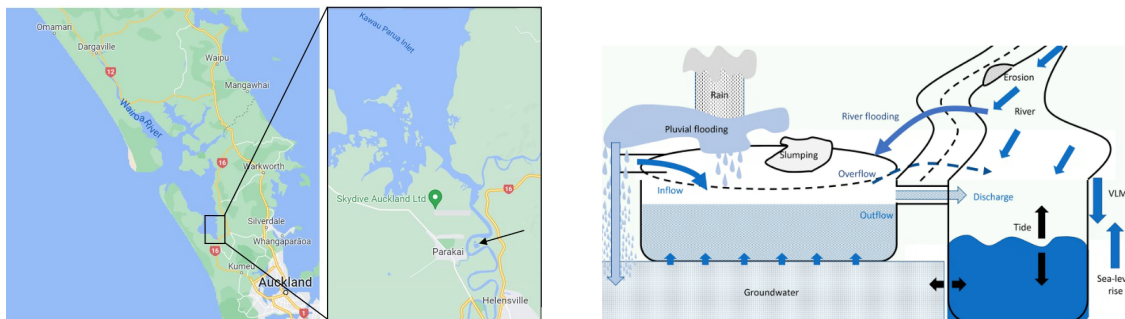
(a) Location of the wastewater treatment plant next to Kaipara river in New Zealand (from google maps)

(b) Diagram of the failure methods and drivers for the wastewater treatment plant. VLM stands for vertical land movement (Stephens et al., 2021).

Figure 1.2: Helensville wastewater treatment plant location and flooding risks

1.3   Problem statement/objective/research questions

1.3.1   Problem statement

The deep south challenge is currently doing research into the future adaptation of a wastewater treatment plant in Helensville, New Zealand. The goal is to use robust decision making to find vulnerabilities for the Helensville wastewater treatment plant, and to use these found vulnerabilities to identify robust policy options to keep the plant operational at its current location for as long as possible.

Robust decision making usually uses simple conceptual models rather than more complex models, due to the large number of runs necessary. The complex topography and compound flooding present at the case site mean using a simple model could potentially be oversimplified. This could in turn lead to potentially wrongly identified vulnerabilities and different policy advice.

1.3.2   Objective

The objective of this research is to compare the model behavior, identified vulnerabilities, and derived policy advice between a simple conceptual and more complex model for the Deep South Challenge's adaptation case study in Helensville.

1.3.3   Research Questions

Main question

How does the use of a more complex model rather than a fast simple model as traditionally used for robust decision making influence predicted system behavior and identified vulnerabilities, and does this have an effect on potential policy advice?

Subquestions

- **How and why does the predicted system behavior differ between the two models?**
  This subquestion focuses on comparing the two models based on their accuracy at the wastewater treatment plant, overall inundation depth and extent, and sensitivities throughout the model domain. This comparison also includes a reflection on where these potential differences come from based on each respective model's aspects.

- **How do the identified vulnerabilities differ between the two models?**
  Vulnerabilities for the wastewater treatment plant are identified using a combination of the sensitivity analysis and the scenario discovery. In general, the sensitivity analysis shows which uncertainties are most important for the results, while the scenario discovery gives specific thresholds for these uncertainties to define scenarios where failure is likely to occur. This comparison also includes a reflection on the effects of differences in the two models.

- **How does the derived policy advice differ between the two models?**
  The vulnerabilities identified, supported with knowledge on system behavior for both models can form the basis of potential policy advice. The question here is if potential differences in predicted system behavior and identified vulnerabilities lead to different policy advice, and if so, how.

1.3.4   Scope and method

This research will focus on the Helensville wastewater treatment plant. In order to compare the predicted system behaviors, identified vulnerabilities, and derived policy advice for two models, the first iteration of robust decision making will be performed for both these models. This mainly consists of running a global sensitivity analysis and scenario discovery for the current situation without any policy to mitigate the effects of climate change.

The two models will be forced by a compound flooding event consisting of rainfall and storm-tide, with failure being defined as overtopping of the wastewater treatment plant's pond embankments. The simple model will be based on a hydrological balance, while the more complex model is based on the Navier-Stokes equations.

1.4 Reader's guide

Chapter 2: Literature review

The goal of this Chapter is to illustrate the gap in knowledge, place the research in the correct context, and give the building blocks for the rest of the report. Section **??** gives a background on robust decision making, and the role the global sensitivity analysis and scenario discovery play in it. Section 2.2 discusses the wastewater treatment plant and surroundings in further detail, including current forcing, potential failure methods, and previous hydraulic modeling. Section 2.3 discusses potential hydraulic modeling approaches, split up into conceptual approaches and those based on the Navier-Stokes equations. Finally, Section 2.4 summarizes relevant aspects of the chapter.

Chapter 3: Research and modeling set up

The goal of this chapter is to further explain the approach taken, as well as the choices made in the modeling set up. The chapter starts with Section 3.1, which outlines the general approach taken. Section 3.2 then provides a framework for the modeling, including a definition of the hydraulic event, the model domain, and the computational configuration. The two models are chosen in Section 3.3. The configuration of these models is given in Section 3.4. Section 3.5 outlines their calibration and validation. Lastly, Section 3.6 discusses the set up of the global sensitivity analysis and the scenario discovery.

Chapter 4: Modeling results and comparison

The goal of this chapter is to present the outcomes of the simulations, and to use these to compare the two models. The chapter starts with Section 4.1, where some aspects of the outcomes are explored. Next, Section 4.2 discusses the results of the global sensitivity analysis. Section 4.3 discusses the results of the scenario discovery. Based on the first part of this chapter, Section 4.4 discusses the implications on potential policy advice. The chapter ends with a comparison on predicted system behavior and accuracy, identified vulnerabilities, and policy advice in Section 4.5.

Chapter 5: Reflection

The goal of this chapter is to reflect on important elements of Chapters 3 and 4 to verify results and discuss limitations. This includes a discussion of modeling choices in Sections 5.1 and 5.2, calibration and validation in Section 5.3, and the sensitivity analysis and scenario discovery in Section 5.4.

Chapter 6: Conclusion and recommendations

This chapter presents the findings of the research based on the research questions stated in this chapter in Section 6.1, and recommends avenues for future research based on those findings in Section 6.2.

Chapter 2

Literature review

The goal of this chapter is to lay the foundation for work done in the rest of the report and further illustrate the gap in knowledge and its relevance. The chapter starts with a primer on robust decision making in Section 2.1. Section 2.2 then introduces important aspects of the wastewater treatment plant and its surroundings. Section 2.3 discusses various hydraulic modeling approaches. Finally, Section 2.4 summarizes relevant aspects of the chapter.

2.1 Robust decision making

Developed by the RAND corporation, robust decision making can be seen as an extension of scenario planning (Lempert, 2019). Compared to scenario planning which uses a selection of a few plausible and mutually exclusive scenarios, robust decision making samples through the entire uncertainty space (every combination of possible uncertainties). The main benefits of sampling through the entire uncertainty space are twofold: a lower reliance on the selection of specific scenarios, and a more precise description of the conditions under which failure is likely to occur for a system.

The primary outcomes of the robust decision making process are provided by the vulnerability analysis. In this step the conditions where the system is vulnerable are described. These identified conditions can then be used to develop robust strategies that better deal with vulnerabilities. This is an iterative process, with a strong role for discussion on potential options, tradeoffs, and uncertainties. This discussion combined with computational experiments has been shown to strengthen both processes by continually testing assumptions and conclusions on both the strategies and the uncertainties taken into account (Groves et al., 2019; Lempert, 2019; Walker et al., 2013).

The straightforward way in which robust decision making identifies a system's vulnerabilities have also been proposed to be helpful for other decision making under deep uncertainty techniques, notably the dynamic adaptive policy pathways approach proposed by Haasnoot et al. (2013). How these two techniques work together, and a further analytical breakdown can be found in the thesis adjacent to this one. This thesis will focus mainly on the identification of said vulnerabilities using two models of differing complexity to see how the results differ and if this significantly influences policy advice.

2.1.1 The robust decision making process

Robust decision making is an iterative process as can be seen in Figure 2.1. Before potential policies are introduced to the system to stress-test their relative performance, the first iteration is usually done for the status quo. This is done to better understand the system, find current vulnerabilities, and identify potential policies. This first iteration is also the scope for this research.
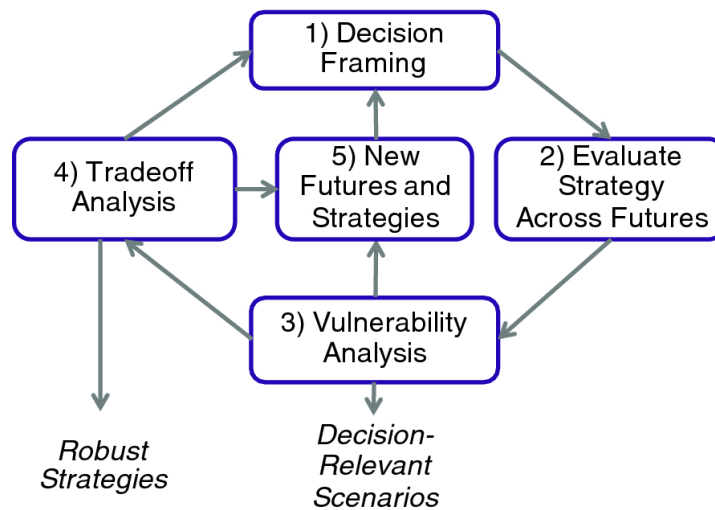
Figure 2.1: A flowchart of the robust decision making process (Lempert, 2019)

Seen in Figure 2.1, the robust decision making process begins by conceptualizing the problem in **step 1** utilizing the XLRM framework. This involves identifying important uncertainties (X), levers (L) representing potential policies, and problem objectives (M) which reflect the relevant outcomes. The relationships (R) show the links between these uncertainties, policy options, and outcomes (Lempert, 2019). After this conceptualization, in **step 2** cases are generated by calculating the outcomes M for different combinations of uncertainties and policies. To do this, various sampling techniques can be employed to sample through all potential combinations of uncertainties. Literature has suggested that using adaptive sampling here could lead to increased efficiency, but most of these techniques are still actively being developed (Groves et al., 2019; Lempert, 2019).

After a database of outcomes for different combinations of uncertainties and policy options is created, a vulnerability analysis is conducted in **step 3** to characterize the conditions where the objectives are not met. The results of the vulnerability analysis are used in **step 5** in two main ways: to help identify policy options to protect against the identified vulnerabilities, or to re-conceptualize the problem when necessary. In later iterations of the process when there are multiple policy options, the results can be used to visualize tradeoffs between these policies for different vulnerabilities in **step 4**.

2.1.2 Vulnerability analysis: scenario discovery and sensitivity analysis

The vulnerability analysis is the analytical heart of the robust decision making, where the outcomes are interpreted to identify vulnerabilities in the system and potential policies. Traditionally this consists only of scenario discovery, but using an additional global sensitivity analysis has been suggested by literature to help in two main ways: to gain a more complete picture of the vulnerabilities, and to help reduce the amount of factors taken into account in later iterations (Herman et al., 2014; Kwakkel & Haasnoot, 2019).

Scenario discovery

As part of the vulnerability analysis, scenario discovery is performed on the database of cases sampled from the entire uncertainty space. The goal is to find statistically significant clusters of cases where the objectives are not met. Although other methods can also be used dependent on the expected characteristics of the results, usually the Patient Rule Induction Method (PRIM) algorithm is initially employed since it is the most robust, easy to interpret, and includes non-linear effects (Bryant & Lempert, 2010; Friedman & Fisher, 1999; Kwakkel, 2017; Kwakkel et al., 2016a; Lempert, 2019).

PRIM defines the clusters of relevant cases using thresholds for each relevant uncertainty, which can be seen in Figure 2.2. This is often defined as a multi-dimensional box (Bryant & Lempert, 2010; Kwakkel et al., 2016a; Ramm et al., 2018).

The quality of a box is usually described through the coverage and density, which is also explained in Figure 2.2. The coverage is defined as the percentage of all cases where the objectives are not met that fall within the thresholds of the selected box, and the density as the percentage of cases that fall within the thresholds of the selected box where the objectives are not met. Ideally, both the coverage and density should be as high as possible, but there is always a tradeoff to be made between the two. If the coverage is high and the density is low, the box includes almost all cases, making the findings a lot less specific. On the other hand if the density is high, but coverage is low, the box's thresholds only describe a few of the cases where the objectives are not reached making the set thresholds less reliable.

Next to coverage and density, a quasi-p value is calculated to estimate the probability that an input value is selected by chance, and whether it is statistically significant. A high quasi-p value can indicate very noisy data, or an insufficient sample size (Bryant & Lempert, 2010; Kwakkel et al., 2016a).
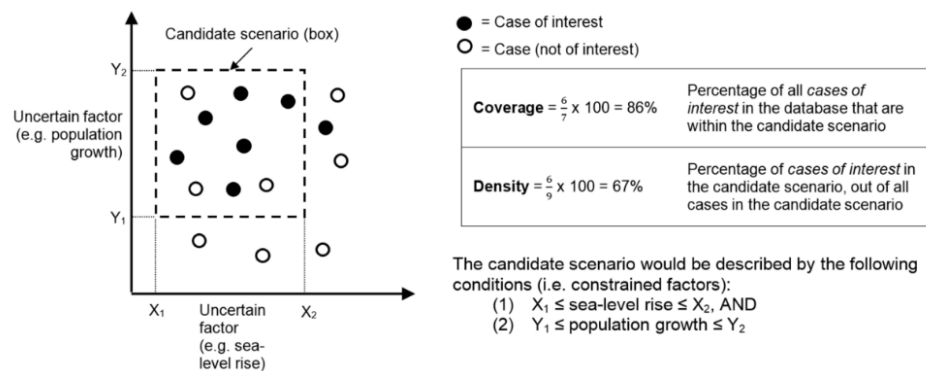
Figure 2.2: Visualization of the results of scenario discovery using the PRIM algorithm. Each point in the graph on the left is a case from the sampled database. A black point is a point where the objectives are not met, whereas a white point is a point where the objectives are met. The box or candidate scenario shows 2 dimensions with thresholds Y_1 and Y_2, and X_1 and X_2. These thresholds are also written out on the bottom right (Ramm et al., 2018).

Sensitivity analysis

Literature suggests a few benefits of using an additional global sensitivity analysis, such as factor prioritization and a better understanding of the model system and outcomes. Factor prioritization is suggested in literature to save computational expense by removing uncertainties in later iterations since they have a negligible influence on the outcomes (Herman et al., 2014; Kwakkel & Haasnoot, 2019). The precise effects of this are questionable, however, since each introduction of a new policy could change the sensitivities of a system. Factor prioritization can help in the identification of policy options, however, by indicating which uncertainties most influence the outcomes.

Using a global sensitivity analysis is also in line with standard practice for hydraulic models (Hall et al., 2009). Compared to local sensitivity methods, global methods offer a broader insight into model behavior, and can also show interaction effects between variables. Two prominent global sensitivity methods are SOBOL and Morris. SOBOL has been shown to be more robust and accurate, and is thus preferred when computationally feasible (Hall et al., 2009; Tang et al., 2006). Morris is usually only employed when many uncertain factors (up to 100) are taken into account, or the runtime of the model is very large (10 minutes or so).

A SOBOL analysis uses a quasi-random sampling scheme, which means that points are strategically chosen to ensure a more uniform and thorough exploration of the uncertainty space compared to a fully random sampling scheme (Saltelli et al., 2010; Sobol, 2001). The results of the analysis include both first and second order effects. First order effects refer to the direct impact on the output of varying one input factor, while second order effects reflect the impact on the output by the interactions between two input factors. The total of these effects should add up to 1 if the results have converged (Saltelli et al., 2010).

2.1.3   Impacts robust decision making on model complexity

Both scenario discovery and sensitivity analysis need many simulations, meaning a high model runtime can be problematic. For a normal sensitivity analysis, this problem is often solved by reducing the complexity of the sensitivity analysis. As mentioned in the previous section, there are different options with differing accuracies for this based on the model and problem at hand. For scenario discovery, however, this is not an option. Instead, to decrease runtime often simplified models are used. The goal of these fast simple or meta-models is to mimic system behavior relatively well while decreasing computational cost (Haasnoot et al., 2014, 2019; Klosterman, 2012; Lempert, 2019; Marchau et al., 2019).

However, the usefulness of these models can decline quickly in cases where a complex system is harder to simplify. In these cases simplifications can impact the behavior of the system and with it, the validity of the results. Notable cases with regards to hydraulic modeling prone to oversimplification are when bathymetry and topography influence flow, or when compound flooding processes are potentially relevant (Alkema, 2007; Eilander, 2022; Herdman et al., 2018; Hoitink & Jay, 2016; O'Neill et al., 2017; Santiago-Collazo et al., 2019; Teng et al., 2017).

There are also reasons other than runtime why these simplified models are traditionally used for robust decision making. They often require fewer parameters, can be more transparent and interpretable for users, and be more robust to small changes in model parameters (Bhave et al., 2016; Groves et al., 2019; Kwakkel et al., 2016a; Lempert, 2019; Molina-Perez, 2016). It is important to recognize the need for models that strike a balance between being complex enough to accurately capture the behavior of a system, while still maintaining interpretability and robustness.

2.2   Helensville case

One of the Deep South Challenge's adaptation cases is the Helensville wastewater treatment plant, which services a small community of less than 4,000 people. This small plant has a two-stage oxidation pond, and discharges its effluent into the small Kaipara river based on gravity (Beca et al., 2020; Ho et al., 2009). More data and the precise operation of the treatment plant can be found in Appendix A.

Like many other wastewater treatment plants, the plant in Helensville is at risk of rising sea levels, increased instensity and frequency of storms, and changing system behavior (Beca et al., 2020; Cao et al., 2020). A managed retreat will most likely be necessary at some point in the future, although the goal is to keep the plant at the same location for as long as possible if it saves costs (Stephens et al., 2021; Watercare Services Limited, 2015).

The goal of this section is to describe relevant aspects of the wastewater treatment plant, explore the surrounding area and system and its effects on forcing, and discuss some of the previous hydraulic modeling undertaken int this area and its relevancy to this research.

2.2.1   The Helensville wastewater treatment plant

Current state of the wastewater treatment plant

From a recent report by Watercare Services Limited (2015) it is clear the wastewater treatment plant is already facing some of the expected effects of climate change. This can be seen in high groundwater levels, increasingly high tides and storm surge, and the increased extent and intensity of precipitation events. Pictures of some of these effects can be found in Appendix A.

High groundwater levels have already led to the placing of a lining combined with a 200 mm thick layer of water to prevent potential seepage. Increasingly high tides and storm surges have led to erosion of the approach road to the wastewater treatment plant, and near overtopping of the plant's embankments in various cases. Lastly, heavy rainfall has caused the plant to exceed its effluent limits numerous times in the past (Stephens et al., 2021).

Main hazards affecting the wastewater treatment plant

The Helensville plant has previously been conceptualized by the Deep South Challenge, which can be seen in Figure 2.3 (Stephens et al., 2021). The main hazards affecting the plant can be split up into two main categories: the treatment ponds overflowing, or external stresses affecting pond functionality. The first is caused by an excess influent due to a combination of pluvial flooding, infiltration, and planned inflow. The second involves stresses due to a combination of sea level rise, increased river flow, storm surge, rainfall, and tidal amplitude. These stresses can lead to slumping or overtopping of the plant's pond embankments, the erosion of the access road, or an increase in the groundwater table.
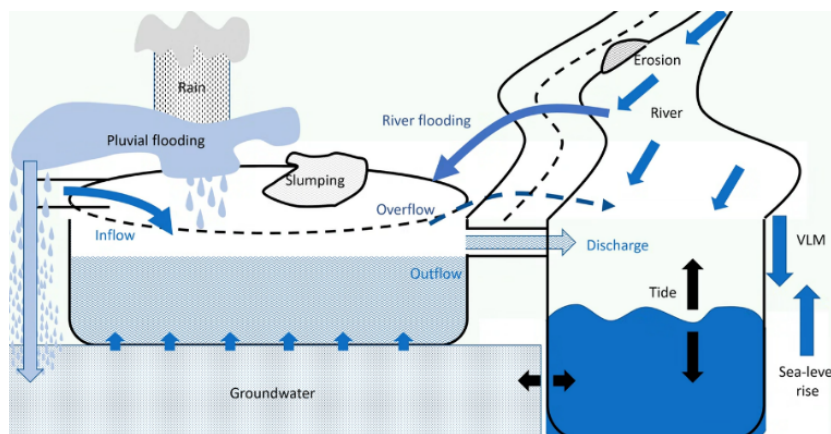
Figure 2.3: Conceptual model of the wastewater treatment plant. The plant is on the left, and the Kaipara river is schematized on the right. The figure also shows various failure mechanisms such as slumping, overflow, and erosion. The hazards facing plant functioning can be placed into two main categories: the treatment ponds overflowing, or external stresses affecting pond functionality (Stephens et al., 2021)

Previous research on the wastewater treatment plant has mostly looked at the first category of hazards: overflowing of the treatment ponds. Even a moderate increase in the projected influent could lead to an increased risk of discharge quality failure by 500% (DSC, personal communication, January 8, 2023) This previous research only included the effects of real sea level rise. The conclusion was that real sea level rise had little effect on the potential functioning of the plant until at least 2060. Only looking at sea level rise rather than including other forcing could be an oversimplification, however.

There is currently no research on the second category of hazards affecting the plant. This is echoed in emails from the Deep South Challenge which mention the lack of knowledge of, and interest in, the effects of compound flooding on the wastewater treatment plant. This compound flooding and its effects on water levels around the wastewater treatment plant will be the focus of this research.

2.2.2 Wastewater treatment plant's surroundings

This subsection dives deeper into the surroundings of the wastewater treatment plant to better understand system behavior and the risks affecting the plant. It discusses, in order, the Kaipara harbor, Kaipara river catchment and the Kaipara river which flows past the plant.

Kaipara harbor

The Kaipara harbor, visible in Figure 2.4, is located on New Zealand's North Island, just north of Auckland. The harbor is quite broad and shallow with clearly defined drainage channels, which can be seen in Figure 2.4b. Almost 43% of the estuary is intertidal, with a surface area of around 947 km^2 at high spring tide and 538 km^2 at low spring tide (Haggitt et al., 2008; Heath, 1975). A large reason for this is the high sedimentation in the harbor, which is also the reason the harbor has become increasingly ebb-dominated (Bosboom & Stive, 2021; Haggitt et al., 2008; Reeve et al., 2009). The high sedimentation rate also leads to the locations of the channels and sandbanks constantly shifting, although there is a general lack of knowledge on the exact speed of these movements (Haggitt et al., 2008; Hume et al., 2003; Reeve et al., 2009).

The important takeaway is that the harbor is a dynamic place, where due to sedimentation intertidal flats and channels are constantly shifting. Over a few decades, this can affect the propagation of storm surge and the tidal amplitude, both of which are important factors for the water level at the wastewater treatment plant.

(a) Location of the wastewater treatment plant in the Kaipara harbor (from google maps)

(b) Bathymetry of the Kaipara Harbor in meters (Haggitt et al., 2008)
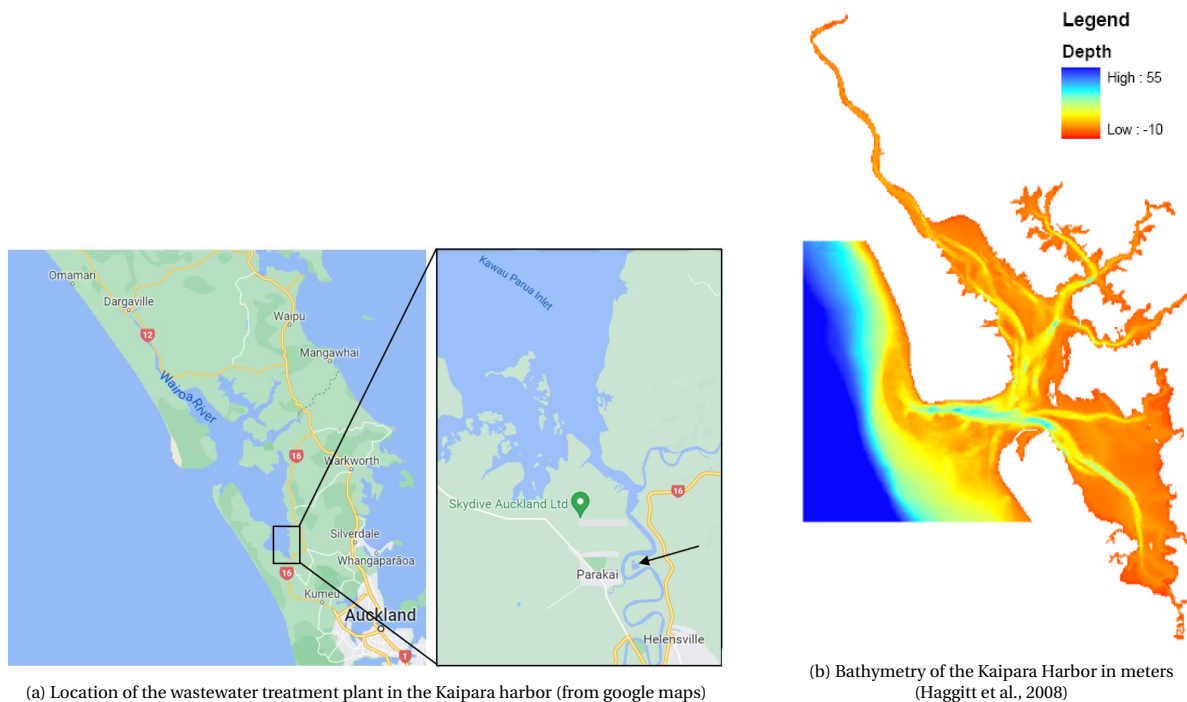
Figure 2.4: Topography and bathymetry of the Kaipara harbor. The estuary is around 60 kilometers long from North to South (Reeve et al., 2009).

Kaipara river catchment

The Kaipara river catchment, where the wastewater treatment plant is located can be seen in Figure 2.5. The topography of the catchment varies significantly. At the downstream end mangrove forests and intertidal flats separate the catchment from the Kaipara harbor, whereas in the upstream areas of the catchment large mountain ranges separate the catchment from both the Auckland harbor and the open coast. This difference in topography leads to slopes up to 17 degrees, with an average around 3.5 (Auckland Council & (LINZ), 2020).

Land use in the catchment is mostly rural. Almost 64% of the catchment is used as pasture for cattle and sheep, while urban use only accounts for about 2.5%. Surface water takes up less than 0.5 percent. (Bibby & Webster-Brown, 2005; Green & Daigneault, 2018; Landcare Research, 2021; Reeve et al., 2009). This has several effects on potential compound flooding of the wastewater treatment plant. First, the main use of the catchment is pasture or small crops, which in general have a low hydraulic roughness compared to cases where more vegetation is present (Chow, 2009; Schneider, Arcement Jr, et al., 1984). This could mean potential storm surge spreads further. Second, the low surface water percentage indicates any rainfall, in general, is not retained upstream but runs off. This quick runoff could be exacerbated by the large slopes in the catchment.

Soil characteristics also vary throughout the catchment, and with depth. In general the shallow soil layers consist mostly of silt and clay in the lower reaches of the catchment, and sand elsewhere (Haggitt et al., 2008; Reeve et al., 2009). Deeper soil layers in the catchment consist mostly of coarser, permeable sands. The small particle size in the lower reaches leads to significant sediment transport, 13.7 tons per year in 2014 (Green & Daigneault, 2018). At those current transport rates, the downstream intertidal flats are growing by 7 mm/year. This growth rate is almost double any of the other intertidal flats found throughout the Kaipara estuary (Green & Daigneault, 2018). The changing bathymetry introduces uncertainty about the propagation of storm surge and tidal amplitude, similarly to the behavior of Kaipara harbor mentioned earlier.
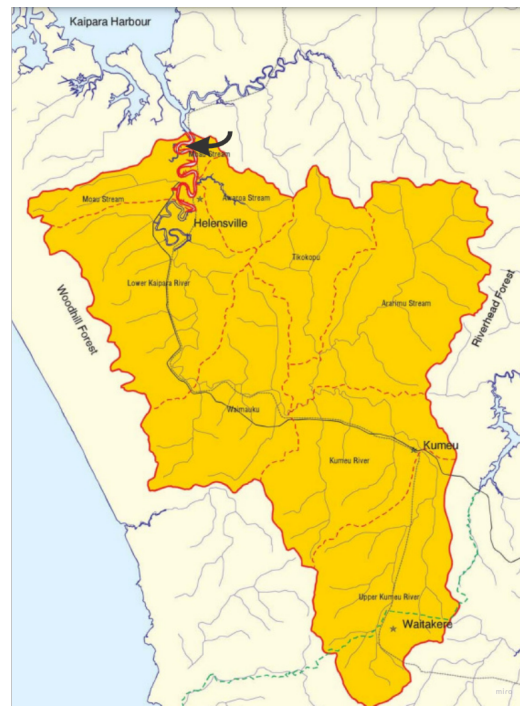
(a) The Kaipara river catchment including the different rivers and streams. The black arrow demarcates the location of the wastewater treatment plant. The Kaipara river flows past the treatment plant. The catchment is 26km long and 6km wide (Auckland Regional Council, 2001).
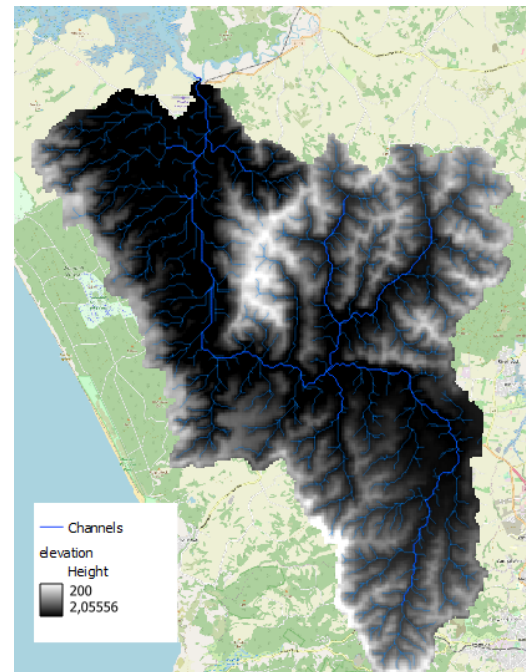
(b) Elevation map for the Kaipara river catchment. The height goes up to 256.8 meters, but is maxed at 200 meters for better visibility (Auckland Council & (LINZ), 2020)

Figure 2.5: Location and elevation of the Kaipara river catchment

Kaipara river

The Kaipara river is the main river that functions as drainage for the entire catchment, and where the wastewater treatment plant discharges its effluent. It also has a strong tidal influence (Dejeans et al., 2022; S. B. Mitchell et al., 2017; Stephens et al., 2016). At the upstream part it is filled by various small streams, after which it flows past Helensville and the wastewater treatment plant as can be seen in Figure 2.5a. River flows are mostly due to drainage, as the streams in the upper part of the catchment are intermittent. These flow can differ greatly. A 50 year ARI event has a peak flow of around 305 m^3/s, while low flows can be down to 0.1653 m^3/s for a 7-day Mean Annual Low Flow (MALF) (Auckland Regional Council, 2001; Ingley, 2021; Stephens et al., 2016). This indicates that flows in the river are most likely only due to either tides or precipitation events.

2.2.3   Hydraulic forcing of the Kaipara river catchment

In this section three main aspects of the current forcing of the Kaipara river catchment will be discussed: precipitation, wave climate and storm surge, and the tides.

Precipitation

The Kaipara river catchment is quite wet. From the Helensville raingauge dataset, which holds records between 2014 and 2019, the rainfall frequency is found to be around 55%. The catchment is also quite warm. Many surrounding measuring stations have not even recorded any temperatures under 0°C. This means that precipitation consists almost exclusively of rainfall (Bell et al., 2018). The amount of rainfall varies somewhat throughout the catchment. In the mountainous areas it is higher, with annual median rainfall levels of 1600 mm, while at the intertidal flats this drops to 1300 mm (Bell et al., 2018).

The current day extreme rainfall for the area can be seen in Figure 2.6. Increases in temperature have been shown to further increase the frequency and intensity of extreme rainfall events. The increase in rainfall depth

can be anywhere between 7% and 9% per extra degree of warming for a 24 hour storm, which is an additional source of uncertainty (Bell et al., 2018).
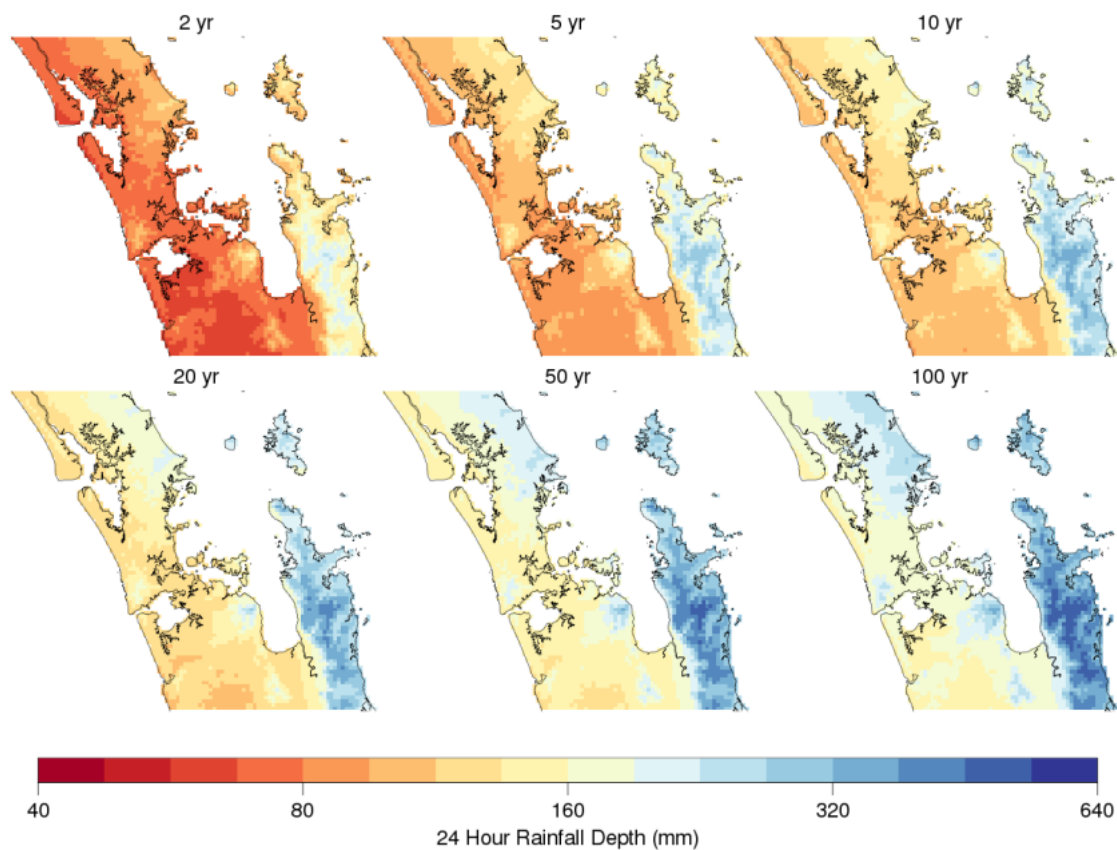
Figure 2.6: Total rainfall for 24 hour storms of differing return periods in the Auckland region. The scale of the rainfall depth is logarithmic (Bell et al., 2018).

Waves and storm surge

Waves are most likely not relevant at the wastewater treatment plant. The waves that are present are wind-driven and created within the estuary. As mentioned before, the Kaipara harbour is around 60 kilometers long (North to South). The wind only comes from this direction less than 5% of the time (Stephens et al., 2016). Looking at a sustained 11 km/hr wind, which happens less than 0.5% from this direction, the significant wave height would be around 20 cm when it reaches the first intertidal flats at the downstream end of the Kaipara river catchment. This wave height most likely damps out on these flats and vegetation before it reaches the wastewater treatment plant, which is 3.5 km upstream.

Using the tidal gauge at Helensville a skew surge analysis was conducted by Stephens et al. (2016) to calculate the difference between the maximum recorded sea-level during a tidal cycle, and the predicted maximum astronomical tidal level (Batstone et al., 2013). Based on this dataset, a generalized pareto distribution was used to calculate extreme values. The 95% confidence range which indicates the interval of values wherein the real value is likely to fall is quite broad as can be seen in Figure 2.7, indicating predictions of the storm surge are not very precise.

AEP = annual exceedance probability; ARI = average recurrence interval; GPD = generalised Pareto distribution fit to independent peaks over 230 mm threshold. All elevations calculated relative to MSL.

AEP	ARI	GPD max. likelihood (mm)	GPD lower 95% confidence interval (mm)	GPD upper 95% confidence interval (mm)
0.63	1	570	445	778
0.39	2	657	486	962
0.18	5	776	535	1252
0.10	10	870	569	1511
0.05	20	967	601	1812
0.02	50	1100	638	2281
0.01	100	1204	664	2700
0.005	200	1311	688	3184
0.002	500	1457	716	3939
0.001	1000	1571	735	4613

Figure 2.7: Storm surges for differing return periods. Note that the 95% confidence intervals are very broad, especially for more extreme events (Stephens et al., 2016)

Tides

Tides have a large influence on the water level in the Kaipara harbor. Due to the large number of intertidal flats throughout the estuary, tides are amplified (Stephens et al., 2016). The wastewater treatment plant uses this high tidal range to discharge its effluent. Data from the tidal gauge at Helensville can be seen in Figure 2.8.
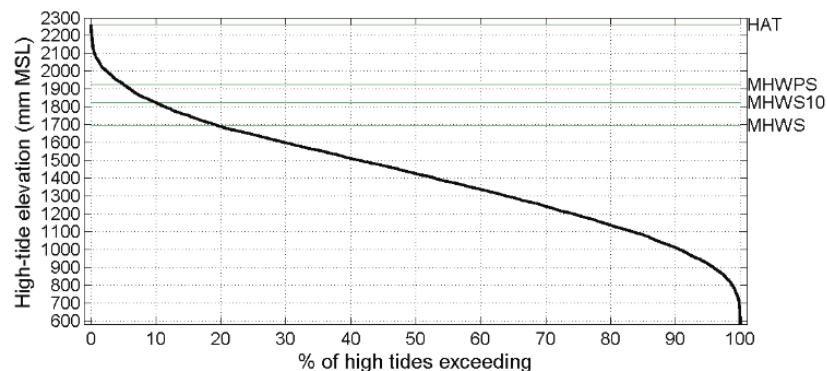
Tide	elevation (mm MSL)
M2	1371
S2	325
N2	231
MHWPS	1926
MHWS	1696
HAT	2264

Figure 2.8: High tide exceedance curve and tidal components for the Helensville tidal gauge (Stephens et al., 2016)

2.2.4   Previous hydraulic modeling

Previous hydraulic modeling of the Kaipara river catchment took place in 2013 and 2016, and might give insight into the use of models of differing complexity (Stephens et al., 2016).

Initially in 2013, a static bathtub model was used to calculate potential inundation for the Helensville area for storm-tides of different return periods (Stephens et al., 2016). This was done by interpolating the results of

a hydrodynamic model for the Auckland coastline, and intersecting this with an elevation map to calculate inundation levels. However, this approach was deemed unsatisfactory due to the large floodplain storage volumes and complex processes in the kaipara river catchment, leading to the commissioning of a full hydrodynamic model of the area. This was done in 2016 with a full-physics flexible mesh 2D MIKE21 model (Stephens et al., 2016).

Comparison between the two approaches showed that the planar method used initially used in 2013 was indeed inaccurate. While for the downstream reaches of the catchment results were similar, results quickly diverge for the upstream reaches where topography becomes more important. Figure 2.9 shows an overestimation of inundation depth by up to 2 meters in these upstream reaches. Next to inundation depths, inundation extent was also overestimated by the planar method.

These results show that a conceptual model is a lot less accurate upstream. The water level at the wastewater treatment plant was also overestimated by more than 0.5 meters, as can be seen in Figure 2.9, indicating the possibility that a conceptual model oversimplifies system behavior at the location of the plant. This makes this case interesting for comparing two hydraulic models of differing complexities for robust decision making (Stephens et al., 2016).
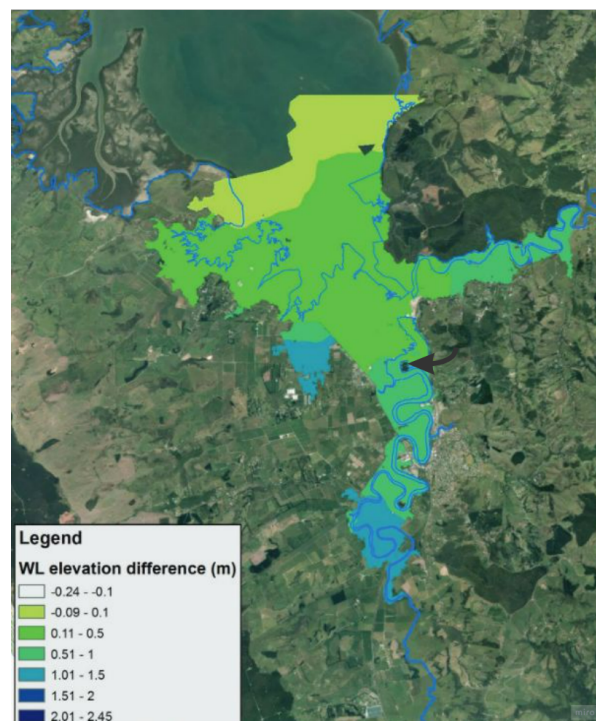
Figure 2.9: Comparison between static planar inundation method from 2013 and the full-physics 2D MIKE21 model from 2016. Only locations where both models gave results are considered. The wastewater treatment plant is located in the 0.51-1 meters difference band, and is shown with a black arrow (Stephens et al., 2016).

2.3 Hydraulic modeling approaches

The goal of this section is to introduce the two main groups of hydraulic modeling approaches which could be used to model water levels at and around the case site. Within these two groups there are various modeling approaches of differing complexities and with different application domains. It is also important to mention that the discernment made between different approaches here is, for a large part, theoretical. In practice, approaches are often combined and many different subgroups thus exist. This is outside the scope of this research, however. The first subsection will discuss the most important conceptual methods, and the second subsection will discuss those based on the Navier-Stokes equations.

2.3.1   0-term/conceptual methods

0-term or conceptual models are often used in situations where computational power is a limiting factor, notably for large study areas (>1000 km^2) or cases where many runs are necessary. Additionally, conceptual models have a high level of interpretability and robustness when dealing with potentially unreliable data compared to more complex methods (Groves et al., 2019; Lempert, 2019; Ramm et al., 2018; Teng et al., 2017; van Berchum et al., 2018).

The main three families of conceptual models are planar or bathtub methods, Rapid Flood Spreading Models (RFSM), and Cellular Automata (CA). In reality, these approaches are not mutually exclusive. CA and RFSM, for example, have developed to be quite similar and are often combined (Jamali et al., 2019; Menendez et al., 2019; Torres et al., 2022; Wijaya & Yang, 2021). For cases where gravity is the dominant driver or when dynamic effects are insignificant, conceptual models such as these can all reach reasonable accuracies for both inundation depth and extent compared to the more complex methods based on the Navier-Stokes equations (Leijnse et al., 2021; Lhomme et al., 2008; H. McGrath et al., 2018).

Planar methods

Planar or bathtub methods assume the water level uniformly rises across the floodplain, and calculate inundation depth and extent by intersecting a calculated water level with the elevation map of the region (Teng et al., 2015). This works best in cases where the river and floodplain storage are clear. The bathtub method is very quick, but can also be inaccurate due to the lack of inclusion of dynamic processes such as precipitation and flood attenuation (Didier et al., 2019; Leijnse et al., 2021; Menendez et al., 2019; Neumann & Ahrendt, 2013).

An example of a planar method can be seen in the previous modeling done at the case site in 2013 discussed in Section 2.2.4. Here, the water level at the downstream end of the Kaipara river was calculated, which was then intersected with a map of the area's elevation to calculate inundation depths and extent. This led to a significant overestimation of the water level in the upstream part of the watershed where dynamic processes are more important (Johnson et al., 2019; H. McGrath et al., 2018; Scriven et al., 2021; Stephens et al., 2016).

Rapid Flood Spreading Method (RFSM)

Developed by Gouldby et al. (2009), Krupka et al. (2007), and Lhomme et al. (2008), RFSM's subdivide the area of interest into "impact zones". For each of these impact zones the volumetric curve is calculated, which is defined as the area for each contour of the impact zone. This is done for each impact zone, and each border's location and elevation is also calculated in order to calculate flow between impact zones. This type of model is robust, computationally efficient, and only needs the elevation for each impact zone and basic forcing data to get started, which is why it is often used for data-sparce urban regions (Menendez et al., 2019; Shen et al., 2016; Teng et al., 2017).

A major benefit of RFSM's compared to planar methods is the ability to include more dynamic processes such as rainfall runoff and infiltration. When using a high resolution elevation map, the results of RFSM's are generally relatively accurate for low-lying regions where dynamic effects are less important (Lhomme et al., 2008; Menendez et al., 2019; Néelz, Pender, et al., 2010; Shen et al., 2016).

Cellular Automata (CA)

Developed by Wolfram (1984), CA based models have already been used in many other fields. The method is based on describing the area of interest in terms of the world (an elevation map), with agents (the water), and transition rules. The elevation map is split up into a grid with each grid cell defining a state such as flooded or dry for the agent. Flooding is then calculated based on simplified transition rules between a grid cell and its neighbors. These transition rules use simplified physics, sometimes loosely based on the Navier-Stokes equations.

A benefit of this method compared to other conceptual methods is that less pre-processing of the elevation map is necessary, which can save time. Additionally, CA methods can be more accurate when the transition rules and the data inputted is of sufficient quality. On the other hand, the algorithms used as transition rules

can be complex to define, and make the model quite complex and less transparent to build compared to the other conceptual methods (Jamali et al., 2019; Menendez et al., 2019; Teng et al., 2017; Torres et al., 2022; Wijaya & Yang, 2021).

2.3.2   Models based on the Navier-Stokes equations

Models based on the Navier-Stokes equations are formulated in 1, 2, and 3 dimensions. In general, 3D modeling requires the most detailed data and computational power and 1D modelling the least. There are however many intermediate methods. A summary of some of these can be found in Appendix **??**. In the next paragraphs the application domains of the 3D, 2D, and 1D methods will be explained. Special interest is given to 2D models, as these are most often used to calculate flood extent and depth.

When selecting between 1D, 2D, or 3D modeling methods, the most important factors are the time and length scales of the processes at hand. When taking these into account, most uncertainties and inaccuracies are usually less a result of model selection, and more due to variations in input data (Dimitriadis et al., 2016).

3D modeling

3D models are typically used for cases where vertical flow can be significant. Examples are the local impacts of catastrophic floods, such as dam breaks, tsunamis or other breaches, where the scale of vertical flow is relevant compared to the other two dimensions (Teng et al., 2017). When vertical flow is less important, such as for shallow flow over broad floodplains, 3D models are most often seen as unnecessary. These models take into account the full Navier-Stokes equations in three dimensions, at the cost of increased computational expense. This increased computational cost leaves 3D models out of reach for most purposes where many runs are necessary, such as for this research. Additionally, the data type and quality required to set up and validate a 3D model make its construction even more difficult (Alcrudo, 2004; Teng et al., 2017).

2D modeling

2D models are the approach used most often to model flood extent and estimate risk (Neélz & Pender, 2009; Teng et al., 2017). 2D methods use the depth averaged Navier-Stokes equations, also called the shallow water equations. These equations assume that the water depth is shallow compared to the other two dimensions. There is a high number of differing approaches that are all 2D, and various studies to benchmark these different approaches (Hunter et al., 2008; Néelz & Pender, 2013; Néelz, Pender, et al., 2010). Teng et al. (2017) states that while 2D models are able to accurately model inundation duration and timing, most full-physics 2D approaches are unviable for very large areas (>1000 km^2), high resolution (<10m), or probabilistic risk assessments where many runs are necessary. This is most likely also the case for this research.

When full-physics 2D approaches are unviable, the shallow water equations can also be simplified when appropriate in order to increase computational speed while still retaining accuracy. Two simplifications that are often used are the Simplified Shallow Water Equations (SSWE) and the Local Inertial Equations (LIE). The SSWE leave out atmospheric forcing, Coriolis and viscosity terms. This is appropriate in most cases, as these effects work on very large temporal and spatial scales. The LIE further simplify these SSWE by neglecting the advection term, which is appropriate when wave dynamics are most likely not relevant (De Almeida & Bates, 2013; Leijnse et al., 2021; Neal et al., 2012).

The LIE can be further simplified when dealing with slowly-varying flow. The diffusive wave equations are used when the flow varies slowly in time, neglecting both local and advective acceleration. When the flow only varies marginally in space as well, quasi-uniform conditions are assumed, and the depth gradient or pressure term is neglected as well to define the kinematic wave equations. These equation only keep the bed slope and local depth. Models based on the diffusive and kinematic wave equations can reasonably accurately model flow when dealing with small variations in time and space. One problem with regards to this research is their lack of accuracy when using a tidal boundary, since this requires the acceleration terms (Hunter et al., 2007; Neal et al., 2012; Néelz & Pender, 2013; Teng et al., 2017).

1D modeling

1D models simplify the Navier-Stokes equations compared to 2D models by assuming the flow is uni-directional. This can be a fair assumption if the length of a channel is much longer than the width of its floodplain. A rule of thumb for this is a length-to-width ratio of 3:1 (Neélz & Pender, 2009). 1D models are useful when the channels are well defined, flows are not expected to spread significantly (uni-directional), or when there is a lack of detailed data. While 1D models are less computationally expensive than their 2D counterparts, in most cases 2D models are preferred over 1D models for coastal flooding and other situations with complex topography where there are no well-defined drainage channels, which is the case for part of the model domain around the wastewater treatment plant (Neélz & Pender, 2009; Teng et al., 2017).

1D models can also be coupled with 2D models. In these cases a 2D approximation is used for the floodplain, while the 1D model describes the drainage channel. This approach is most often used when both the drainage streams and floodplains are clearly defined. Both accuracy and computational cost are, in this case, usually comparable to the 2D approach used for the modeling of the floodplain (Dimitriadis et al., 2016; Kalimisetty et al., 2021).

2.4 Conclusion of the literature review

Exploration of the case site shows that the wastewater treatment plant is at risk to compound flooding, and that there is significant uncertainty present. The amount of rainfall will vary based on future temperature changes, the intertidal flats that influence tidal amplitudes and storm surge propagation are dynamic due to high levels of sedimentation, and there is a large uncertainty in the projected storm surge. This makes this case interesting for the use of robust decision making in order to make effective policy in the face of these uncertainties.

The main process behind robust decision making consists of the vulnerability analysis, which consists of a scenario discovery and a global sensitivity analysis. These both many simulations, necessitating a model with a shorter run time in order to thoroughly search through the uncertainty space. For this, simplified models are often used. This can become problematic when a complex system is harder to simplify, in which case the simplifications impact system behavior and the validity of the results.

Looking into previous hydraulic modeling at the case site from 2013 and 2016 shows that a conceptual bathtub model is a lot less accurate upstream in the model domain. This indicates the possibility that a conceptual model also oversimplifies system behavior at the location of the wastewater treatment plant (Stephens et al., 2016).

Looking at the various hydraulic modeling options available show that on the conceptual side the most logical options are a rapid flood spreading model, or a cellular automata model. These two options take into account more processes compared to a model using the bathtub approach such as the 2013 study done previously at the case site. For the more complex model based on the shallow water equations, a 3D model and full-physics 2D model have high computational demands making them unfeasible. Additionally, a 1D model is a less obvious selection for coastal flooding or when drainage channels are largely undefined. This leaves the options of a simplified 2D model, or a 1D-2D coupled model. Both these options have similar computational demands and accuracy.

While on the one hand a conceptual model might oversimplify the behavior, the computational expense of running a full-physics 2D model is not viable for exploratory modeling. The question is then twofold: is the use of a simplified 2D model feasible for the vulnerability analysis? If so, what are the impacts of the increased model complexity on system behavior, identified vulnerabilities, and policy advice?

Chapter 3

Research and modeling set up

The goal of this chapter is to further explain the approach taken in this research, as well as explain the choices made in the modeling. Section 3.1 outlines the general approach taken. Section 3.2 presents a schematization of the system. This includes a conceptual diagram of the system's scope, a definition of the hydraulic event and failure mechanism, and the model domain.

After these initial two sections that broadly explain the approach taken and some of the choices made, the rest of the chapter goes into more detail. The two models of differing complexity are chosen in Section 3.3. The configuration of these models is given in Section 3.4. Section 3.5 explains their calibration and validation. Lastly, Section 3.6 discusses the configuration of the global sensitivity analysis and the scenario discovery.

3.1   General research set up

The goal of this research is to find whether using a more complex model is worth the added computational demand compared to the simple conceptual models usually used for robust decision making. The approach taken to reach this objective can be seen in Figure 3.1 and is further explained below.
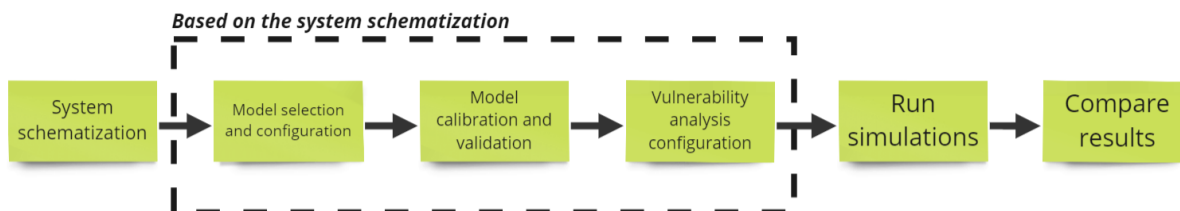
Figure 3.1: General approach taken to reach the objective of this research

First the system will be schematized. This involves introducing the scope of the system, the model domain, the forcing taken into account, and the failure mechanisms. This schematization forms the basis for the rest of the choices made in this chapter.

After the system is schematized, two models are selected. These two models are configured, calibrated, and validated for both an extreme storm-tide and rainfall event. This is followed by the configuration of the vulnerability analysis, consisting of a global sensitivity analysis and scenario discovery. The main uncertainties taken into account and their chosen ranges are also explained here.

After the configurations of the models and the vulnerability analysis done in this chapter, the global sensitivity analysis and scenario discovery are run and their results are explained in the next chapter. This explanation is followed by a comparison of both models. This comparison is based on predicted system behavior at the wastewater treatment plant, the identified vulnerabilities, and the implications for policy making of these results.

3.2   System schematization

From the case exploration in Section 2.2, it was found the most interesting risk facing the wastewater treatment plant was the effects of compound flooding on the wastewater treatment plant. A diagram of the compound flooding can be found in Figure 3.2. The storm-tide boundary found in this diagram can also be seen in Figure 3.3.

This section provides more detail on the scope of the system, the way the models will be forced, and what constitutes failure. This includes several simplifications. These simplifications help to focus on the big picture of model comparison while keeping computational demands lower. In future work, based on the results of this research, some of the questions regarding forcing and failure methods can be investigated in more detail.
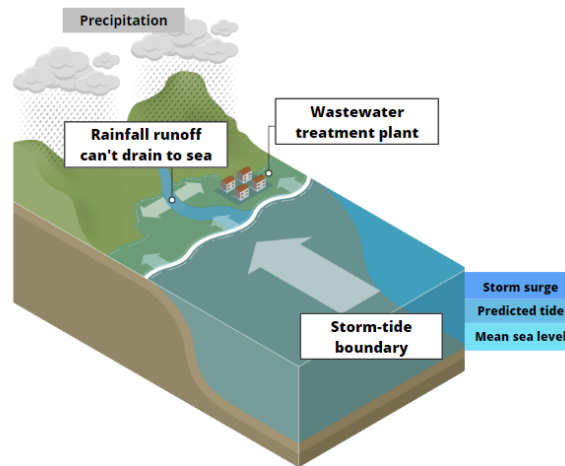
Figure 3.2: Conceptual diagram of compound flooding for the wastewater treatment plant. Diagram is based on a picture by M. McGrath (2019).
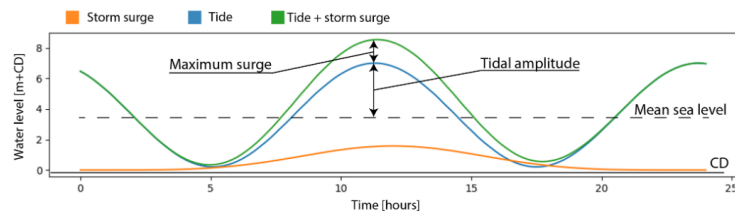
Figure 3.3: Breakdown of the storm-tide boundary used in Figure 3.2 (van Berchum et al., 2020)

3.2.1   Model domain

The model domain will encompass the entire Kaipara river watershed, bound by the intertidal flats at the downstream end, and the mountain ranges upstream. Taking the entire watershed within the model domain ensures the inclusion of all rainfall within the system. Setting the lower boundary at the intertidal flats also enhances the representation of flood attenuation in the models.

The Kaipara river basin is quite steep, meaning rainfall runoff will be quick. This is why the storm event taken as a basis will have a duration of 24 hours. This has also been used in previous work in the region (Council, 1999). An added benefit of using a 24 hour storm duration is that computational demands are kept lower.

3.2.2   Forcing

The compound flooding is due to a combination of precipitation and storm-tide. From the flow data of the Kaipara river, also given in Section 2.2, it can be concluded that nearly all the flow in the Kaipara river is due to drainage. This is why it was chosen not to include a river flow in the system.

Precipitation

The rainfall is assumed to be both spatially and temporally uniform for the duration of the storm in this research, which should be sufficient for the comparison of the two models. Spatially and temporally varying the rainfall would introduce additional uncertainties and complexity with regards to their proposed distribution, significantly increasing computational time needed. Using a uniformly distributed rainfall most likely underestimates the runoff as the drainage is constant, although this is also dependent on various additional factors including catchment size, timescale, catchment slope, infiltration, and the height of the peak (Zhou et al., 2021).

Storm-tide

The storm-tide is modeled as a water level boundary where the maximum tide reaches a peak at the same time as the storm surge, which can be seen in Figure 3.3. This is similar to previous work (Stephens et al., 2016; van Berchum, 2019), and should give a good insight into the effects of peak storm-tides. For the vulnerability analysis the storm surge and tidal amplitude will be split up to assess their individual effects.

3.2.3   Failure mechanism: overtopping

The high water levels around the wastewater treatment plant due to compound flooding place external stress on the functioning of the wastewater treatment plant. Potential failure mechanisms include slumping or overtopping of the plant's pond embankments, the erosion of the access road, or an increase in the groundwater table. With the exception of erosion, which is less crucial to the functioning of the plant, the failure mechanisms are all based on a combination of high water levels and geotechnical information.

Since the goal of this research is to compare the two models of differing complexity, this research will focus on the overtopping of the pond embankments. This failure mechanism is on the same timescale as the compound flooding event chosen, gives good insight into which factors lead to high water levels, and doesn't require additional geotechnical information.

The lowest point of the embankment is 3.38 meters NZVD2016, while the highest is 3.8 meters. This can all be seen in the last PDF in Appendix A. Overtopping is assumed to happen when the average maximum water level around the wastewater treatment plant reaches 3.60 meters. 33 of the 70 spot heights around the embankment are below this threshold. The duration of the water level exceeding this threshold is not considered in this research. Again, the key focus is on understanding the main processes and comparing both models, and the specific number chosen for the water level serves as a practical threshold for analysis.

3.3   Model selection

Based on the system schematization and case exploration, as well as the known restrictions for the global sensitivity analysis and scenario discovery, requirements can be defined for the models to be selected. The models selected should be able to be forced by compound flooding. Potential models should be able to represent rainfall runoff, and the effects of the intertidal flats on flood attenuation. It is also necessary that the model has a low enough runtime to be able to simulate a large number of experiments.

3.3.1   Conceptual model

The planar approach is less successful in replicating flooding behavior in the area, which was discussed in Section 2.2.4. A rapid flood spreading model or cellular automata model would be a better fit for this purpose, since they take into account more processes, as mentioned in Section 2.3. While there are multiple fast options for such models, most of these are focused only on fluvial flooding (Jamali et al., 2018, 2019; Teng et al., 2017; Wijaya & Yang, 2021). The addition of storm-tide and pluvial flooding to simulate compound flooding is less prominent. Models that do include these processes usually focus on urban flooding due to higher economic risks and more complex drainage patterns. FLORES is one such model that has already previously been used for scenario discovery (van Berchum, 2019).

Rapid flood spreading model (RFSM): FLORES

FLORES is a model based on the rapid flood spreading model. It is, in part, a continuation of previous work by Shen et al. (2016), which will be used as the basis for the conceptual model used in this research. It has already been used and validated for scenario discovery in the past. Additionally, it includes rainfall run-off and the effects of flow over the intertidal flats. This method is computationally cheap and relatively straight forward to implement, even in data-scarce environments (van Berchum et al., 2020).

In previous work modeling inundation depth and extent for a combined storm-tide and rainfall event, it had an error of around 20% while saving minutes in runtime compared to a full-physics 2D hydraulic model. While this is a lot less accurate, it showed similar behavior to the more complex model (van Berchum, 2019; van Berchum et al., 2018).

3.3.2   Complex model

The second model should take into account more of the relevant physical processes. For this, most 2D and 3D methods are out of reach due to their computational demand as was discussed in section 2.3. This includes the MIKE-21 model used previously as described in Section 2.2.4. Additionally, there are simplified 2D versions of the shallow water equations such as models based on the diffusive and kinematic wave equations. The main problem with these models is their lack of accuracy when using a tidal boundary, since this requires the acceleration terms (Neal et al., 2012; Néelz & Pender, 2013; Teng et al., 2017).

This leaves three main options: a model based on the simplified shallow water equations, local inertial equations, or a 1D-2D coupled model. The choice here was made for the SFINCS model using the local inertial equations, called SFINCS-LIE (Leijnse et al., 2021). The main reasons for the selection of SFINCS-LIE are twofold. The simplified shallow water equations are most likely not necessary, since the case exploration found waves would damp out before reaching the wastewater treatment plant. Second, a 1D-2D coupled model is most likely less effective due to a lack of definition of the drainage streams, while the computational costs and accuracy are oftentimes relatively similar to those of full-physics 2D methods (Dimitriadis et al., 2016).

2D reduced physics model: SFINCS

Developed in 2020 by Leijnse et al. (2021), SFINCS (Super-Fast INundation of CoastS) is a reduced-physics solver which uses simplified versions of the shallow water equations. The main goal for its development was to lower computational costs while keeping its accuracy similar to a model using the full shallow water equations such as Delft-3D. The model is meant to model compound flooding in coastal areas, and thus takes into account various flooding drivers, including fluvial, pluvial, tidal processes (Eilander, Couasnon, Leijnse, et al., 2022a; Eilander, Couasnon, Leijnse, et al., 2022b; Eilander, Couasnon, Sperna Weiland, et al., 2022; Leijnse et al., 2021).

SFINCS has two main benefits for the purpose of this research. First off, it fits the proposed case in New Zealand well. It covers compound flooding for coasts, and due to SFINCS's open-source, open-access nature it can be used in potential further research in the area. Second, its runtime is a lot quicker than full-process solvers. To give an indication of its runtime, for another case modeling a compound storm-tide and rainfall event, it had a reduction of a factor of 100 compared to the structured full-physics Delft3D model while maintaining similar accuracy (Eilander, Couasnon, Leijnse, et al., 2022a; Eilander, Leijnse, & Winsemius, 2022; Leijnse et al., 2021).

3.4   Model configuration

This section builds on the previous sections by explaining the configurations for both models. This starts with a description of the computational specifications and the data used for each model. After this, both models are explored based on the schematizations of the model domain, model boundaries and forcing, water level calculations, and outputs.

3.4.1 Computational specifications and data use

Both models were run from a home laptop, which is an Acer Swift 5 Pro SF514-55T-77BX. This laptop has an Intel Core i7 processor with 4 cores and 16 GB of RAM. The models themselves were built using Python using the same (global) data when possible, although SFINCS includes more data sources. More information on the way the datasets were used can be found in Sections 3.4.2 and 3.4.3 respectively as well as in Appendix C for FLORES and Appendix D for SFINCS.

FLORES

QGIS 3.22.11 is a gis program used to pre-process and post-process some of the data for FLORES. The main functions were to define the watershed and subbasins, calculate their volumetric curves, and define border heights. The collection of python packages can be found at https://github.com/xan-source/FLORES_Helensville.git.

Data necessary for FLORES was the elevation map from Auckland Council and (LINZ) (2020) and, to a lesser extent, the land use data from Landcare Research (2021). The land use data was not used directly, but rather to estimate values such as water retention.

SFINCS

The SFINCS model was built in Python using the Hydromt-SFINCS plugin developed by Eilander, Couasnon, Leijnse, et al. (2022a). The exact version of this and its dependent python packages can be found in the requirements.txt in the github linked to this project. To run the model itself, an executable for SFINCS was also needed for which the Blockhaus executable (v2.0.2) was used. No pre- or post-processing was necessary for the data used for the SFINCS model. The collection of python packages used to set up the virtual environment can be found at https://github.com/xan-source/SFINCS_helensville.git.

Although similarly to FLORES, SFINCS can be run using only an elevation map of the region, this can be supplemented using global datasets for more detailed information. SFINCS uses a digital elevation model of the region from Auckland Council and (LINZ) (2020), bathymetry data from J. Mitchell et al. (2012), and a rivers shapefile from Lin et al. (2019) to schematize the region. Next to this, infiltration data from Jaafar and Ahmad (2019) is used. The land cover dataset from Landcare Research (2021) is also used, although only to differentiate between land and sea for different locations.

3.4.2 Configuration of Flood Risk Reduction Evaluation and Screening model (FLORES)

Model domain

The model domain for FLORES is schematized as subbasins with borders between them. These are input into the Python model using .csv files. These files are created using pre-processing in QGIS of the elevation map from Auckland Council and (LINZ) (2020). Following the pre-processing steps below, which are also outlined by van Berchum (2019), lead to the schematization of the model domain as found in Figure 3.4.

Figure 3.4: Subbasin schematization for the Kaipara river basin. Flow outside the model domain is schematized as basin 0.

The pre-processing steps involve three key steps. First, the model domain, in this case the Kaipara river basin, is divided up into subbasins based on a minimum size threshold. Second, these subbasins are all divided up into contours. Using the total area of each contour, volume-depth curves can be constructed as can be seen in Figure 3.5. Third, additional information is added for each basin. This includes the elevations of the borders, surface water retention, and infiltration.
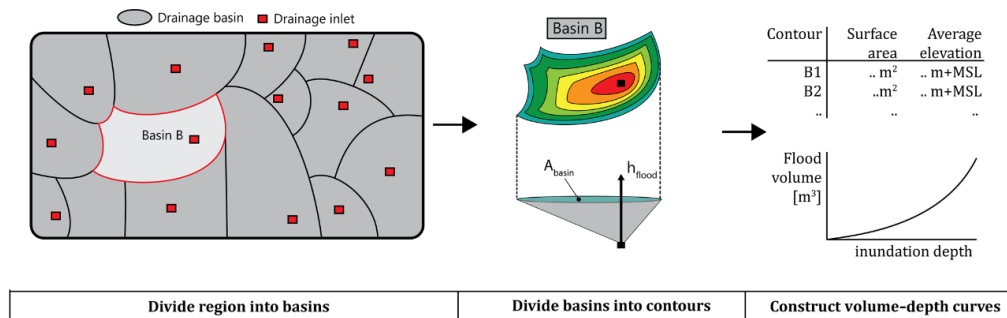
Figure 3.5: Steps from left to right in creating volumetric curves for each of the subbasins in the FLORES model (van Berchum et al., 2020)

This additional information was derived as follows. For the original FLORES model, where the model domain was relatively flat, the border elevation was defined as the mean of the lowest 25% of the border between two basins. For this research, due to the much larger elevation differences this was redefined to the lowest 10%. The surface water retention, similarly to the original FLORES model, is defined as the amount of surface water on the land use map from Landcare Research (2021) for each subbasin. Infiltration is assumed to be constant throughout the model domain, also similar to the original FLORES model.

Model boundaries and forcing

FLORES is forced by rainfall and storm-tide. The rainfall is modeled as an individual inflow for each subbasin per timestep. The storm-tide is modeled as a time series of water levels, which flow into basin 1 based on the equations for the lines of defense. From basin 1, the storm-tide then flows further to other basins based on the hydrological balance.

The lines of defense used in the FLORES model dampen the effects of the storm-tide. Similar effects are also present when the water level within the model domain is higher than the outside water level. If no lines of defense are present such as for the Helensville case, there are two main ways used to calculate inflow into the model domain, which are kept the same as the original FLORES model and can also be seen in Figure 3.6. In the case of flow over land, the coast is modeled as a broad weir. In the case of flow through a river, open channel flow is assumed. Further explanation on the formulas used for this can be found in Appendix C.
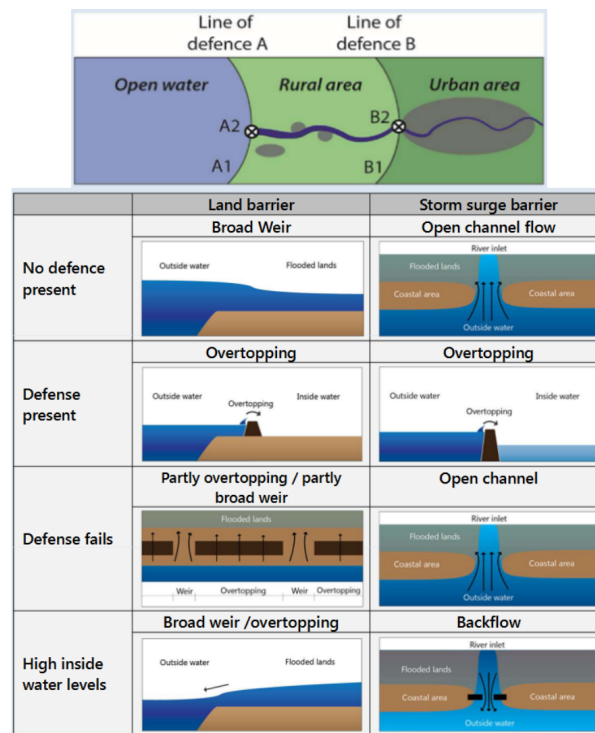
Figure 3.6: Lines of defense from van Berchum (2019)

Water level calculation

FLORES uses a simple hydrological balance to calculate the water levels at each timestep for each basin for the storm's duration. As mentioned before, the storm duration is 24 hours. The timestep chosen was 0.1 hours, or 6 minute increments. While very simplified compared to 2D models, processes like infiltration, drainage, retention, and flood attenuation due to a line of defense are still taken into account. The different variables that can be found here are explained based on van Berchum et al. (2020).

Hydrological balance
$$V_i = V_{i-1} + (Q_{r,i} + Q_{s,i} + Q_{fi,i} + Q_{di,i} - Q_{in,i} - Q_{rt,i} - Q_{do,i} - Q_{fo,i}) * t$$

General:

- V_i: water volume in a basin for time step i

- Q_{rt}: the retention of the basin due to surface water. If the capacity for a basin is reached, the basin starts to flood.

- t: the length of the time step

Inflows:

- Q_r: Inflow due to the total rainfall in the basin

- Q_s: Inflow due to storm surge passing the lines of defense for the basin

- Q_{fi}: Inflow from neighboring basins due to filling and spilling in the last timestep

- Q_{di}: Inflow due to drainage from upstream basins in the last timestep

Outflows:

- Q_{in}: Outflow due to infiltration for the basin

- Q_{do}**:** Outflow due to drainage for the basin. This becomes inflow for the basins it drains to in the next timestep

- Q_{fo}**:** Outflow of surface flow towards neighboring basins due to filling and spilling. This becomes inflow for those basins in the next timestep

Filling and spilling

The process behind Q_{fi} and Q_{fo} is filling and spilling, which is the main way water flows between different subbasins. Filling happens when the inflows exceed the outflows for a basin, which means the basin slowly fills up. Spilling occurs when the water level in a basin reaches the boundary level of an adjacent basin and the extra water starts spilling into this adjacent basin (Lhomme et al., 2008; Shen et al., 2016; Teng et al., 2017; van Berchum, 2019). The FLORES model conceptualizes a basin as seen in figure 3.7b, and follows the steps in figure 3.7a to model the redistribution of water between all basins where the water spills.
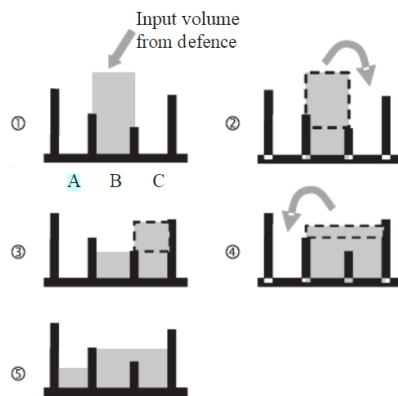
(a) Steps in filling and spilling process (Lhomme et al., 2008)
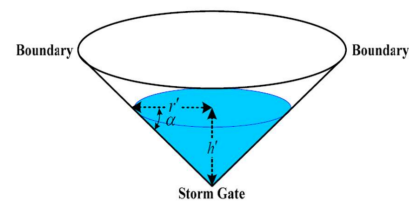
(b) The filling conceptualization for a basin in the NSRIM (Shen et al., 2016)

Figure 3.7: Filling and spilling conceptualization for a rapid flood spreading model such as FLORES. Subfigure 3.7a shows the process behind the transfer of water volumes betweens basins, and subfigure 3.7b shows the way a basin is conceptualized to fill up.

Outputs

FLORES calculates the value of each variable in the hydrological balance for the entire storm duration. Both the global sensitivity analysis and scenario discovery use integers rather than time-series, so the outputs will represent the peak inundation. The outputs of the model will be the maximum absolute water levels reached for each subbasin.

3.4.3 Super-Fast INundation of CoastS (SFINCS)

Model domain

SFINCS schematizes the model domain using an equidistant rectilinear grid in UTM coordinates. After defining this model grid, a maskfile is created to define the purpose of each gridcell within it. This can be seen in Figure 3.8b. Active maskcells are calculated, inactive maskcells are not. Boundary maskcells are those where the boundary conditions are implemented. Lastly, the outflow maskcells show where outflows from the model grid are possible (Eilander, Leijnse, & Winsemius, 2022).

The model domain for SFINCS can be seen in Figure 3.9. While the grid is rectangular, the model domain for SFINCS also encompasses the entire Kaipara river basin, similarly to FLORES. For this research, this grid is 800 by 400 cells with a resolution of 50 meters in both directions. The mask is given by -2 meters NZVD2016. This means that all points within the model grid above this elevation are defined as active cells.

The roughness of the model domain is split up into three parts. The first is 'sea', which is set at a manning number of 0.04 when the elevation of a grid point is below the mean sea level. The second is 'land', which is set at 0.02 when the elevation of a grid point is above mean sea level. Lastly, 'river' is set at 0.03 at points

above mean sea level where said river is burned into the model domain using a shapefile of the river line with a certain width.
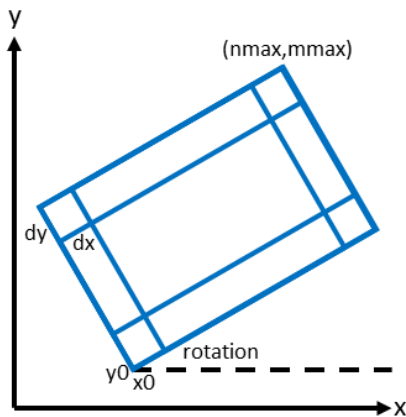
(a) How to define a model grid (Leijnse, 2023). dx and dy are both 50 meters for this research.
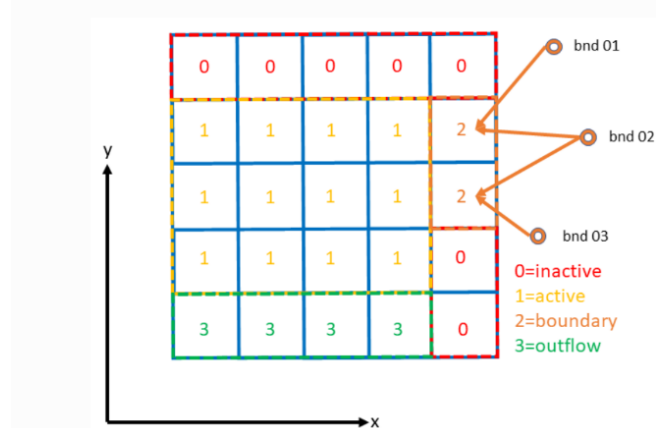
(b) Definitions of the mask file and boundary conditions used to defince every grid cell (Leijnse, 2023)

Figure 3.8: Region layout in SFINCS. First a model grid is defined as seen in subfigure a, then a mask file is used to define the role of every grid cell as seen in subfigure b
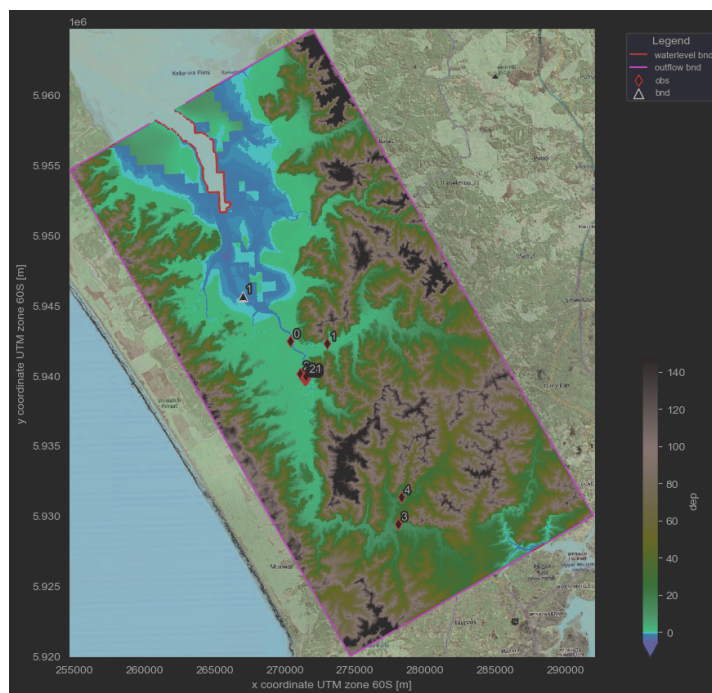
Figure 3.9: Map of the SFINCS set up, including waterlevel boundaries, active cells, inactive cells, and outflow boundaries. The map is set up using the steps in Figure 3.8

Model boundaries and forcing

Rainfall is forced for each active gridcell per timestep for the entire model domain, and is set up using a time-series.

The storm-tide is forced at the boundary 'bnd' point marked as 1 in Figure 3.9, similarly to the 'bnd 01', 'bnd 02', and 'bnd 03' points in Figure 3.8b. The location of this 'bnd' point was taken to be at a similar location to that of the FLORES model.

This forcing point is interpolated to the waterlevel boundary (mask cell 2). This boundary is given at -1.5 meters NZVD2016, making sure only active mask cells are used. SFINCS uses a weakly reflecting water level boundary. Water levels at the boundary cells, which are the red cells found in figure 3.9 are slowly varying, which is the case for tides.

Water level calculations

As mentioned before, the water level calculations are done using the local inertial equations. The numerical discretization for this can be found in Appendix D. To calculate the fluxes, water levels, and water depths for each gridcell SFINCS uses the Arakawa C-grid which can be seen in Figure D.1. This scheme has a history of being used in coastal modeling, being used in about 85% of shallow water models, including Delft-3D as well (De Goede, 2020; Gibson et al., 2002).

Forcing is implemented as a timeseries for the 24 hour storm with increments of 0.1 hours or six minutes, similar to FLORES. The timestep for which SFINCS calculates the water levels is determined dynamically within SFINCS to adhere to the CFL-condition, however (Leijnse et al., 2021).

Outputs

The output of SFINCS is a map or animation of the flooding extent and depth. This can be done for both water level and water depth. SFINCS has an additional option to include observation points ('obs' in Figure 3.9). These points calculate the evolution of the water level through time. Similarly to FLORES, the maximum absolute water levels reached for each observation point were calculated.

3.5 Calibration and validation

This section describes the calibration and validation of SFINCS and FLORES. This is done in three parts. First, both models are calibrated. Second, both models are validated based on the calculated inundation depth and extent for a storm-tide event, and for the addition of a rainfall event. The last part concludes the calibration and validation to discuss whether the models are useful for their intended goal.

3.5.1 Calibration

It was not feasible to calibrate FLORES and SFINCS using the same events that were used to calibrate the previous models discussed in Section 2.2.4. This had different reasons. The 2013 study using the bathtub method calibrated the model for extreme water levels measured at Pouto point, which is at the mouth of the Kaipara harbour and far outside the model domain in this case. The 2016 study using the MIKE21 model calibrated the model using the extreme water levels at the Helensville tidal gauge. This required building a second model that did not take into account any of the floodplains (Stephens et al., 2016). Creating a second model is not feasible within the timescale of this project however.

Even though both these previous models were calibrated for different events and show very different inundation depth and extent in the upstream part of the basin, the behavior in the lower part of the basin is similar as can be seen in Figure 2.9. This is why it was chosen to calibrate the FLORES and SFINCS for a maximum storm-tide of 3.0 meters at the most downstream part of the basin, which is the same for both the 2013 and 2016 studies. A storm-tide of 3.0 meters aligns with a 1%AEP flood as calculated by Stephens et al. (2016).

The storm-tide boundary was split into three parts for FLORES and SFINCS, as can also be seen in Figure 3.3: the tidal amplitude, the mean sea level, and the storm surge. The calibration was done for both FLORES and SFINCS using an offset of -0.13 mean sea level to account for the NZVD-16 vertical datum, a rainfall intensity of 0, and a tidal amplitude of 1.9 meters, which is the MHWPS tide at the helensville gauge. The estimated storm surge for a 100 year ARI was very uncertain as mentioned earlier, with a 95% confidence range, between 0.66 and 2.7 meters (Stephens et al., 2020; Stephens et al., 2016). Using these values and varying the storm surge, for both FLORES and SFINCS a storm surge of 1.3 meters, which is well within the confidence bounds, was necessary to get a water level of 3.0 meters.

(a) Inundation level and extent for a 1%AEP storm-tide for the 2013 study using the bathtub method

(b) Inundation level and extent for a 1%AEP storm-tide for the 2016 study using the MIKE21 model
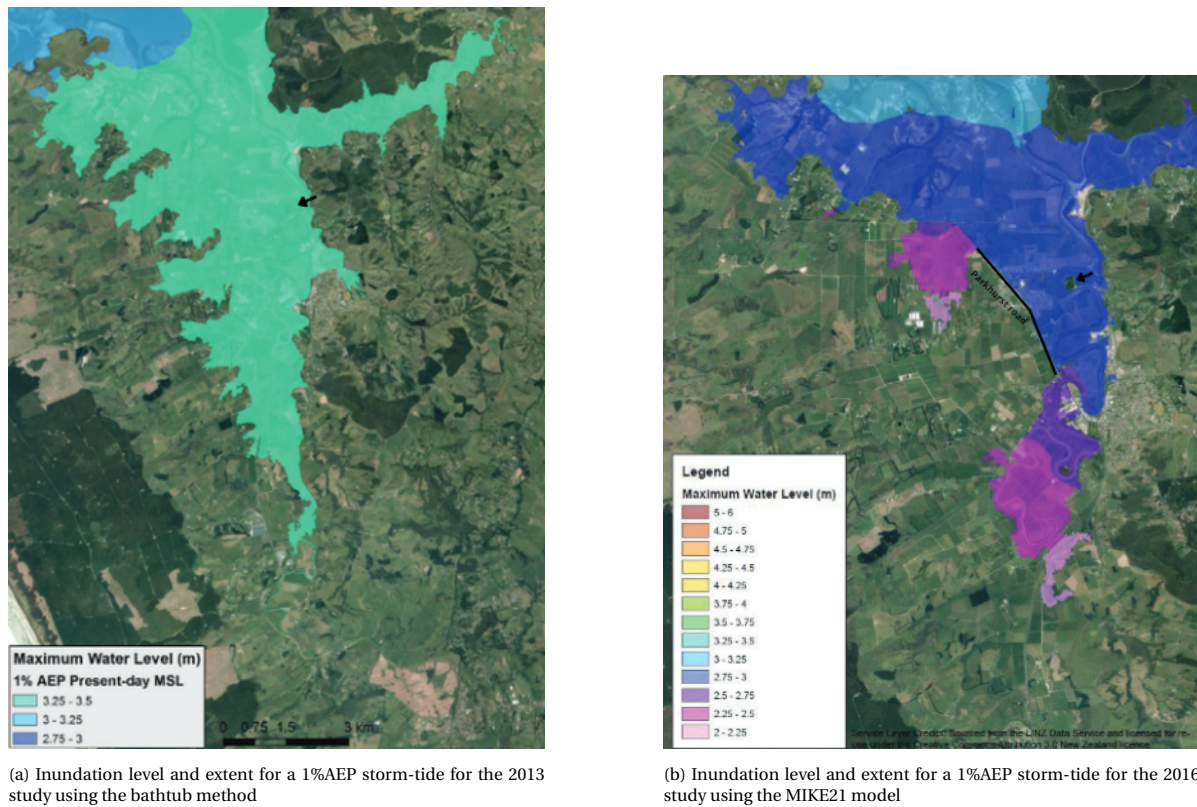
Figure 3.10: Inundation level and extent from 2013 and 2016 studies described earlier in Section 2.2.4. Arrows indicate the location of the wastewater treatment plant, and the MIKE21 plot on the right also shows Parkhurst road. Note that length scales are not the same for these two plots (Stephens et al., 2016).

3.5.2   Validation storm-tide

After calibration, both SFINCS and FLORES were validated for a storm-tide event by comparing them against the inundation extent and depth of each other, and of the MIKE21 model study done previously. Both SFINCS and FLORES were forced by a -0.13 meters mean sea level, a tidal amplitude of 1.9 meters, and a storm surge of 1.3 meters.

(a) FLORES inundation level and extent for 1%AEP storm-tide

(b) SFINCS inundation level and extent for 1%AEP storm-tide
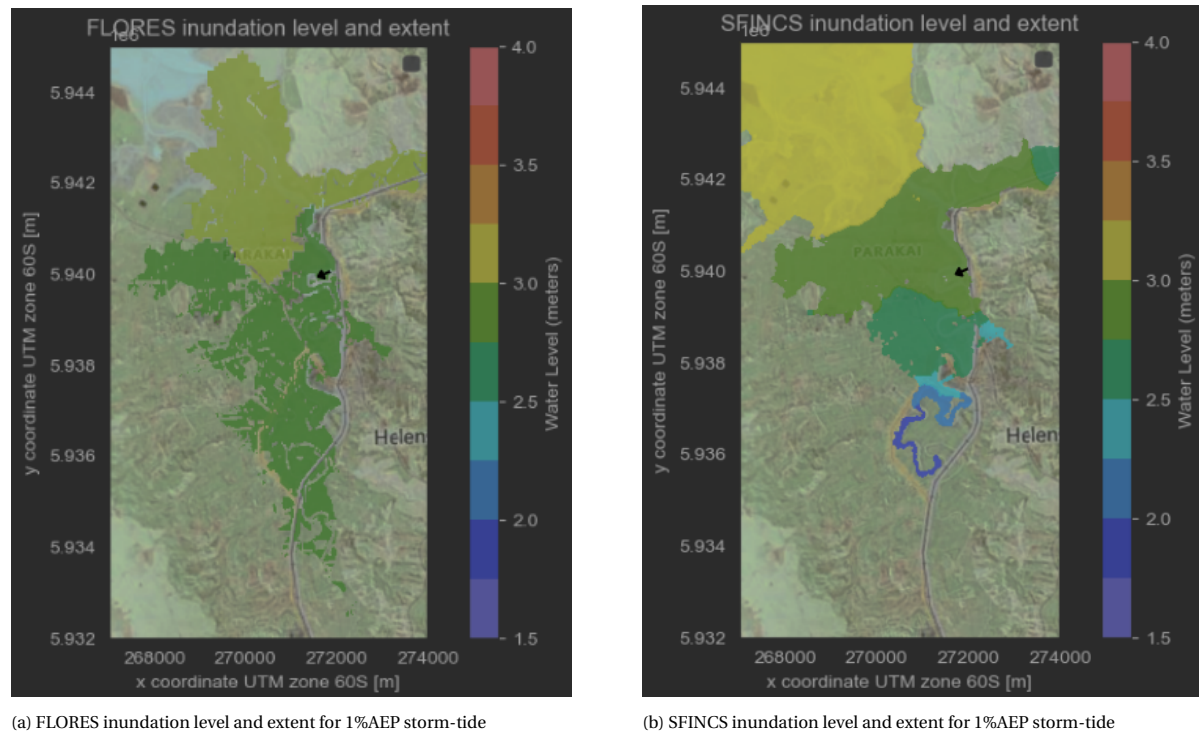
Figure 3.11: Inundation levels and extent for a 1%AEP storm-tide for both the SFINCS and FLORES models. The arrow demarcates the location of the wastewater treatment plant. SFINCS has a value of 2.8 meters here, while FLORES has a value of 2.98 meters.

SFINCS

At the downstream part of the model domain, inundation levels are similar between SFINCS, MIKE21, and FLORES. This can be expected due to the calibration being for a similar storm-tide here. For the upstream part inundation depths are most similar to the MIKE21 model, since SFINCS also accounts for the attenuation of the flood wave across the floodplain, something not seen in either the bathtub model or FLORES which can be seen in Figures 3.10a and 3.11a. SFINCS gives a maximum water level at the wastewater treatment plant of 2.8 meters.

Differences of inundation extent between MIKE21 and SFINCS are most likely due to the inclusion of stop-banks for the MIKE21 model, as explained in Section 3.5.1. These stopbanks lead to the flooding being more contained to areas adjoining the river. Compared to the MIKE21 model, SFINCS overestimates the flooding extent. This is most likely due to the absence of local features like Parkhurst road, which influence flow dynamics. Parkhurst road strems the flow in the MIKE21 model, which is not the case for the other models. The absence of this road can be explained by the grid used. The MIKE21 model was very detailed, and used a flexible mesh. Compared to this, the SFINCS model is less detailed in order to facilitate a quick enough runtime, using a rectangular grid of 50x50 meters.

FLORES

The results of FLORES were post-processed in a similar manner to the bathtub method. For each subbasin, the maximum water level was calculated in Python, and an elevation map for each subbasin was intersected with this water level in QGIS. The map with these results was plotted in Python using the same format as for SFINCS, resulting in Figure 3.11. The similar post-processing leads the inundation extent for FLORES to look similar to that of the bathtub method found in Figure 3.10a. Comparable to the the 2013 study, FLORES over-estimates inundation depth and extent in the upstream part of the basin, since attenuation of the flooding is not explicitly taken into account. This is in contrast to MIKE21 and SFINCS, which do show this.

FLORES reasonably estimates flooding extent and depth compared to SFINCS in the rest of the model domain as can be seen in Figure 3.12. Differences in the downstream part of the domain are due to the smaller model domain for FLORES compared to SFINCS. This smaller model domain does not seem to affect flooding extent

or depth in the rest of the basin, however. Inundation depth at the location of the wastewater treatment plant is similar for SFINCS, MIKE21 and FLORES.
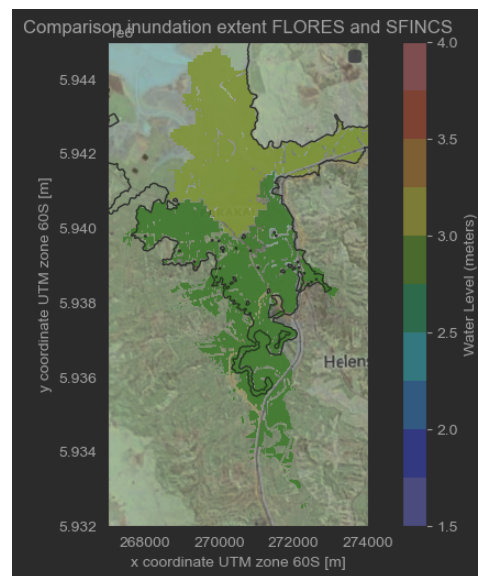
Figure 3.12: SFINCS inundation extent overlayed on the FLORES inundation map. This is reasonably similar at the downstream end, but varies significantly in the upstream end.

3.5.3   Validation rainfall

While no events exist to validate the compound flooding due to storm-tide and pluvial flooding, the MIKE21 model was run with a combination of a 50 year ARI storm-tide and 50 year ARI river flow, which can be seen in Figure 3.13. As discussed in Section 3.2, it is assumed that river flows are mostly due to drainage of rainfall falling in the Kaipara river basin. For the location of the wastewater treatment plant, the effect of this was around an additional 20 centimeters of inundation depth. The effect of this added river flow was more pronounced upstream, however, showing that including the effects of rainfall could potentially be significant.

Comparing the results of both FLORES and SFINCS for the same boundary conditions can also give some insight. The difference in water level from a combination of a 100 year ARI rainfall event combined with a 100 year ARI storm-tide can be seen in Figure 3.14. Compared to the water level from just the storm-tide, as shown in Figure 3.11, the effect of the added rainfall only has a small influence. The max water levels in the basins for FLORES are increased by a couple of centimeters, and for SFINCS inundation extent and depth is changed slightly. Notably, the distribution of the differences in water level are similar between FLORES and SFINCS.

There does seem to be a significant difference between the effects of a 100 year ARI precipitation as used in this research and the 50 year ARI river flow as used for the MIKE21 model, especially in the upstream part of the model domain. This could be due to a number of things. Most importantly, forcing a river flow assumes a constant discharge, while for rainfall the river discharge varies based on the upstream area assuming spatially and temporally uniform rainfall. This leads to more pronounced effects in the upstream part of the domain where the river flow is overstated, which is less the case when using rainfall. Second, the 50 year ARI river flow was combined with a 50 year ARI storm-tide. Due to the lower value for the storm-tide for MIKE21 compared to FLORES and SFINCS, the added effect of the river flow could be more pronounced. Third, the rainfall for this research was assumed to be spatially and temporally uniform. Using a rainfall peak while keeping the total average 24 hour rainfall the same might lead to a larger inundation extent and depth. Last, there could be other sources of flow in the river.
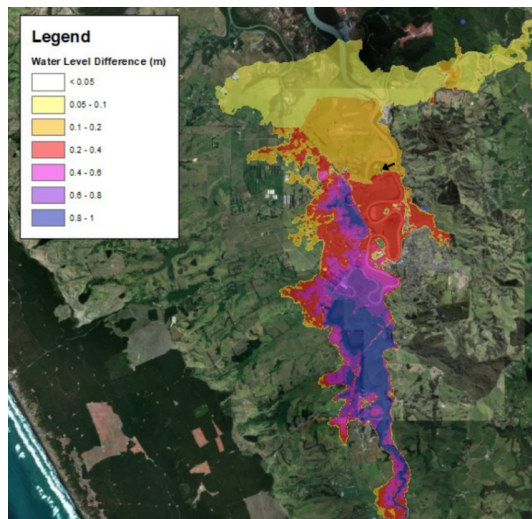
Figure 3.13: Water level difference when adding a 50 year ARI river flow to a 50 year ARI storm-tide for the MIKE21 study. At the location of the wastewater treatment plant, this difference is around 20 centimeters (Stephens et al., 2016)
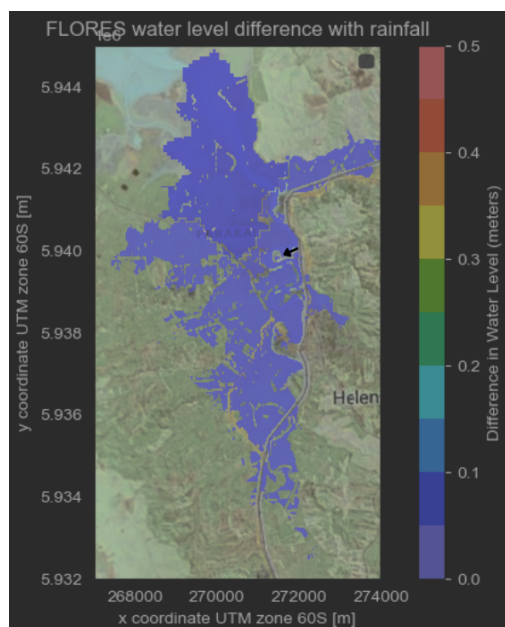
(a) Water level difference for FLORES when adding a 100 year ARI 24 hour rainfall event to a 100 year ARI storm-tide
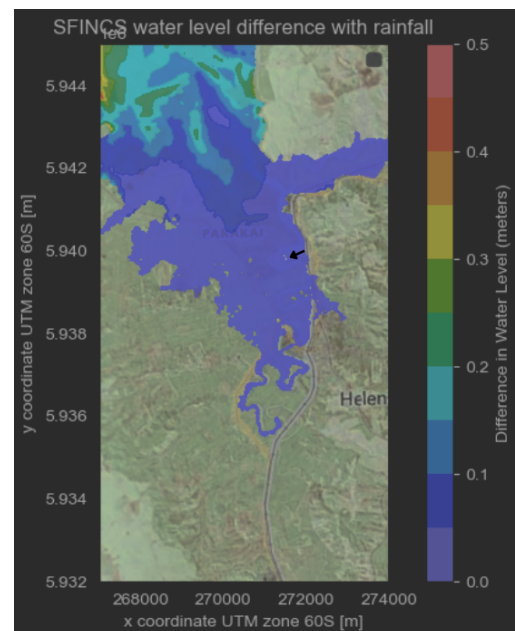
(b) Water level difference for SFINCS when adding a 100 year ARI 24 hour rainfall event to a 100 year ARI storm-tide

Figure 3.14: Maps of the water level difference when adding a 1%AEP rainfall event to a 1%AEP storm-tide for FLORES and SFINCS. The black arrows denote the location of the wastewater treatment plant. Both figures show the same general distribution of water level differences due to rainfall.

3.5.4 Conclusion of calibration and validation

FLORES and SFINCS will both be forced for combination of extreme storm-tides and rainfall. To facilitate this, both models were validated against previous studies exploring flooding due to extreme storm-tides. Compared to the MIKE21 model, SFINCS gave similar water levels, at around 2.75-3 meters with an average of 2.80 meters at the wastewater treatment plant. FLORES slightly overestimated the water level, at around 2.98 meters for subbasin 4. The bathtub model further overestimated this water level, giving 3.25-3.5 meters.

The main differences between FLORES and SFINCS seem to be driven by the flood attenuation included for SFINCS. While flooding extent and depth are similar downstream, the lack of this process leads to overesti-

mation of the water level at the wastewater treatment plant and an overestimation of inundation extent and depth further upstream as can be seen in Figures 3.11 and 3.12.

Both FLORES and SFINCS also show similar effects when adding rainfall. While there is a significant difference between the inclusion of a river flow and that of a rainfall, the effects of the additional rainfall seem to be similar for FLORES and SFINCS, allowing for their comparison.

Overall, both models show relatively similar magnitudes of flooding extent and depth for both a storm-tide event and a rainfall event. While FLORES slightly overestimates inundation level and extent for a storm-tide event, the behavior overall is generally similar. Additionally, the encountered differences can be explained. This leads to reason that both models are reasonably able to model the behavior of the system and water levels at the wastewater treatment plant, and comparison between the two models is possible.

3.6   Vulnerability analysis configuration

This section will describe the configuration of the vulnerability analysis, which consists of the scenario discovery and the global sensitivity analysis. Both of these will be run using the same uncertainties described in the following sections. The global sensitivity analysis will be run for points throughout the model domain in order to compare behavior of the models as well. The scenario discovery will be run using just the water level at the wastewater treatment plant.

While the vulnerability analysis done through robust decision making is an iterative process, for this research only the first iteration will be done. Finding the vulnerabilities for the status quo is also the first step undertaken for robust decision making, and should give insight into the way both models differ in their results.

3.6.1   Outputs taken into account

As mentioned before in Sections 3.4.2 and 3.4.3, the calculated outputs are the maximum water levels for the storm duration. In order to compare behavior between SFINCS and FLORES, observation points were added for SFINCS in similar locations to the FLORES subbasins. These observation points can be seen in Figure 3.16.

The scenario discovery is run for the maximum water level at the wastewater treatment plant. This is subbasin 4 in the case of FLORES, and for the avgWTP as defined in Figure 3.15 in the case of SFINCS.
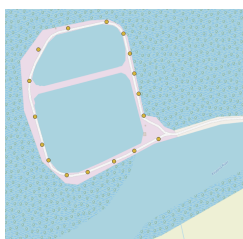
Figure 3.15: The way the observation points are placed around the wastewater treatment plant embankments. These observation points lead to two outputs: avgWTP and maxWTP. AvgWTP is the average of the maximum water level observed by the points, while maxWTP is the maximum of their maximum water levels.

The global sensitivity analysis is run using the maximum water level for each basin in the case of FLORES, and for observation points 0 through 4, as well as for the avgWTP as defined in the case of SFINCS. These points can be seen in Figure 3.16.
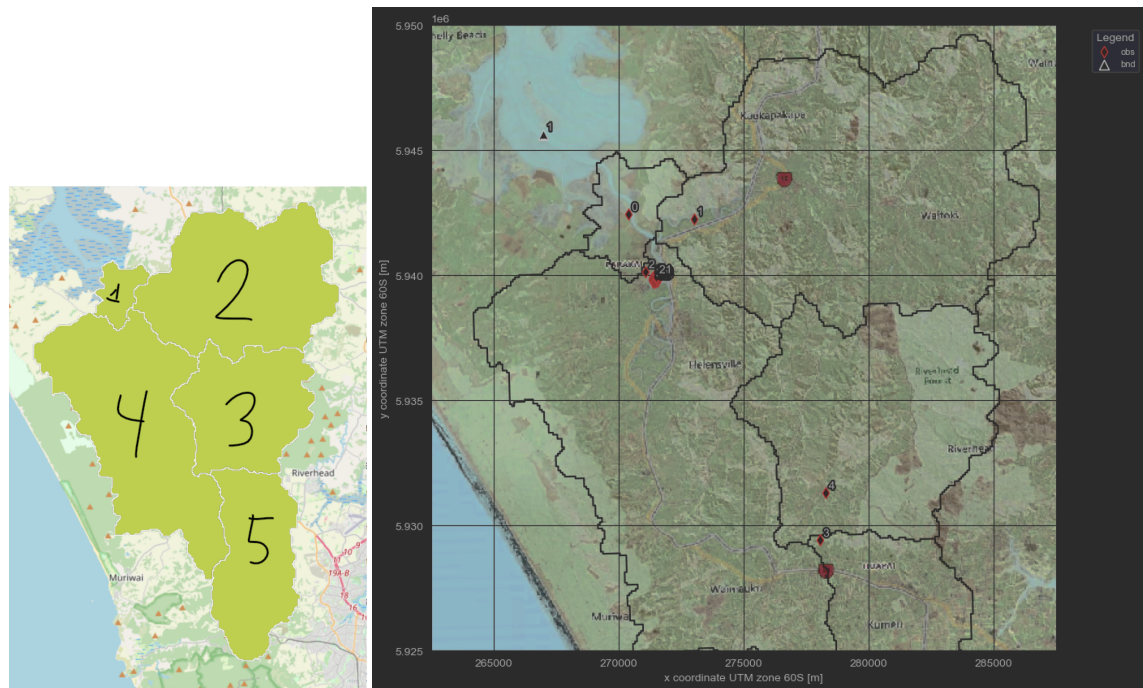
Figure 3.16: Locations of observation points for SFINCS compared to FLORES. On the left are the subbasins for the FLORES model, and on the right are the observation points for SFINCS with an overlay of the FLORES subbasins.

3.6.2 Uncertainties taken into account

When conducting a sensitivity analysis it is important the ranges of the chosen uncertainties are relatively representative, as otherwise the results can be skewed. This is less of a factor for the scenario discovery, since the focus is on identifying specific scenarios that lead to particular outcomes, so the emphasis is on exploring the uncertainty space rather than quantifying the overall sensitivity to uncertainties. Next to the forcing uncertainties, there are also uncertainties in the modeling choices. These model uncertainties are explained further in the coming subsections.

The ranges chosen for each uncertainty can be found in Table 3.1 with an explanation as to why these values were chosen. For the forcings, a timescale of around 100 years was chosen. More in depth explanations on these can mostly be found in previous sections, including Section 2.2.

FLORES model uncertainties

Two modeling choices that present additional uncertainty are the infiltration rate chosen, and the boundary heights, which will be explained in the next paragraphs. Some other model choices were not looked at, as it would mean altering the model in a significant way in order to test their sensitivity which was not possible due to time constraints. The three biggest include the number of basins chosen, the formulas that were used for the lines of defense, and the shape of the rainfall (i.e. using a rainfall peak while keeping the average rain intensity over 24 hours the same).

From the geological inspection done earlier in Section 2.2 and supplemented by Appendix B, it can be seen the soil distribution for the Kaipara river watershed is mostly loamy clay and sandy loam, with smaller sections that have larger or smaller sediment sizes. Finding the right infiltration rate can be especially challenging as the aquifers that run below the top layers of soil have a high transmissivity, and the layer above them consists of smaller deposits with very low transmissivity. Infiltration rates taken into account were between clay loam (5 mm/hour) and sandy loam (20 mm/hour).

The way boundaries between basins were schematized for the original FLORES model was by using the lowest 25% of border heights. However, Beira, where this initial model was tested, is a lot more level than Helensville, where the height differences within the model domain are upwards of 200 meters. This is why the lowest

Uncertainty	Range	Explanation
Storm surge	0 - 1.3 m	Both FLORES and the SFINCS model have been calibrated for 1.3 meters for a 100 ARI storm-tide event
Tidal amplitude	1.5 - 2.3 m	The Kaipara harbour is a dynamic place, with lots of tidal flats and deep channels. This means the tidal amplitude could potentially change in the future. The amplitude at Pouto point, at the mouth of the Kaipara harbour, for the highest astronomical tide is around 1.5 meters, and for the Helensville tidal gauge this is 2.3 meters.
Mean sea level	-0.13 - 1.05 m	Currently, the mean sea level is currently at -0.13 meters NZVD2016. Taking into account current sea level projections for New Zealand, this could rise to 1.05 by 2100 (Tonkin+Taylor, 2021).
Rain intensity	0 - 8.6 mm/hour	The rain intensity is in mm/hour. A 100 year ARI rainfall event is 8.6 mm/hour for a 24 hour event in the Auckland region.
Infiltration rate (FLORES)	5 - 20 mm/hour	From geological inspection in Appendix B, it can be seen the soil distribution for the Kaipara river watershed is mostly loamy clay and sandy loam, with smaller parts that have potentially larger or smaller sediment sizes.
Border heights (FLORES)	10% or 25%	To calculate the border heights, the average of the lowest 10% of the border was calculated since the topography of the basin is steep. In the original research by van Berchum (2019), however, the average of the lowest 25% was used.
Roughness river (SFINCS)	0.02 - 0.04	The manning's values selected were based on those suggested in the SFINCS manual, combined with extra info from Chow (2009).
Roughness sea (SFINCS)	0.01 - 0.03	The manning's values selected were based on those suggested in the SFINCS manual, combined with extra info from Chow (2009).
Roughness land (SFINCS)	0.03 - 0.05	The manning's values selected were based on those suggested in the SFINCS manual, combined with extra info from Chow (2009).

Table 3.1: Inputs for the global sensitivity analysis and the scenario discovery.

10% of the border heights was used for this research. Experiments for both border heights using the same uncertainty ranges were done, to investigate the effect of this choice.

SFINCS model sensitivities

One potentially important process also mentioned by Stephens et al. (2016) is the effect on roughnesses due to increases in MSL. This process is also included in SFINCS. If MSL increases, more of the model domain is labeled as "sea", which has a lower roughness which in turn leads to less flood attenuation. A similar process happens when the Kaipara river becomes larger. This is why the main model sensitivities taken into account were the influence of the various roughnesses on the calculated water levels. The manning's values taken were based on the suggested values in the SFINCS manual combined with extra info from Chow (2009).

Some extra model uncertainties that could be looked at for SFINCS are the location of the forcing boundary, the effects of the chosen grid size, the width of the river, and the quality of the provided elevation and bathymetry data set. These likely have at least some effect, but due to time constraints they could not be investigated further.

3.6.3   Python implementation

The EMA workbench will be used to run the scenario discovery and global sensitivity analysis in addition to the computational specifications as outlined in Section 3.4.1. The EMA workbench is a Python package that facilitates scenario discovery by sampling through the uncertainty space, analyzing, and visualizing the results. Multiple sampling techniques such as Latin hypercube, Monte Carlo, factorial, and partial factorial sampling, as well as FAST, SOBOL, and MORRIS are all supported for this using the SALib library (Kwakkel, 2017; Usher et al., 2021). The results can then also be easily visualized, through links with seaborn and matplotlib.

In order to save time, both the sensitivity analysis and the scenario discovery were run in one go. This is done by using the SOBOL sampling method to calculate values for both the sensitivity analysis and the scenario discovery. SOBOL uses a quasi-random sampling scheme. Quasi-random sampling improves the distribution of sampled points compared to random sampling by using sequences that achieve a more uniform coverage of the uncertainty space, as also mentioned in Section 2.1.2 (Saltelli et al., 2010).

Chapter 4

Modeling results and comparison

The goal of this chapter is to present the outcomes of the simulations, and to use these to compare FLORES and SFINCS. The chapter starts with Section 4.1, where the correlations and distributions of the outcomes are discussed. Next, Section 4.2 discusses the results of the global sensitivity analysis. Section 4.3 discusses the results of the scenario discovery. Based on this first part of the chapter, Section 4.4 discusses the implications on potential policy advice. The chapter ends with a comparison on predicted system behavior and accuracy, identified vulnerabilities, and policy advice in Section 4.5.

4.1 Outcomes

Outcomes are generated by simulating the experiments as described in Section 3.6 outcomes. SFINCS has 4096 outcomes for each output, while FLORES has 6144 outcomes for each output. This section uses these outcomes to describe the correlations between different model outputs, and to describe the distribution of outcomes at the wastewater treatment plant.

4.1.1 Correlations between outputs

Output correlations FLORES

As mentioned before, the outputs for FLORES consist of the maximum water level calculated in each sub-basin for the storm duration. The correlations between the maximum water level in the different basins can be seen in Figure 4.1. The x and y axis give the water level in meters for these subbasins. This water level is quite high for subbasins 3 and 5, due to the way the subbasins are schematized. Since the border height is higher than the lowest part of the subbasin, some water accumulates. For the very steep upper basins, this effect is more pronounced leading to high water levels. As mentioned before, the FLORES model is run with two different border heights to test the sensitivity to this model uncertainty. This doesn't seem to influence correlations, however

Certain subbasins for the FLORES model are perfectly correlated with each other, while being totally un-correlated with other subbasins. This behavior can be seen in figure 4.1. This is most likely due to two main reasons. The first is the filling and spilling mechanism spreading the water between basins that have low boundaries, which is the case for basins 1, 2, and 4. The water levels in these subbasins are thus very similar. The second is similar behavior due to similar forcing, which is the case for basins 3 and 5. As mentioned in the previous paragraph, These two basins are both at the most upstream part of the catchment, and are both almost exclusively influenced by rainfall, leading to strong correlation.
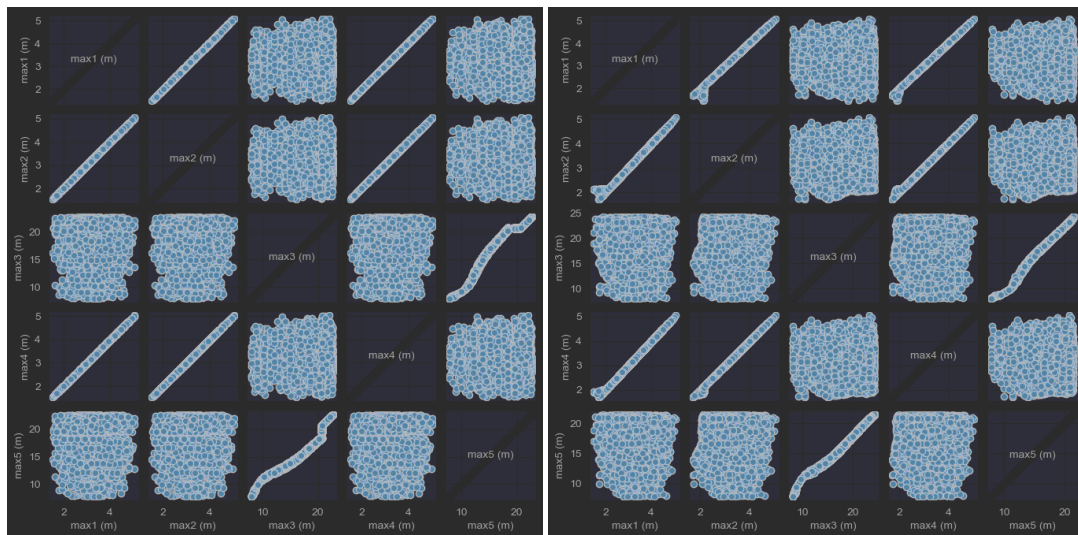
(a) Correlations between the outputs per subbasin when using the lowest 10% of border heights

(b) Correlations between the outputs per subbasin when using the lowest 25% of border heights

Figure 4.1: Correlations between the maximum water levels for different subbasins for the FLORES model. The x and y axis show the water levels in meters.

Output correlations SFINCS

The outputs for SFINCS consist of the maximum water level calculated at various observation points for the duration of the storm. There are also two additional outputs at the wastewater treatment plant: avgWTP and maxWTP. The observation points were placed in similar places to the FLORES subbasins. 'obs0' is placed in subbasin 1, 'obs1' in subbasin 2, 'obs2' in subbasin 4, 'obs3' in subbasin 5, and 'obs4' in subbasin 3. This can also be seen in Figure 3.16. The correlations between these outputs can be found in Figure 4.2.

The correlations in Figure 4.2 for observation points 0 (basin 1), 1 (basin 2), and 2 (basin 4) show a strong correlation to each other, but only after a certain height. This height is the bed level, and correlation only starts once the water level reaches the bed level or higher. These results show points 1 and 2 flood at pretty much the same time, while point 2 only floods when the water level at point 0 reaches 3 meters.

Two interesting points are observation points 3 and 4, which are related to FLORES subbasins 5 and 3 respectively. For these two observation points there are very few outcomes, and they are not correlated with any other observation points. In Figure 4.2, an offset of around 16.6 meters can be seen to account for them being very far upstream. Flooding depths are also extremely small, with the largest being 0.001 meters. These small floodings are most likely due to small calculation errors, where a high rainfall has not yet drained from a grid cell. This can also be seen in the self-correlation plot, where for observation points 3 and 4 almost no points exist. From these results, it can be assumed these two observation points never flood for the forcing described in the previous chapter.

The avgWTP and maxWTP are also correlated with each other. MaxWTP is systematically higher than avgWTP, with correlation only starting at 2.96 meters, which is apparently the highest bed level around the embankments as calculated by SFINCS. AvgWTP is only equal to the maxWTP once the water level reaches above this bed level.

Figure 4.2: Correlations for all different SFINCS outputs. The locations of the observation points can be found in Section 3.6 in Figure 3.16. A vertical line can be seen in the correlation matrix when the water level that floods the observation point on the y axis does not yet flood the observation point on the x axis.

Comparison correlations FLORES and SFINCS

The difference in model structures between FLORES and SFINCS is reflected in the results of the correlations. The biggest reason for this are the differences in schematization of the model domain. FLORES schematizes each subbasin using a volumetric curve where the basin is allowed to fill with water, and only spills to adjacent basins once a certain level is reached. SFINCS uses a numerical grid to model the domain.

For the downstream basins 1, 2, and 4 (observation points 0, 1, and 2 respectively), this shows in an immediate correlation in the case of FLORES since rainfall immediately starts filling up each basins and correlation occurs when the relatively low border heights between basins 1, 2, and 4 are reached. This can also be seen in Subfigure 4.1b, where the border heights are slightly higher and two lines can be seen for the correlation between max1 and max2, for example. When the output is forced by rainfall it is correlated, and when it is not, the line is not (in these cases the line is horizontal or vertical). For the case of SFINCS, rainfall falling in the model domain drains straight away, leading to no correlation until the total water level reaches the bed level of the observation point.

This difference in domains also shows in the upstream basins 3 (observation point 4) and 5 (observation point 3). FLORES shows that these basins can flood, albeit only due to rainfall, while SFINCS shows the observation points linked to these basins never flood.

4.1.2   Outcome distribution at the wastewater treatment plant

Below the calculated water levels at the location of the wastewater treatment plant are discussed. For the FLORES model this corresponds with the maximum water level calculated in basin 4. For SFINCS, there are

two potential outputs called avgWTP and maxWTP.

FLORES

The left boxplot in Figure 4.3 shows the maximum water level outcomes at the wastewater treatment plant have a minimum value of 1.5 meters and a maximum of around 4.5 meters. This is distributed normally, with the middle of the boxplot being almost perfectly in the middle of the graph. The water level where the treatment plant is overtopped, which was set at 3.6 meters in Section 3.2 is reached around 25% of the time. There is almost no discernible difference between the outcomes at the wastewater treatment plant between the two different border heights.
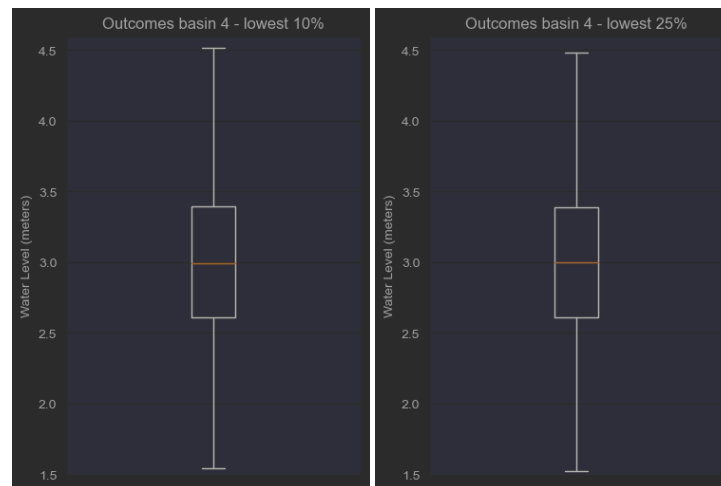
Figure 4.3: Distribution of the calculated water levels for FLORES at the wastewater treatment plant. The left subfigure shows the basin 4 water levels using the average of the lowest 10% of the border heights, the right shows basin 4 water levels using the average of the lowest 25%.

SFINCS

The boxplots in Figure 4.4 show the avgWTP and maxWTP outcomes. As mentioned before, these consist of the mean and the maximum of the maximum water levels found at the observation points around the wastewater treatment plant embankments, which is also explained in Section 3.6. The maxWTP shows a different distribution to the avgWTP by only starting when the water level reaches the highest bed level of the observation points surrounding the embankments, which is at 2.96 meters. This is deemed less complete compared to the avgWTP outcome since it cuts out this lower portion of the results.
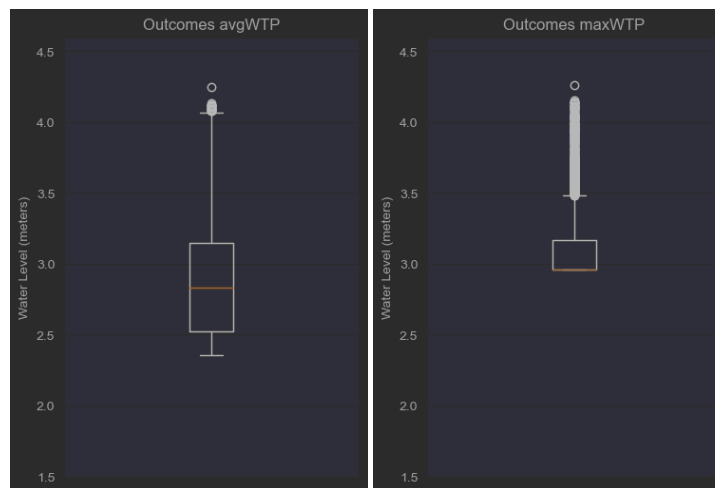
Figure 4.4: Calculated water levels for SFINCS at the wastewater treatment plant. The left subplot shows the avgWTP outcomes, while the right subplot shows the maxWTP outcomes.

Comparison of outcomes FLORES and SFINCS

The SFINCS boxplot which shows the avgWTP outcomes, has a minimum outcome of around 2.25 meters around the wastewater treatment plant, and a maximum of 4.25 meters. This is compared to a minimum outcome of 1.5 meters and a maximum of 4.5 meters for FLORES. There are two main differences when comparing the maximum water levels at the wastewater treatment plant between FLORES and SFINCS. The distribution has a larger range for FLORES, and the mean outcome is higher. This is most likely due to two things, the higher bed level for SFINCS as opposed to basin 4 for FLORES, and the flood attenuation taken into account by SFINCS as opposed to FLORES.

The 'avgWTP' output for SFINCS has a higher bed level than the output for FLORES, since basin 4 for FLORES is larger and already starts downstream of the wastewater treatment plant. The higher bed level affects the minimum outcome that can be seen, as the water level needs to reach at least this level before an outcome is calculated in the case of SFINCS.

The flood attenuation taken into account for SFINCS due to roughness leads to a lower upper bound for the outcomes, and overall lower outcomes. In combination with the higher bed level for SFINCS, this leads to the skewed distribution for SFINCS compared to FLORES.

4.2   Sensitivity analysis

The sensitivity analysis calculates the relative influence of the different uncertainties on the different outputs. These uncertainties are split up into two: model uncertainties and forcing uncertainties. Due to the large number of graphs for the sensitivity analyses, only the main conclusions will be given here, while the graphs themselves can be found in Appendix E. The reasoning behind the chosen model and forcing uncertainties can be found in Section 3.6.

4.2.1   Model uncertainties

FLORES

The two model uncertainties taken into account for FLORES were the infiltration rate and the border heights. From the sensitivity analysis it is clear that the maximum water level is not sensitive at all to the chosen infiltration rate for any of the subbasins. This means that this variable can potentially be left out in future iterations, and the choice of variable here is less important.

Changing the border heights also does not influence the found sensitivities, for either the downstream basins 1, 2, and 4, or the upstream basins 3 and 5. This makes sense, as the upper basins 3 and 5 are not influenced by

the storm-tide in any case. Basins 1, 2, and 4 have very similar border heights when comparing the lowest 10% of the border heights and the lowest 25%. These border heights are quite low, meaning minimal differences in water level would occur since they would most often just flood.

SFINCS

The model uncertainty taken into account were potential changes in roughness of the sea, the river, and the land. From the results of the sensitivity analysis, these have a negligible effect on the maximum water level for most observation points. While the effect of flood attenuation is not negligible as could be seen from the outcome distribution, the ranges chosen for the roughness seem to indicate that small differences in this choice are not relevant.

4.2.2   Forcing uncertainties

FLORES

The forcing sensitivities are very similar for basins 1, 2, and 4, as are those for basins 3 and 5. The water levels in the upstream basins 3 and 5 are almost exclusively sensitive to the rain intensity, showing that the storm-tide does not reach to these basins.

The downstream basins 1, 2, and 4 are mostly sensitive to storm surge and mean sea level. Interestingly enough, the tidal amplitude had less of an effect. This is most likely due to the chosen range being smaller for the tidal amplitude compared to mean sea level and storm surge (0.8 compared to 1.18 and 1.3 meters respectively), and tidal amplitude having less of an effect on high water level in general since it is divided into flood and ebb tides. These downstream basins are also not sensitive at all to the rainfall. This aligns with the findings of the validation, where the added rainfall only led to a couple of extra centimeters of inundation.

SFINCS

Similarly to FLORES the maximum water levels of observation points 3 and 4, which are at the most upstream part of the basin, are almost exclusively responsive to the chosen rainfall intensity.

For the rest of the observation points, the biggest factors influencing behavior are the max surge and mean sea level, with a smaller role for the tidal amplitude. Like FLORES, this is most likely due to the chosen range for the tidal amplitude being smaller.

4.2.3   Sensitivity at the wastewater treatment plant

The graphs in this section show both S1 (first-order sensitivity), and ST (total sensitivity) as well as a confidence bounds. First-order sensitivity measures the direct impact of the variable on the model output, while total sensitivity considers both the direct and indirect effects, including potential second order interactions with other parameters. If the results have fully converged, the sum of all values of ST should add up to 1.

FLORES

The wastewater treatment plant lies in subbasin 4, which is correlated with basins 1 and 2 as shown earlier in this section. These basins are most sensitive to the storm surge and mean sea level, and then to the tidal amplitude which can be seen in Figure 4.5. This is in part due to the smaller range for tidal amplitude, and in part due to the division of tidal amplitude into flood and ebb as described in Section 4.2.2.
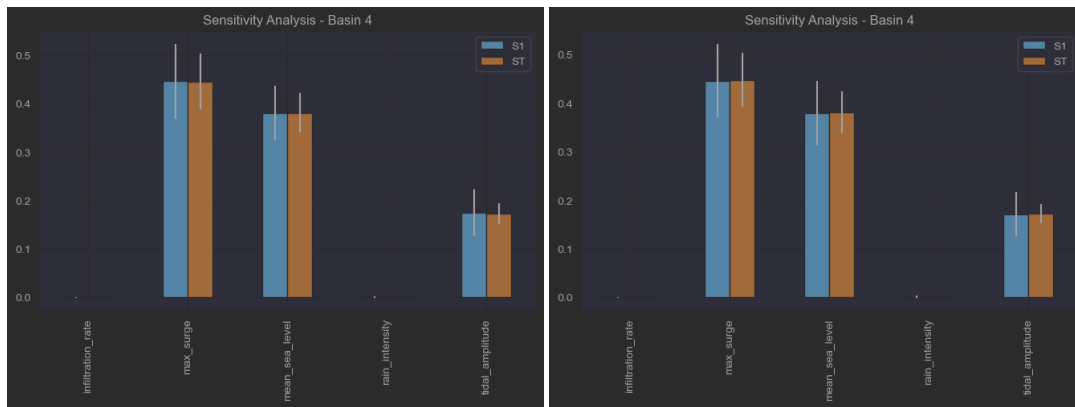
Figure 4.5: Sensitivity analysis for both variations of FLORES: using the lowest 10% and 25% of borders respectively. The y-axis gives the percentage of sensitivity explained by the variable. All sensitivities for all variables should add up to 1. S1 gives the first order sensitivity, while ST gives the total sensitivity. The white line gives the confidence bounds. Explanations on these are given at the start of this subsection.

SFINCS

In order to calculate the sensitivities around the wastewater treatment plant, multiple observation points were placed around its borders, which can be seen in Figure 3.15. For these points, both the maximum and the average of their maximum water levels were calculated as outputs. This is in part to see if the behavior of the sensitivities changes significantly between the two, and in turn whether the "highest high" has similar behavior to the "average high".

The main sensitivities at the wastewater treatment plant are similar to the rest of the observation points in the downstream part of the model domain, and are the same for both maxWTP and avgWTP. The main factors are storm surge and mean sea level, with a lesser role for the tidal amplitude. The reasoning for this is similar to that for the FLORES model. Rainfall and the differing river, sea, and land roughnesses have little to no effect.

Interestingly, Figure 4.6 shows that all values of ST added together of the maxWTP output are higher than 1, with very high confidence bounds. This indicates that the results for this output have not yet converged fully. Currently, the total sensitivities for maxWTP do show very similar behavior to those of avgWTP, however, while the confidence bounds are quite large. This indicates there are simply less outcomes where the uncertainties have an effect for the maxWTP output compared to the avgWTP, something also seen in the outcome distribution at the wastewater treatment plant earlier in this chapter.
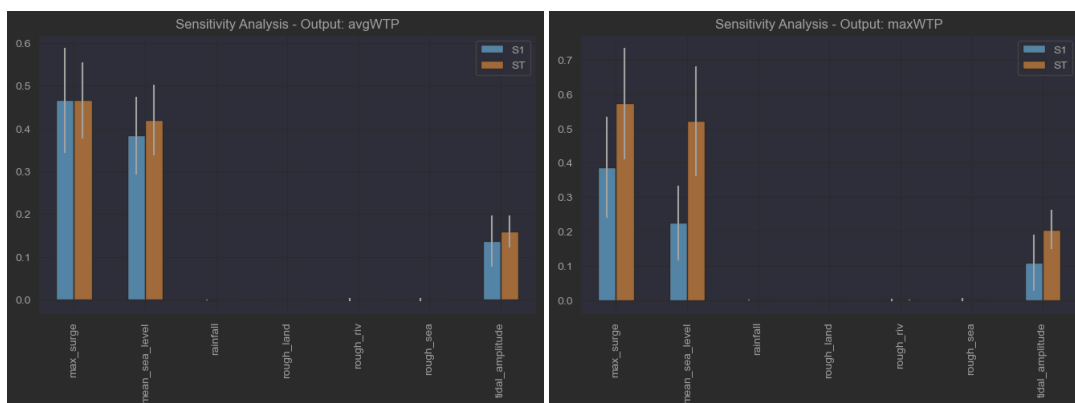
Figure 4.6: Sensitivity analysis for avgWTP and maxWTP. Definitions of these outputs can be found earlier in this chapter or in Section 3.6. The y-axis gives the percentage of sensitivity explained by the variable. All sensitivities for all variables should add up to 1, although due to lack of convergence this can differ slightly. S1 gives the first order sensitivity, while ST gives the total sensitivity. The white line gives the confidence bounds. Explanations on these are given at the start of this subsection.

4.2.4   Comparison sensitivities FLORES and SFINCS

In general, FLORES and SFINCS show very similar sensitivity. In the upstream part of the model domain both models are only sensitive to rainfall, while in the downstream part of the domain they are sensitive to storm surge, mean sea level, and tidal amplitude.

At the location of the wastewater treatment plant, Figure 4.5 shows the sensitivities for FLORES and Figure 4.6 those for SFINCS. The total variability for FLORES was made up for 44.5% of storm surge, 38.2% of mean sea level, and 17.9% of tidal amplitude. For SFINCS, this is 46.6% due to storm surge, 41.9% due to mean sea level, and 16.0% due to tidal amplitude.

The small difference between the sensitivities at the wastewater treatment plant for FLORES and SFINCS mainly consists of less influence of the tidal amplitude on the total variability for SFINCS. This could be due to a number of things. First, the flood attenuation taken into account by SFINCS which was shown earlier to affect the outcomes could have more impact on a more dynamic process such as tidal amplitude compared to mean sea level and storm surge. Second, the results of SFINCS had not converged completely yet, which means small errors could be possible based on the samples chosen, although this is less likely for a quasi-random approach such as SOBOL sampling.

4.3   Scenario discovery

The steps behind the scenario discovery process is further explained in Section 2.1.2. The goal is to find a description of the conditions where failure occurs. Failure in this case is defined when the maximum water level around the wastewater treatment plant is higher than 3.60 meters. The FLORES output used is the maximum water level in basin 4 for the lowest 10% border heights. The SFINCS output used is the avgWTP.

4.3.1   Box selection using the Patient Rule Induction Method (PRIM)

A description of the process behind PRIM is given in Section 2.1.2. The selection of a box is based on coverage and density. As mentioned earlier, coverage is a measure of the percentage of all cases of interest (failure) that fall within a box's thresholds. Density is the percentage of all cases located within a box's thresholds that are of interest. Ideally, both coverage and density are as high as possible. There is always a tradeoff, however. A high coverage often leads to a low density, since the box includes a lot more cases. A high density could lead to a low coverage, where the box misses a lot of the cases of interest.

The results from the PRIM analysis for both FLORES and SFINCS can be found in Figure 4.7. Interestingly, more dimensions need to be restricted for SFINCS compared to FLORES, which indicates there are less total cases of interest for SFINCS. This is further supported by the low density for SFINCS compared to FLORES. This lower density for SFINCS is most likely since less simulations were performed compared to FLORES.

Based on Figure 4.7a, the box chosen for FLORES has a coverage of 73.7%, and a density of 73.3%. This means that 73.7% of all outcomes where failure occurs can be explained by the selected box, and 82% of the outcomes within the selected box are outcomes where failure occurs. To allow for better comparison, the coverage selected for SFINCS is similar to that of the box chosen for FLORES. The box chosen for SFINCS balances a coverage of 73.2% with a density of 74.2%.

(a) Coverage density tradeoffs for FLORES   (b) Coverage density tradeoffs for SFINCS
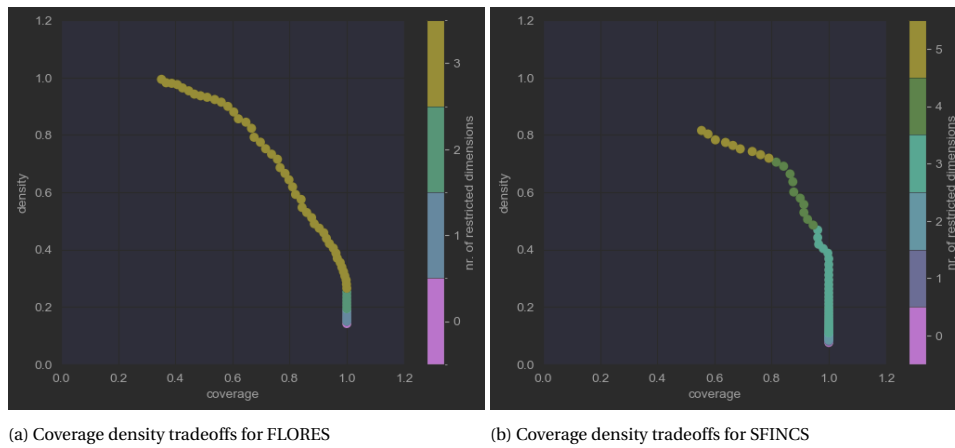
Figure 4.7: PRIM results for both models. The graphs show the tradeoffs between coverage and density for a maximum water level greater than 3.60 meters. This is done for the max water level in basin 4 for FLORES, and for the output avgWTP for SFINCS. Each point on the graph represents a potential box. The legend shows the number of restrictions, this is how many variables are taken into account to arrive at the points of interest.

4.3.2 Box descriptions

A box is made up of certain limits, which are also sometimes called thresholds. The boxes for both models can be compared due to their similar coverage, even though SFINCS has less outcomes. This assumes that using SOBOL's quasi-random sampling method does indeed lead to a more diverse and balanced exploration of the uncertainty space.

Box description FLORES

For FLORES, three uncertainties have to be restricted to describe failure. These three factors also followed from the sensitivity analysis as the most influential factors: mean sea level, storm surge, and tidal amplitude. The quasi-p score, which is the number behind the uncertainties in Figure 4.8, also indicates these found values are statistically significant.

The box indicates the following: any outcome where the mean sea level is above 0.54 meters combined with a storm surge of at least 0.64 meters and tidal amplitude of at least 1.8 meters has approximately a 73.3% chance of leading to failure. Additionally, this combination of factors describe 73.7% of all failure events.
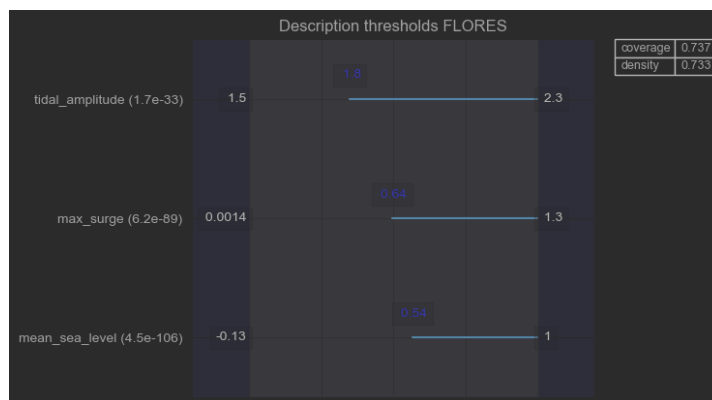
Figure 4.8: Description of the chosen box for FLORES. The coverage and density can be seen in the top right, and the quasi-p score is behind the variables on the left. These terms are explained further in Section 2.1.2. The numbers in blue are the thresholds of the box

The scatter plot in Figure 4.9 is a visual representation of the box described in Figure 4.8. It can be seen that the relationship between the two uncertainties is linear. Still, the box covers 73.7% of all cases where failure occurs. A linear relationship indicates that for following research, another scenario discovery method such

as a logistic regression or principal components analysis could achieve better coverage while keeping similar density.
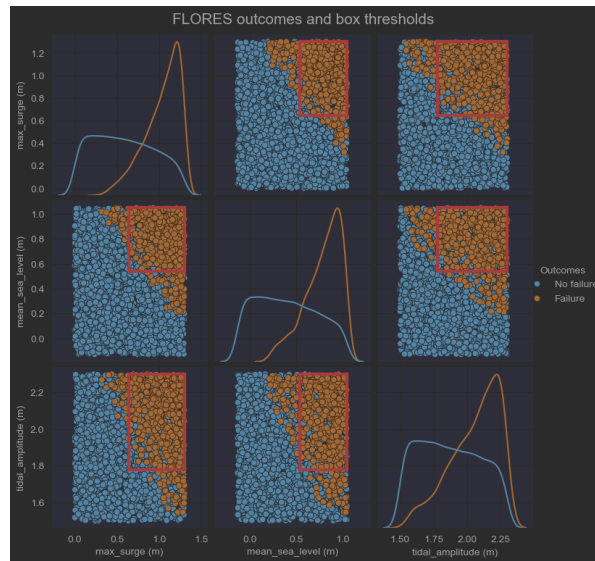
Figure 4.9: Scatter plot showing all outcomes for FLORES. Each outcome is a combination of the uncertainties for the maximum water level in basin 4. The points are binary: orange points are where the water level is greater than 3.60 meters and failure occurs, while for blue points no failure occurs. A probability distribution function for both these types of points can also be seen. Lastly, the box described in detail in Figure 4.8 can be seen in red.

Box description SFINCS

Figure 4.10 describes the selected box for SFINCS. One interesting point for SFINCS is the quasi-p score, which is the number behind each variable. A high quasi-p value suggests that the restriction as placed by the box on the variable is not statistically significant. Currently, the quasi-p scores indicate that the restrictions placed on rainfall and the roughness of the sea are not statistically significant, and that the main factors are tidal amplitude, mean sea level, and storm surge. In the case of SFINCS, this indicates that more runs should be done to investigate whether rainfall and sea roughness are indeed relevant.

The box indicates the following: when the mean sea level is above 0.57 meters, combined with a storm surge of 0.85 meters, and where the tidal amplitude is above 1.8 meters, there is approximately a 74.2% chance of failure. Additionally, this combination of factors describe 73.2% of the outcomes where failure occurs for SFINCS.
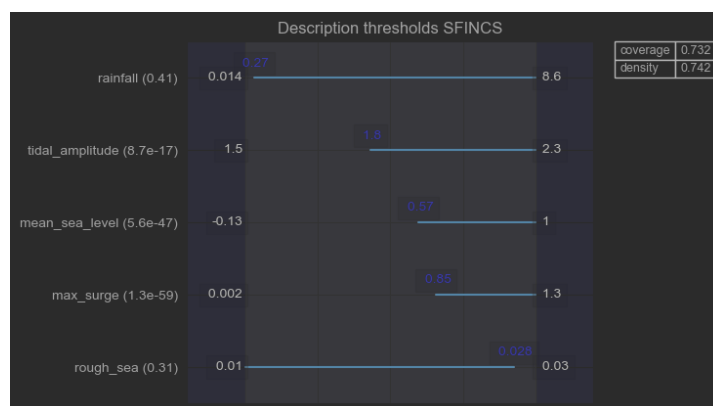
Figure 4.10: Description of the box selected for SFINCS. Coverage and density can be found in the top right. The number after each variable is their quasi-p score. These terms are explained further in Section 2.1.2. The numbers in blue are the thresholds of the box.

For the scatter plot shown in Figure 4.11, the factors "rough_sea" and "rainfall" were removed, since they

were most likely not statistically significant. Similarly to the scatter plot for FLORES in Figure 4.9, a linear relationship can be seen between the three uncertainties, although this is less pronounced for SFINCS due to the lower number of runs. Similarly to FLORES, this indicates another scenario discovery technique such as principal components analysis or logistic regression would most likely improve the fit of the box.
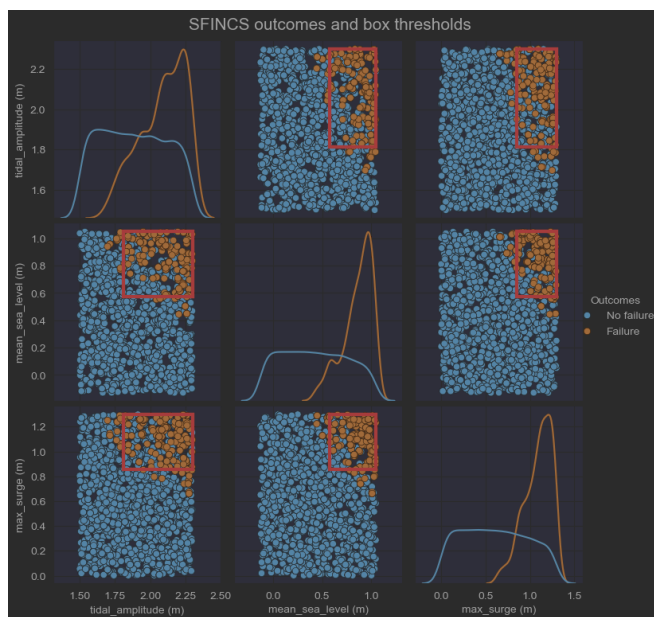
Figure 4.11: Scatter plot showing all results for SFINCS. Each point is an outcome for the avgWTP output described previously. The points are binary: orange points are where the water level is greater than 3.60 meters and failure occurs, while for blue points no failure occurs. A probability distribution function for both these types of points can also be seen. Lastly, the box described in detail in Figure 4.10 can be seen.

4.3.3   Comparison of the found boxes for FLORES and SFINCS

The boxes found through scenario discovery for FLORES and SFINCS are very similar. The same three factors were important for both: mean sea level, storm surge, and tidal amplitude. The mean sea level threshold is at least 0.54 meters for FLORES, and 0.57 meters for SFINCS. The tidal amplitude threshold is 1.8 meters for both. The storm surge difference was slightly different, with 0.64 meters for FLORES, and 0.85 meters for SFINCS. These boxes have the same coverage, meaning they describe the same percentage of outcomes where failure occurs.

The similarity in boxes shows that the relation between these three variable is similar for both the models. The only real difference is for the storm surge, where the SFINCS threshold is higher by 19 centimeters. This again shows the overestimation of inundation level by FLORES as also found earlier looking at the distribution of the outcomes. The other difference between the boxes is a slightly higher density for the SFINCS box, offset by a slightly higher coverage for the FLORES box. Drawing specific conclusions from this is questionable however, due to the lower amount of runs done for SFINCS compared to FLORES.

SFINCS has 4096 outcomes, compared to 6144 for FLORES. This lower number of outcomes lead to the inclusion of rainfall and sea roughness as extra thresholds with very high quasi-p values. Increasing the number of runs should show whether these two additional factors are indeed important, and increase the density of the box by more clearly illustrating when failure occurs.

4.4   Implications for policy making

The results mentioned in this chapter also have implications for potential policy advice. This is done mostly in broad lines. Important to note is that while the scenario discovery showed that the relationship between

the uncertainties is linear, they still have similar percentages for coverage, indicating they both explain the same ratio of the total cases where failure occurs. This allows for some comparison between the two.

Policy based on FLORES results

The box found in the scenario discovery for FLORES which describes 73.7% of the cases where failure occurs has a mean sea level of at least 0.54 meters, combined with a storm surge of 0.64 meters and tidal amplitude of 1.8 meters. A mean sea level of 0.54 meters could be reached before 2070 for a high emissions trajectory, and around 2120 for a low emissions trajectory (Tonkin+Taylor, 2021). A storm surge of 0.64 meters under current conditions has a return period of around 2 years (Stephens et al., 2016). A tidal amplitude of 1.8 meters under current conditions is around equal to the mean high water spring tide that is exceeded 10% of the time (Stephens et al., 2016).

Looking at the linear relationship in Figure 4.9, the FLORES model potentially starts flooding for a mean sea level of 0.25 meters, which is likely to occur around 2050 (Tonkin+Taylor, 2021). For this mean sea level, the upper range of storm surge and tidal amplitude would also be necessary for flooding to occur, which is unlikely.

The wastewater treatment plant only flooding at around 2050 for a RCP4.5 scenario would mean there is still time for adaptation. The primary goal of policy would be to try to mitigate the storm surge in order to keep the plant operable at the same location for longer. This has two reasons. First, the storm surge currently carries the most uncertainty compared to mean sea level and tidal amplitude, as described in Sections 2.2.3 and 3.5.1. Second, from the sensitivity analysis it was found this factor had the most influence on the maximum water level. Policy to address this would have to have a timeline of around 20-30 years, depending on sea level rise. After this, most policy would likely focus on relocating the wastewater treatment plant.

Policy based on SFINCS results

The box found for SFINCS which describes 73.2% of the cases where failure occurs had a mean sea level of above 0.57 meters, combined with a storm surge of 0.85 meters, as well as a tidal amplitude above 1.8 meters. The mean sea level may reach the constrained value of 0.57 before 2070 for a high emissions trajectory, and around 2120 for a low emission one (Tonkin+Taylor, 2021). The storm surge of 0.85 meters correlates to that of around a 10 year return period, while the tidal amplitude is around the same as the MHWS10, or the mean of the highest 10% of all high tides (Stephens et al., 2016).

From the linear relationship it can be seen that according to SFINCS, flooding only occurs when mean sea level is above 0.4 meters, combined with the highest tidal amplitude and storm surge. This mean sea level is expected to be reached around 2075 for a RCP4.5 emissions scenario.

Based on the sensitivity analysis, policy would be focused on reducing the effects of storm surge, since this has the most effect on the maximum water level at the wastewater treatment plant. Additionally, this is also the most uncertain factor compared to mean sea level and tidal amplitude as discussed in Sections 2.2.3 and 3.5.1. Policy with the goal of mitigating this storm surge to keep the treatment plant at the current location longer would have a timeline of around 50 years. After this, policy would focus on the relocation of the wastewater treatment plant long-term.

4.5 Comparison FLORES and SFINCS models

4.5.1 General

Both models were built in Python, which made analysis relatively easy. Compared to SFINCS, FLORES requires more pre- and post-processing which was done using QGIS. This took a significant time. Once this is set up, however, the run time per simulation is much quicker often only taking a few seconds compared to slightly more than a minute for SFINCS. FLORES and SFINCS also both work with globally available data, the most important of which is an elevation map.

4.5.2 Model behavior and accuracy

Both FLORES and SFINCS show similar behavior throughout the model domain. A comparison of their inundation extent can be found in Figure 3.12. They are both only sensitive to rainfall in the upstream part of the model domain, and have the same three main factors that lead to the variability of the maximum water level at the wastewater treatment plant: mean sea level, storm surge, and tidal amplitude.

At the location of the wastewater treatment plant, Figure 4.5 shows the sensitivities for FLORES and Figure 4.6 those for SFINCS. The total variability for FLORES was made up for 44.5% of storm surge, 38.2% of mean sea level, and 17.9% of tidal amplitude. For SFINCS, this is 46.6% due to storm surge, 41.9% due to mean sea level, and 16.0% due to tidal amplitude. This is also nearly identical. Small differences could be due to the flood attenuation taken into account by SFINCS, or by small differences in the samples taken.

FLORES overestimates the inundation level at the wastewater treatment plant when compared to SFINCS. This could be seen in the validation, in the outcomes section, and from the results of scenario discovery. The outcomes at the plant also indicate a larger spread in the results compared to SFINCS.

4.5.3 Identified vulnerabilities

The vulnerabilities identified for both FLORES and SFINCS are also very similar. They had a similar coverage and density, and the same main three factors: mean sea level, storm surge, and tidal amplitude. The main difference between the two were the increase in storm surge necessary for SFINCS to flood, which was around 20 centimeters more. SFINCS also showed rain intensity and the sea roughness to be potentially relevant, although more runs would be necessary to prove this.

4.5.4 Policy advice

Continued from the last subsection, the conditions required for the FLORES model to flood are slightly lower than those for the SFINCS model. This affects the timeline of policy advice, as the vulnerabilities identifed for FLORES indicate that relocation of the treatment plant should happen earlier than the vulnerabilities identified for SFINCS. For FLORES the timeline for adaptation measures is around 20-30 years, while for SFINCS this is 50 years.

In both cases the wastewater treatment plant can stay at its current location longer. When designing policy, the main factor to mitigate would be the storm surge, which has the largest current uncertainty and the largest effects on the maximum water level at the wastewater treatment plant.

While both models show relatively similar behavior, the overestimation of water levels by the FLORES model leads to lower flooding thresholds, which would ultimately most likely affect the timeline of potential policies.

Chapter 5

Discussion

This chapter discusses the choices made in the research and their implications on the results. It starts with Section 5.1 discussing the system schematization used to force both FLORES and SFINCS. Next, specific modeling choices for each model are discussed in Section 5.2. This mostly consists of the way the region is schematized. After this, limitations of the calibration and validation for FLORES and SFINCS are discussed in Section 5.3. Lastly, Section 5.4 discusses the way the sensitivity analysis and scenario discovery were set up, and the validity of their results.

5.1 Forcing

Both FLORES and SFINCS were forced using the same event discussed in Section 3.2. The storm duration was taken to be 24 hours, rain was assumed to be constant over the duration of the storm, and the same mean sea level and tidal amplitude were taken. These conditions are obviously simplified, but made comparison between the two models easier.

Storm duration

The chosen storm duration for the model domain was 24 hours. This is assumed to be a good duration since all the rainfall most likely drains within this time domain, and the average rainfall intensity is higher than for storms of a longer duration, which means it correctly simulates an extreme event. Using longer storm durations would most likely lead to lower inundation depths, although this is uncertain, especially in combination with different rainfall intensities and distributions. Whether this is the case, and insight into model behavior can be tested by also using longer storm durations such as 48 and 72 hours.

Rainfall

The effects of rainfall on maximum water levels was found to be almost negligible in the downstream part of model domain. The forcing due to rainfall was simplified however, taken to be uniform over the storm duration. This distribution was used to be able to compare FLORES and SFINCS without the added complexity of spatial and temporal variation in the rainfall. Using a spatially and temporally uniform rainfall distribution most likely underestimates runoff, however, since in this case the runoff is also constant instead of leading to peak discharges. Testing the behavior of both models to changes in rainfall distribution and timing could give interesting information on rainfall drainage and its interplay with storm-tides.

Storm-tide

Rather than using storm-tide elevation as done in previous modeling of the area, for this research the storm surge and tidal amplitude were separated to look at each variable separately. This worked well, since it did indeed give more information used in the comparison of FLORES and SFINCS.

The range of potential tidal amplitudes where based on potential changes in the bathymetry of the river or local floodplains due to sedimentation or erosion. These potential changes were taken into account by choosing an amplitude between 1.5 and 2.3 meters. However, the wastewater treatment plant discharges its effluent into the tidal river, meaning it needs certain tidal conditions in order to discharge. Future work could include a reflection on the tidal ranges between which the treatment plant is operable.

Fluvial flooding

When setting up the forcing, it was assumed that since the model domain encompassed the entire watershed any rainfall would either infiltrate or runoff, especially due to the extremely low mean annual river flow of the Kaipara river.

Comparison of both FLORES and SFINCS forced by a 100 year ARI rainfall event against the previous work where MIKE21 was forced by a 50 year ARI river flow showed that both FLORES and SFINCS most likely underestimated the effect of rainfall. This could be due to two things, the rainfall being uniform which was mentioned before, or a missing latent river flow missing.

A potentially missing latent river flow could influence model behavior, as FLORES and SFINCS schematize a river flow differently. Added river flows could potentially mean inundation depths and extents are underestimated by this research. In order to combat this more validation events should be looked into. This could also lead to further insight into the order of potential river flows when setting up the forcing for future models.

5.2   Modeling choices

The modeling choices made in Sections 3.3 and 3.4 also have some discussion points. FLORES and SFINCS were chosen as representative of conceptual and more complex models respectively. While there were other potential models that could have been chosen, the chosen models were aligned with the research objectives and took into compound flooding. Additionally, both models meshed well with python and the EMA workbench. The validation showed both models represented the model domain relatively well and the choice for them was valid.

FLORES and SFINCS already showed similar behavior, and SFINCS was relatively accurate compared to the MIKE21 model. This means a more complex model is almost certainly not necessary. Additionally, from the previous modeling efforts it was shown that the bathtub model was a lot less accurate than FLORES. Comparing other available models with complexities somewhere in between FLORES and SFINCS such as cellular automata, 1D-2D, or quasi-2D models could give even more insight into the combination of factors that would lead to the need for a more complex modeling approach.

5.2.1   Failure schematization

Failure for both models was defined as a maximum water level higher than 50% of the measuring points around the wastewater treatment plant's embankments, which was 3.60 meters. There were several simplifications made here: only the maximum water level was looked at rather than including flood duration, and potential failure mechanisms other than overtopping were ignored. For the purpose of this research to compare the two models, this was fine. In future research where more precise results are needed, this should be reassessed.

5.2.2   FLORES

FLORES was used as the conceptual model. This had several benefits compared to alternatives, including the possible implementation of coastal defenses and the inclusion of compound flooding. Initially, the addition of processes such as rainfall, infiltration, drainage, and flow between basins were seen as an improvement on even more conceptual approaches. However, most of these processes were not found to be important to the maximum water level for this research.

Originally, FLORES was meant for damage calculations in urban regions, meaning it had to be adapted for the purposes of this research. This meant additional time was needed to rework the python code. Additionally,

pre- and post-processing needed to make FLORES work was lengthy, since most of the basin delineation and file creation had to be done by hand in QGIS. This extra work outside of the pure runtime, which was in the order of seconds, might be less of an issue for more experienced modelers, but was non-trivial compared to the total runtime for this research.

Model domain

The model domain for FLORES was schematized as one watershed in order to include all rainfall flowing past the wastewater treatment plant. This watershed was delineated into 5 subbasins where the storm-tide flowed into subbasin 1 as a product of two formulas, representing flow over a broad weir and open channel flow. However, for a high enough storm-tide the water might not flow through subbasin 1, but reach high enough to flow directly into basins 2 and 4. Whether this is the case, and how much this actually affects the water levels in those basins could be looked into further.

As mentioned before, a lengthy pre-processing step was required to delineate the subbasins, calculate their contours, and calculate border heights between subbasins. This limited the number of subbasins used for this research, potentially affecting the results, especially since the storm-tide never reached subbasins 3 and 5. It would be interesting to further investigate the effects of adding additional subbasins while keeping pre- and post-processing feasible in order to see whether this leads to more accurate results. If it does, seeing if a balance can be found where adding additional subbasins leads to diminishing returns could also be interesting.

FLORES also used a uniform infiltration value for the whole model domain, while exploration of the geology showed infiltration is much higher in the upstream part of the domain compared to the downstream part. This was not found to be an issue, however, as the sensitivity analysis showed the effect on water level due to infiltration was minimal. Future work including groundwater levels, could be affected by this choice though.

Formulas

FLORES uses two formulas to simulate storm surge flowing into the model domain: a broad weir formula for land flow, and an open channel flow formula for river flow. Since the coastal boundary was relatively similar to the initial work by van Berchum (2019), these formulas were not changed.

The broad weir formula uses a constant typically set at 0.55 but which can potentially go as low as 0.46. While this should be correct for this research, other potential broad weir formulas and even different schematizations of overland flow more focused on intertidal flats could be implemented and investigated. Similarly, the open channel flow formula assumes a rectangular river profile with a set slope. Sensitivities within this formula to the river's characteristics, as well as the performance of other open channel flow formulas should also be checked.

5.2.3   SFINCS

SFINCS was chosen as the more complex model. As a reduced physics approach, it saves significant time compared to full 2D models while maintaining accuracy. It was feasible to run SFINCS on a home laptop with the specifications outlined in Section 3.4.1. While a full run with SFINCS took much longer than for FLORES, this model was much easier to set up, with limited pre- or post-processing necessary. In this regard, there is also a balance to be found between the run time of the model and the time needed to get both models ready.

Model domain

The speed SFINCS can work with is based in part on the size of the datasets used. One of the larger datasets is often the elevation map. To accommodate this, the elevation map can be downscaled. However, when downscaling an elevation map, there is a possibility that the quality of the data set is lowered. This in turn could, in the worst case, change the flood routing or other behavior of the model. This was likely not a problem for this research as it used a grid size of 50 meters by 50 meters. However, research on the interplay of the chosen grid size and the the quality of the elevation map should be done to look at the trade-offs between run time and accuracy could be very interesting.

The forcing of SFINCS is done by means of a water level boundary at a certain chosen elevation. This is usually at around -2 meters for a coastal region. For the Helensville case, rather than just a coast, there are large intertidal flats with deep channels running through them where the water was forced. This made choosing the boundary finicky compared to a coastal boundary condition, as the flood wave was damped and changed more by the intertidal flats compared to a normal coast. While SFINCS was calibrated and validated for these large intertidal flats, further research into their effects on the storm-tide boundary could be interesting.

5.3   Calibration and validation

Due to a lack of better data sources, both FLORES and SFINCS were calibrated and validated using the previous modeling efforts from 2013 and 2016. Unfortunately, neither of these two previous efforts were calibrated or validated for a rainfall event. While the calibration and validation done for FLORES and SFINCS were deemed sufficient for the purposes of this research in comparing the two, care should be put into further calibration and validation of these models. This especially pertains to the rainfall and potential river flow, which showed a difference compared to the MIKE21 model with a 50 year ARI river flow.

The validation also showed that one of the main factors influencing flow is Parkhurst road, which strems the flow in the MIKE21 model. While the found inundation levels are relatively similar between SFINCS, FLORES, and MIKE21 are still similar, inclusion of this feature might slightly influence them.

5.4   Sensitivity analysis and scenario discovery

Both the sensitivity analysis and the scenario discovery were ran using SOBOL, which uses a quasi-random sampling scheme. This had two major benefits. First, this allowed both the sensitivity analysis and the scenario discovery to be run at the same time. Second, while the results for SFINCS were not converged due to the lower amount of runs, the quasi-random sampling allowed for a more full exploration of the uncertainty space making conclusions possible.

SFINCS was run for 4096 runs, and FLORES for 6144 runs. This discrepancy in outcomes showed in part in the scatter plots for the scenario discovery, where a much stronger linear relationship was found for FLORES than for SFINCS. While this lower number of runs for SFINCS did not alter the conclusions of this research, in order to better compare the box coverage and density it would be nice if both models had a similar number of outcomes.

5.4.1   Sensitivity analysis

The ranges used for the sensitivity analysis were all chosen with the same timescales in mind, and explained in Section 3.6. However, the choice of range is an extra source of sensitivity. This could already be seen in the sensitivity of the water levels to the tidal amplitude, which has a smaller range compared to mean sea level and storm surge. Extra effort should be put into further assessing the influence of the range boundaries on the outcomes of the sensitivity analyses.

There are also other model factors not taken into account for the sensitivity analysis due to time constraints, which were mentioned earlier in Section 3.6. For FLORES these include the number of basins chosen and the formulas for the lines of defense, while for SFINCS this includes the location of the boundary condition, the chosen grid size, and the quality of the elevation map.

5.4.2   Scenario discovery

The scenario discovery showed the three main factors to be similar for both FLORES and SFINCS. PRIM was used to find a box that had a similar coverage. From the results, however, it could be seen that there was a linear relationship between the tidal amplitude, storm surge, and mean sea level. This means that while the box found through PRIM is still useful in understanding around 73% of the cases where failure occurs for both models, using another technique for scenario discovery such as a logistic regression or a principal components analysis might give an even better description of the conditions under which failure occurs.

Scenario discovery with regards to robust decision making is an iterative process where different policies are designed and compared to each other based on earlier results. This was outside the scope of this research, however. For this research, only one iteration was done using the status quo. This is fine for the goal of the research of comparing FLORES and SFINCS. For further research, the problem definition and potential policies should be fine-tuned using the results described in this report.

Chapter 6

Conclusion and recommendations

6.1 Conclusions

As a reminder, the main question for this report was "How does the use of a more complex model rather than a fast simple model as traditionally used for robust decision making influence predicted system behavior and identified vulnerabilities, and does this have an effect on potential policy advice?".

This was answered by selecting both a conceptual model (FLORES) and more complex model (SFINCS). The predicted outcomes of both these models were described and compared to each other. Additionally, a vulnerability analysis consisting of a sensitivity analysis and scenario discovery was run for the wastewater treatment plant, and compared for both models. Lastly, the model behavior combined with the identified vulnerabilities were used to determine potential policy advice for both models, which was in turn also compared.

6.1.1 Comparison of predicted system behavior

The validation of FLORES and SFINCS showed that inundation level and extent were mostly similar in the downstream part of the domain, although FLORES significantly overestimated inundation depth and extent more upstream. This makes sense, since both models were calibrated for the same water level at the downstream boundary. The overestimation by FLORES upstream is most likely due to the flood attenuation present in the SFINCS model. Compared to the full-physics MIKE21 model, SFINCS calculated similar inundation levels close to the wastewater treatment plant while FLORES overestimated the water level here slightly.

The boxplot of the outcomes at the wastewater treatment plant also showed this overestimation of the water levels by FLORES compared to SFINCS. The range of potential outcomes was larger, and the distribution between the lower and upper threshold were distributed normally. For SFINCS, on the other hand, the range of outcomes was smaller and skewed towards the lower part of the plot. This shows that FLORES on average overestimates the water level at the wastewater treatment plant, which is most likely due to the lack of inclusion of flood attenuation.

Both models showed relatively similar sensitivities throughout the model domain. For both, outputs in the upstream part of the model domain were almost exclusively sensitive to rainfall. In the downstream part of the model domain, the outputs were predominantly sensitive to mean sea level, storm surge, and tidal amplitude. Infiltration and roughness, which were taken into account for FLORES and SFINCS respectively, were found not to be important for outputs anywhere in the model domain.

6.1.2 Comparison of identified vulnerabilities

The results of the sensitivity analysis showed the three most important factors influencing extreme water levels at the wastewater treatment plant were the same for both models: mean sea level, storm surge, and tidal amplitude. There were only small differences in magnitude of the sensitivities between the two models.

The small differences in this magnitude are most likely due to the flood attenuation described by SFINCS. This lead to a weaker effect of the tidal amplitude on the water level.

Differences in model behaviors, while small, also influenced the results of scenario discovery. For both FLORES and SFINCS, the thresholds explained around 73% of the cases where failure occurs. SFINCS needed a significant mean sea level of 0.57 meters combined with a storm surge of 0.85 meters and a tidal amplitude above 1.8 meters to flood, while scenario discovery for FLORES showed flooding at a mean sea level of 0.54 meters combined with a storm surge of 0.64 meters and tidal amplitude of at least 1.8 meters.

For both FLORES and SFINCS, the scenario discovery showed a linear relationship between tidal amplitude, mean sea level, and storm surge. This relationship indicated that for SFINCS the wastewater treatment plant only started flooding when a mean sea level of at least 0.4 meters was reached, while for FLORES a mean sea level of 0.25 meters was necessary. This difference is again due to the overestimation of water levels by FLORES due to the lack of inclusion of flood attenuation.

6.1.3   Comparison of potential policy advice

The differences in predicted system behavior and identified vulnerabilities are small, which can be seen in the types of policy advice as well. The vulnerabilities identified for both models indicate the wastewater treatment plant can stay at the current location for a while longer. In the case of FLORES, the mean sea level of 0.25 meters where failure starts to occur is reached in around 20-30 years. For SFINCS, the mean sea level of 0.4 meters where failure starts to occur is only reached in around 50 years.

Potential policy advice would, in both cases, first focus on mitigating the effects of storm surge, and then on relocation of the wastewater treatment plant. The focus would be on storm surge since the maximum water level at the wastewater treatment plant was most sensitive to this factor for both models. Which adaptation measures to choose is also in part dependent on the timeline before relocation is necessary. This timeline is longer for the results of the SFINCS model than that of the FLORES model.

The results show that while the behaviors exhibited by both models is relatively similar, the small differences in accuracy affect the timing of proposed adaptation. This leads to reason that while a conceptual model such as FLORES works well to identify important factors within the system, a more accurate model such as SFINCS is potentially more useful once timing of adaptation becomes important. In this case, the biggest reason for the lower accuracy of FLORES was due to the lack of the flood attenuation taken into account.

6.2   Recommendations

There are three main recommendations. The first has to do with the simplifications done to schematize the forcing and failure of the case. The second with the selection, calibration, and validation of the current models, and the last with the vulnerability analysis done for this research.

6.2.1   Forcing and failure schematization

FLORES and SFINCS were both forced for a uniform rainfall. From the validation it became clear that a 100 year ARI uniform rainfall underestimated inundation compared to a 50 year ARI river flow. The recommendation is to research why this is. One start could be to include temporally and spatially varying rainfall events, or to include a latent river flow to see the effects on inundation levels at the wastewater treatment plant.

Failure in this case was described as a maximum water level higher than around 50% of the spot heights around the wastewater treatment pond embankments. This was reasonable for this research where the focus was on the comparison of the two models. A more realistic schematization of flooding, as well as taking into account additional failure mechanisms would help to better describe the combinations of uncertainties under which failure occurs.

6.2.2 Model selection, calibration, and validation

The two models that were selected, FLORES and SFINCS, were deemed sufficient for this research. In order to further validate the results and give even more insight into the combination of factors that would lead to the need for a more complex modeling approach, it is recommended to repeat the steps taken in this research for different models of varying complexity such as 1D-2D coupled, cellular automata, or quasi-2D models. Models more complex than SFINCS are most likely not necessary, since SFINCS inundation levels at the location of the wastewater treatment plant were similar compared to MIKE21.

The calibration and validation of both models was done using previous modeling efforts. This, while not perfect, worked for the purposes of this research of comparing both models. However, if policy advice is to be given based on these results, more work should be put into further calibration and validation, especially taking into account rainfall and compound flooding events.

6.2.3 Vulnerability analysis

SFINCS was run for less combinations of uncertainties than FLORES. The first recommendation would be to run it for a similar amount to FLORES, in order for convergence to occur and to better compare the two. There are also ways to further speed up the process in order to make the use of SFINCS feasible for future projects, such as the inclusion of subgrid features for SFINCS which was not done for this research due to time and modeling constraints.

The scenario discovery showed the relationship between tidal amplitude, mean sea level, and storm surge to be linear. In order to better describe the conditions under which failure occurs for this case, it is recommended to use scenario discovery methods that deal better with this linear relation, such as a logistic regression or a principal component analysis for future iterations of the robust decision making process.

Bibliography

Alcrudo, F. (2004). A state of the art review on mathematical modelling of flood propagation. impact project.

Alkema, D. (2007). Simulating floods: On the application of a 2d hydraulic model for flood hazard and risk assessment.

Arias, P., Bellouin, N., Coppola, E., Jones, R., Krinner, G., Marotzke, J., Naik, V., Palmer, M., Plattner, G.-K., Rogelj, J., Rojas, M., Sillmann, J., Storelvmo, T., Thorne, P., Trewin, B., Rao, K. A., Adhikary, B., Allan, R., Armour, K., . . . Zickfeld, K. (2021). Technical summary [Masson-Delmotte, V., P. Zhai, A. Pirani, S.L. Connors, C. Péan, S. Berger, N. Caud, Y. Chen, L. Goldfarb, M.I. Gomis, M. Huang, K. Leitzell, E. Lonnoy, J.B.R. Matthews, T.K. Maycock, T. Waterfield, O. Yelekçi, R. Yu, and B. Zhou (eds.)]. In Climate Change 2021: The Physical Science Basis. Contribution of Working Group I to the Sixth Assessment Report of the Intergovernmental Panel on Climate Change (pp. 33–144). Cambridge University Press. https://doi.org/10.1017/9781009157896.002

Auckland Council & (LINZ), T. T. W. L. I. N. Z. (2020). Auckland north, new zealand 2016-2018 [https://doi.org/10.5069/G92R3

Auckland Regional Council. (1993, April). Tp25 draft parakai geothermal groundwater resource statement and management plan 1993.pdf. http://www.aucklandcity.govt.nz/council/documents/technicalpublications/TP25%20Draft%20Parakai%20geothermal%20groundwater%20resource%20statement%20and%20management%20plan%201993.pdf

Auckland Regional Council. (2001). Kaipara river catchment water allocation strategy 2001.

Batstone, C., Lawless, M., Tawn, J., Horsburgh, K., Blackman, D., McMillan, A., Worth, D., Laeger, S., & Hunt, T. (2013). A uk best-practice approach for extreme sea-level analysis along complex topographic coastlines. Ocean Engineering, 71, 28–39.

Beca, GHD, & Miskell, B. (2020, October). The new zealand wastewater sector. https://environment.govt.nz/assets/Publications/Files/wastewater-sector-report.pdf

Bell, R. G., Bostock, H., Carey-Smith, T., Collins, D. B., Fedaeff, N., Kachhara, A., Macara, G. R., Mullan, B., Paulik, R., Somervell, E., et al. (2018). Auckland region climate change projections and impacts: Prepared for auckland council, council controlled organisations, and district health boards/prepared by petra pearce (climate scientist), rob bell (principal scientist-coastal and estuarine processes), helen bostock (marine geologist), trevor carey-smith (climate scientist), daniel collins (hydrologist), nava fedaeff (climate scientist), ayushi kachhara (air quality technician), gregor macara (climate scientist), brett mullan (principal scientist-climate variability), ryan paulik (hazards analyst), elizabeth somervell (air quality scientist), abha sood (climate scientist), andrew tait (principal scientist-climate), sanjay wadhwa (gis analyst), john-mark woolley (climate research scientist).

Bhave, A. G., Conway, D., Dessai, S., & Stainforth, D. A. (2016). Barriers and opportunities for robust decision making approaches to support climate change adaptation in the developing world. Climate Risk Management, 14, 1–10. https://doi.org/https://doi.org/10.1016/j.crm.2016.09.004

Bibby, R. L., & Webster-Brown, J. G. (2005). Characterisation of urban catchment suspended particulate matter (auckland region, new zealand); a comparison with non-urban spm. Science of The Total Environment, 343(1), 177–197. https://doi.org/https://doi.org/10.1016/j.scitotenv.2004.09.041

Bosboom, J., & Stive, M. J. (2021). Coastal dynamics. TU Delft Open.

Brunner, G. W. (2016). Hec-ras river analysis system: Hydraulic reference manual, version 5.0. US Army Corps of Engineers–Hydrologic Engineering Center, 547.

Bryant, B. P., & Lempert, R. J. (2010). Thinking inside the box: A participatory, computer-assisted approach to scenario discovery. Technological Forecasting and Social Change, 77(1), 34–49.

Cao, A., Esteban, M., & Mino, T. (2020). Adapting wastewater treatment plants to sea level rise: Learning from land subsidence in tohoku, japan. Natural Hazards, 103(1), 885–902.

Chow, V. T. (2009, January 1). Open-channel hydraulics (Paperback). The Blackburn Press.

Council, A. R. (1999). Guidelines for stormwater runoff modelling in the auckland region. Auckland Regional Council Technical Publication No, 108.

De Almeida, G. A., & Bates, P. (2013). Applicability of the local inertial approximation of the shallow water equations to flood modeling. Water Resources Research, 49(8), 4833–4844.

De Goede, E. D. (2020). Historical overview of 2d and 3d hydrodynamic modelling of shallow water flows in the netherlands. Ocean Dynamics, 70(4), 521–539.

De Vries, P. (2014). The bolivar roads surge barrier: A conceptual design for the environmental section.

de Almeida, G. A., Bates, P., Freer, J. E., & Souvignet, M. (2012). Improving the stability of a simple formulation of the shallow water equations for 2-d flood modeling. Water Resources Research, 48(5).

Dejeans, B. S., Mullarney, J. C., & MacDonald, I. T. (2022). Lagrangian observations and modelling of turbulence along a tidally influenced river. Water Resources Research, e2020WR027894.

Didier, D., Baudry, J., Bernatchez, P., Dumont, D., Sadegh, M., Bismuth, E., Bandet, M., Dugas, S., & Sévigny, C. (2019). Multihazard simulation for coastal flood mapping: Bathtub versus numerical modelling in an open estuary, eastern canada. Journal of Flood Risk Management, 12, e12505.

Dimitriadis, P., Tegos, A., Oikonomou, A., Pagana, V., Koukouvinos, A., Mamassis, N., Koutsoyiannis, D., & Efstratiadis, A. (2016). Comparative evaluation of 1d and quasi-2d hydraulic models based on benchmark and real-world applications for uncertainty assessment in flood mapping. Journal of Hydrology, 534, 478–492.

Dongeren, A. V., & Svendsen, I. A. (1997). Absorbing-generating boundary condition for shallow water models. Journal of waterway, port, coastal, and ocean engineering, 123(6), 303–313.

Eilander, D. (2022). Towards global-scale compound flood risk modeling.

Eilander, D., Couasnon, A., Leijnse, T., Ikeuchi, H., Yamazaki, D., Muis, S., Dullaart, J., Winsemius, H. C., & Ward, P. J. (2022a). A globally-applicable framework for compound flood hazard modeling. https://doi.org/10.5194/egusphere-2022-149

Eilander, D., Couasnon, A., Leijnse, T., Ikeuchi, H., Yamazaki, D., Muis, S., Dullaart, J., Winsemius, H. C., & Ward, P. J. (2022b). A globally-applicable framework for compound flood hazard modeling. EGUsphere, 1–40.

Eilander, D., Couasnon, A., Sperna Weiland, F. C., Ligtvoet, W., Bouwman, A., Winsemius, H. C., & Ward, P. J. (2022). Modeling compound flood risk and risk reduction using a globally-applicable framework: A case study in the sofala region. Natural Hazards and Earth System Sciences Discussions, 1–31.

Eilander, D., Leijnse, T., & Winsemius, H. C. (2022). Hydromt-sfincs. https://doi.org/10.5281/ZENODO.6244556

Friedman, J. H., & Fisher, N. I. (1999). Bump hunting in high-dimensional data. Statistics and computing, 9(2), 123–143.

Friedrich, E., & Kretzinger, D. (2011). Vulnerability of wastewater infrastructure of coastal cities to sea level rise: A south african case study. Water SA, 38, 755–764. https://doi.org/10.4314/wsa.v38i5.15

Gibson, R., Barnes, M., & Atkinson, R. (2002). Coastal and shelf-sea modelling in the european context. Oceanography and marine biology: an annual review, 40, 37–141.

Gouldby, B., Sayers, P., Mulet-Marti, J., Hassan, M., & Benwell, D. (2009). A methodology for regional-scale flood risk assessment. Water Management, 090708021753010–1. https://doi.org/10.1680/wama.2009.00084

Green, M., & Daigneault, A. (2018). Kaipara harbour sediment mitigation study: Summary. Prepared for Northland Regional Council and Auckland Council by Streamlined Environmental, Report NRC170-1 (minor revision), Hamilton.

Groves, D., Molina-Perez, E., Bloom, E., & Fischbach, J. R. (2019). Robust decision making (rdm): Application to water planning and climate policy. In V. A. W. J. Marchau, W. E. Walker, P. J. T. M. Bloemen, & S. W. Popper (Eds.), Decision making under deep uncertainty (pp. 135–164). Springer.

Haasnoot, M., Kwakkel, J. H., Walker, W., & Ter Maat, J. (2013). Dynamic adaptive policy pathways: A method for crafting robust decisions for a deeply uncertain world. Global environmental change, 23(2), 485–498.

Haasnoot, M., Van Deursen, W., Guillaume, J. H., Kwakkel, J. H., van Beek, E., & Middelkoop, H. (2014). Fit for purpose? building and evaluating a fast, integrated model for exploring water policy pathways. Environmental modelling & software, 60, 99–120.

Haasnoot, M., Warren, A., & Kwakkel, J. H. (2019). Dynamic adaptive policy pathways (dapp). In V. A. W. J. Marchau, W. E. Walker, P. J. T. M. Bloemen, & S. W. Popper (Eds.), Decision making under deep uncertainty (pp. 71–92). Springer.

Haggitt, T., Mead, S. T., & Bellingham, M. (2008). Review of environmental information on the kaipara harbour marine environment. Auckland Regional Council.

Hall, J. W., Boyce, S. A., Wang, Y., Dawson, R. J., Tarantola, S., & Saltelli, A. (2009). Sensitivity analysis for hydraulic models. Journal of Hydraulic Engineering, 135(11), 959–969. https://doi.org/10.1061/(asce) hy.1943-7900.0000098

Heath, R. (1975). Stability of some new zealand coastal inlets. New Zealand journal of marine and freshwater research, 9(4), 449–457.

Herdman, L., Erikson, L., & Barnard, P. (2018). Storm surge propagation and flooding in small tidal rivers during events of mixed coastal and fluvial influence. Journal of Marine Science and Engineering, 6(4), 158.

Herman, J. D., Zeff, H. B., Reed, P. M., & Characklis, G. W. (2014). Beyond optimality: Multistakeholder robustness tradeoffs for regional water portfolio planning under deep uncertainty. Water Resources Research, 50(10), 7692–7713.

Ho, I., Deshpande, A., & Floyd, J. (2009). Wastewater reclaimation for high quality reuse - a case study in helensville [(Accessed on 17/02/2022)].

Hoitink, A., & Jay, D. A. (2016). Tidal river dynamics: Implications for deltas. Reviews of Geophysics, 54(1), 240–272.

Hume, T., Nichol, S., Smith, K., & Liefting, R. (2003). Kaipara sand study: Component 1b: Geomorphic evidence of sand movement and storage in historical times. NIWA Client Report: HAM2003-028.

Hummel, M. A., Berry, M. S., & Stacey, M. T. (2018). Sea level rise impacts on wastewater treatment systems along the us coasts. Earth's Future, 6(4), 622–633.

Hunter, N. M., Bates, P. D., Horritt, M. S., & Wilson, M. D. (2007). Simple spatially-distributed models for predicting flood inundation: A review. Geomorphology, 90(3-4), 208–225.

Hunter, N. M., Bates, P., Neelz, S., Pender, G., Villanueva, I., Wright, N., Liang, D., Falconer, R. A., Lin, B., Waller, S., et al. (2008). Benchmarking 2d hydraulic models for urban flooding. Proceedings of the institution of civil engineers-water management, 161(1), 13–30.

Ingley, R. (2021). River water quality state and trends in tāmaki makaurau: Auckland 2010-2019: State of the environment reporting. Auckland Council, Te Kaunihera o Tāmaki Makaurau.

Jaafar, H., & Ahmad, F. (2019). GCN250, global curve number datasets for hydrologic modeling and design. https://doi.org/10.6084/m9.figshare.7756202.v1

Jamali, B., Bach, P. M., Cunningham, L., & Deletic, A. (2019). A cellular automata fast flood evaluation (ca-ffé) model. Water Resources Research, 55(6), 4936–4953.

Jamali, B., Löwe, R., Bach, P. M., Urich, C., Arnbjerg-Nielsen, K., & Deletic, A. (2018). A rapid urban flood inundation and damage assessment model. Journal of Hydrology, 564, 1085–1098.

Johnson, J. M., Munasinghe, D., Eyelade, D., & Cohen, S. (2019). An integrated evaluation of the national water model (nwm)–height above nearest drainage (hand) flood mapping methodology. Natural Hazards and Earth System Sciences, 19(11), 2405–2420.

Kalbus, E., Buckthought, L., Perks, A., & Boyle, J. (2016). State of the environment: Groundwater state and trends in the auckland region 2016.

Kalimisetty, S., Singh, A., Korada Hari Venkata, D. R., & Mahammood, V. (2021). 1d and 2d model coupling approach for the development of operational spatial flood early warning system. Geocarto International, 1–16.

Klosterman, R. (2012). Simple and complex models. Environment and Planning B: Planning and Design, 39. https://doi.org/10.1068/b38155

Krupka, M., Pender, G., Wallis, S., Sayers, P., & Mulet-Marti, J. (2007). A rapid flood inundation model. Proceedings of the congress-international association for hydraulic research, 32(1), 28.

Kwakkel, J. (2017). The exploratory modeling workbench: An open source toolkit for exploratory modeling, scenario discovery, and (multi-objective) robust decision making. Environmental Modelling & Software, 96, 239–250.

Kwakkel, J., & Haasnoot, M. (2019). Supporting dmdu: A taxonomy of approaches and tools. In V. A. W. J. Marchau, W. E. Walker, P. J. T. M. Bloemen, & S. W. Popper (Eds.), Decision making under deep uncertainty (pp. 355–374). Springer.

Kwakkel, J., Haasnoot, M., & Walker, W. (2016a). Comparing robust decision-making and dynamic adaptive policy pathways for model-based decision support under deep uncertainty. Environmental Modelling & Software, 86, 168–183.

Landcare Research, M. W. (2021). Lcdb v5.0 - land cover database version 5.0, mainland, new zealand [data retrieved from LRIS Portal, https://lris.scinfo.org.nz/layer/104400-lcdb-v50-land-cover-database-version-50-mainland-new-zealand/]. https://doi.org/doi:10.26060/W5B4-WK93

Lawrence, J., Bell, R., Blackett, P., Stephens, S., & Allan, S. (2018). National guidance for adapting to coastal hazards and sea-level rise: Anticipating change, when and how to change pathway. Environmental science & policy, 82, 100–107.

Leijnse, T. (2023, August). User manual - general¶. https://sfincs.readthedocs.io/en/latest/input.html

Leijnse, T., van Ormondt, M., Nederhoff, K., & van Dongeren, A. (2021). Modeling compound flooding in coastal systems using a computationally efficient reduced-physics solver: Including fluvial, pluvial, tidal, wind-and wave-driven processes. Coastal Engineering, 163, 103796.

Lempert, R. J. (2019). Robust decision making (rdm). In V. A. W. J. Marchau, W. E. Walker, P. J. T. M. Bloemen, & S. W. Popper (Eds.), Decision making under deep uncertainty (pp. 23–51). Springer.

level. (2021). Site analysis. http://www.level.org.nz/site-analysis/hazards/rising-sea-levels/

LGNZ. (2019, January). Vulnerable: The quantum of local government infrastructure exposed to sea level rise. https://www.lgnz.co.nz/assets/Uploads/0bb3c3d32a/Planning-for-Sea-Level-Rise-v7-FINAL.pdf

Lhomme, J., Sayers, P., Gouldby, B., Samuels, P., & Wills, M. (2008). Recent development and application of a rapid flood spreading method, 15–24. https://doi.org/10.1201/9780203883020.ch2

Lin, P., Pan, M., Allen, G., Frasson, R., Zeng, Z., Yamazaki, D., & Wood, E. (2019). Global estimates of reach-level bankfull river width leveraging big-data geospatial analysis. https://doi.org/10.5281/ZENODO.3552775

Marchau, V. A. W. J., Walker, W. E., Bloemen, P. J. T. M., & Popper, S. W. (2019). Introduction. In V. A. W. J. Marchau, W. E. Walker, P. J. T. M. Bloemen, & S. W. Popper (Eds.), Decision making under deep uncertainty (pp. 1–20). Springer.

McGrath, H., Bourgon, J.-F., Proulx-Bourque, J.-S., Nastev, M., & Abo El Ezz, A. (2018). A comparison of simplified conceptual models for rapid web-based flood inundation mapping. Natural Hazards, 93(2), 905–920.

McGrath, M. (2019). Climate change: Warming to drive 'robust increase' in UK flooding — bbc.com [[Accessed 9-03-2024]].

Menendez, P., Losada, I. J., Torres-Ortega, S., Toimil, A., & Beck, M. W. (2019). Assessing the effects of using high-quality data and high-resolution models in valuing flood protection services of mangroves. PloS one, 14(8), e0220941.

Mitchell, J., Mackay, K., Neil, H., Mackay, E., Pallentin, A., & Notman, P. (2012). Undersea new zealand. https://catalogue.data.govt.nz/dataset/nz-bathymetry-250m-imagery-raster-layer1

Mitchell, S. B., Green, M. O., MacDonald, I. T., & Pritchard, M. (2017). Field studies of estuarine turbidity under different freshwater flow conditions, kaipara river, new zealand. Estuarine, Coastal and Shelf Science, 198, 542–554.

Molina-Perez, E. (2016). Directed international technological change and climate policy: New methods for identifying robust policies under conditions of deep uncertainty [PhD Dissertation]. Pardee RAND Graduate School. https://doi.org/10.7249/RGSD369

Mullan, M. (2018). Climate-resilient infrastructure: Policy perspectives [(Accessed on 04/13/2022)]. OECD.

Neal, J., Villanueva, I., Wright, N., Willis, T., Fewtrell, T., & Bates, P. (2012). How much physical complexity is needed to model flood inundation? Hydrological Processes, 26(15), 2264–2282.

Neélz, S., & Pender, G. (2009, July). Desktop review of 2D hydraulic modelling packages. Environment Agency.

Néelz, S., & Pender, G. (2013). Benchmarking the latest generation of 2d hydraulic modelling packages. Environment Agency: Bristol, UK.

Néelz, S., Pender, G., et al. (2010). Benchmarking of 2d hydraulic modelling packages.

Neumann, T., & Ahrendt, K. (2013). Comparing the" bathtub method" with mike 21 hd flow model for modelling storm surge inundation. Ecologic Institute, Berlin, Germany.

Ngo, H., Ranasinghe, R., Zevenbergen, C., Kirezci, E., Maheng, D., Radhakrishnan, M., & Pathirana, A. (2020). An efficient modelling approach for probabilistic assessments of present-day and future fluvial flooding. Natural Hazards and Earth System Sciences Discussions, 1–42.

O'Neill, A. C., Erikson, L. H., & Barnard, P. L. (2017). Downscaling wind and wavefields for 21st century coastal flood hazard projections in a region of complex terrain. Earth and Space Science, 4(5), 314–334.

Ramm, T. D., Watson, C. S., & White, C. J. (2018). Describing adaptation tipping points in coastal flood risk management. Computers, Environment and Urban Systems, 69, 74–86.

Reeve, G., Swales, A., & Reed, J. (2009). Kaipara harbour sediments: Information review. Auckland Regional Council.

Saltelli, A., Annoni, P., Azzini, I., Campolongo, F., Ratto, M., & Tarantola, S. (2010). Variance based sensitivity analysis of model output. design and estimator for the total sensitivity index. Computer physics communications, 181(2), 259–270.

Santiago-Collazo, F. L., Bilskie, M. V., & Hagen, S. C. (2019). A comprehensive review of compound inundation models in low-gradient coastal watersheds. Environmental Modelling & Software, 119, 166–181.

Schneider, V., Arcement Jr, G., et al. (1984). Guide for selecting manning's roughness coefficients for natural channels and flood plains (tech. rep.). United States. Federal Highway Administration.

Scriven, B. W. G., McGrath, H., & Stefanakis, E. (2021). GIS derived synthetic rating curves and HAND model to support on-the-fly flood mapping. Natural Hazards, 109(2), 1629–1653. https://doi.org/10.1007/s11069-021-04892-6

Shen, J., Tong, Z., Zhu, J., Liu, X., & Yan, F. (2016). A new rapid simplified model for urban rainstorm inundation with low data requirements. Water, 8(11). https://doi.org/10.3390/w8110512

Sobol, I. M. (2001). Global sensitivity indices for nonlinear mathematical models and their monte carlo estimates. Mathematics and computers in simulation, 55(1-3), 271–280.

Stanton, M. C. B., & Roelich, K. (2021). Decision making under deep uncertainties: A review of the applicability of methods in practice. Technological Forecasting and Social Change, 171, 120939.

Stephens, S. A., Bell, R. G., & Haigh, I. (2020). Supplementary material - spatial and temporal analysis of extreme sea level and skew surge events around the coastline of new zealand. https://nhess.copernicus.org/articles/20/783/2020/nhess-20-783-2020-supplement.pdf

Stephens, S. A., Bell, R. G., & Lawrence, J. (2018). Developing signals to trigger adaptation to sea-level rise. Environmental Research Letters, 13(10), 104004. https://doi.org/10.1088/1748-9326/aadf96

Stephens, S. A., Lwarence, J., Allison, A., & Boyle-Gotta, A. (2021). Adaptive tools for decisions on compounding climate change impacts on water infrastructure.

Stephens, S. A., Wadhwa, S., & Tuckey, B. (2016). Coastal inundation by storm-tides and waves in the auckland region. Auckland Council, Te Kaunihera o Tāmaki Makaurau.

Stoeten, K. (2013). Hurricane surge risk reduction for galveston bay.

Tang, T., Reed, P., Wagener, T., & van Werkhoven, K. (2006). Comparing sensitivity analysis methods to advance lumped watershed model identification and evaluation. Hydrology and Earth System Sciences Discussions, 3(6), 3333–3395. https://hal.science/hal-00298785

Teng, J., Vaze, J., Dutta, D., & Marvanek, S. (2015). Rapid inundation modelling in large floodplains using LiDAR DEM. Water Resources Management, 29(8), 2619–2636. https://doi.org/10.1007/s11269-015-0960-8

Teng, J., Jakeman, A. J., Vaze, J., Croke, B. F., Dutta, D., & Kim, S. (2017). Flood inundation modelling: A review of methods, recent advances and uncertainty analysis. Environmental modelling & software, 90, 201–216.

Tonkin+Taylor. (2021). Coastal flood hazard assessment for northland region 2019-2020. (1012360.1000.v4). https://www.nrc.govt.nz/media/nfbhwhgs/t-t-cfhz-report-2021.pdf

Torres, M. A., Chávez-Cifuentes, J. F., & Reinoso, E. (2022). A conceptual flood model based on cellular automata for probabilistic risk applications. Environmental Modelling & Software, 157, 105530.

Usher, W., Herman, J., Iwanaga, T., Teixeira, L., CELLIER, N., Whealton, C., Hadka, D., Xantares, Bernardoct, Rios, F., Mutel, C., Cederstrand, E., TobiasKAndersen, Van Engelen, J., ANtlord, Kranas, H., Foramitti, J., Menegon, S., Vaibhav Kumar Dixit, & Bsteubing. (2021). Salib/salib: V1.3.13. https://doi.org/10.5281/ZENODO.598306

van Berchum, E. (2019). Rapid screening and evaluation of flood risk reduction strategies.

van Berchum, E., Mobley, W., Jonkman, S., Timmermans, J., Kwakkel, J., & Brody, S. (2018). Evaluation of flood risk reduction strategies through combinations of interventions, j. flood risk manage., 12, e12506.

van Berchum, E., van Ledden, M., Timmermans, J., Kwakkel, J., & Jonkman, S. (2020). Rapid flood risk screening model for compound flood events in beira, mozambique. Natural Hazards and Earth System Sciences, 20(10), 2633–2646.

van Ormondt, M., Leijnse, T., Nederhoff, K., de Goede, R., & van Dongeren, A. (2023). Sfincs: Super-fast inundation of coasts model. https://doi.org/10.5281/ZENODO.8038565

Vatvani, D., Zweers, N., Van Ormondt, M., Smale, A., De Vries, H., & Makin, V. (2012). Storm surge and wave simulations in the gulf of mexico using a consistent drag relation for atmospheric and storm surge models. Natural Hazards and Earth System Sciences, 12(7), 2399–2410.

Walker, W. E., Haasnoot, M., & Kwakkel, J. (2013). Adapt or perish: A review of planning approaches for adaptation under deep uncertainty. Sustainability, 5(3), 955–979.

Watercare Services Limited. (2015). Wastewater treatment performance. %7Bhttps://www.watercare.co.nz/CMSPages/GetAzureFile.aspx?path=~%5Cwatercarepublicweb%5Cmedia%5Cwatercare-media-library%5Cwastewater-collection-treatment%5C2015_wastewater_treatment_performance_watercare.pdf&hash=aaa332c69c252b093aca40752be05827cd0497adaa91e27b5fa8dc7412d19085%7D

Wijaya, O. T., & Yang, T.-H. (2021). A novel hybrid approach based on cellular automata and a digital elevation model for rapid flood assessment. Water, 13(9), 1311.

WMO. (2019, September). United in science 2021. https://public.wmo.int/en/resources/united_in_science

Woetzel, J., Pinner, D., Samandari, H., Engel, H., Krishnan, M., Boland, B., Cooper, P., & Ruby, B. (2020, June). Will infrastructure bend or break under climate stress? (Tech. rep.). https://www.mckinsey.com/business-functions/sustainability/our-insights/will-infrastructure-bend-or-break-under-climate-stress

Wolfram, S. (1984). Cellular automata as models of complexity. Nature, 311(5985), 419–424.

Zhou, W., Zhu, Z., Xie, Y., & Cai, Y. (2021). Impacts of rainfall spatial and temporal variabilities on runoff quality and quantity at the watershed scale. Journal of Hydrology, 603, 127057.

Appendix A

Helensville wastewater treatment plant

In this appendix additional data on the Helensville wastewater treatment plant will be given. The current dynamic adaptive policy pathways map can be found in figure A.1. This shows a clear choice to be made between making small upgrades for the next 20 year to keep the plant at the current location longer, and just relocating the plant once the current forcing is too much.

This appendix also contains different photos of the case site as provided by Watercare New Zealand. This includes pictures of the location of the treatment plant, pictures of high water events, pictures of high pond levels, and finally a topographic survey of the plant's embankments.
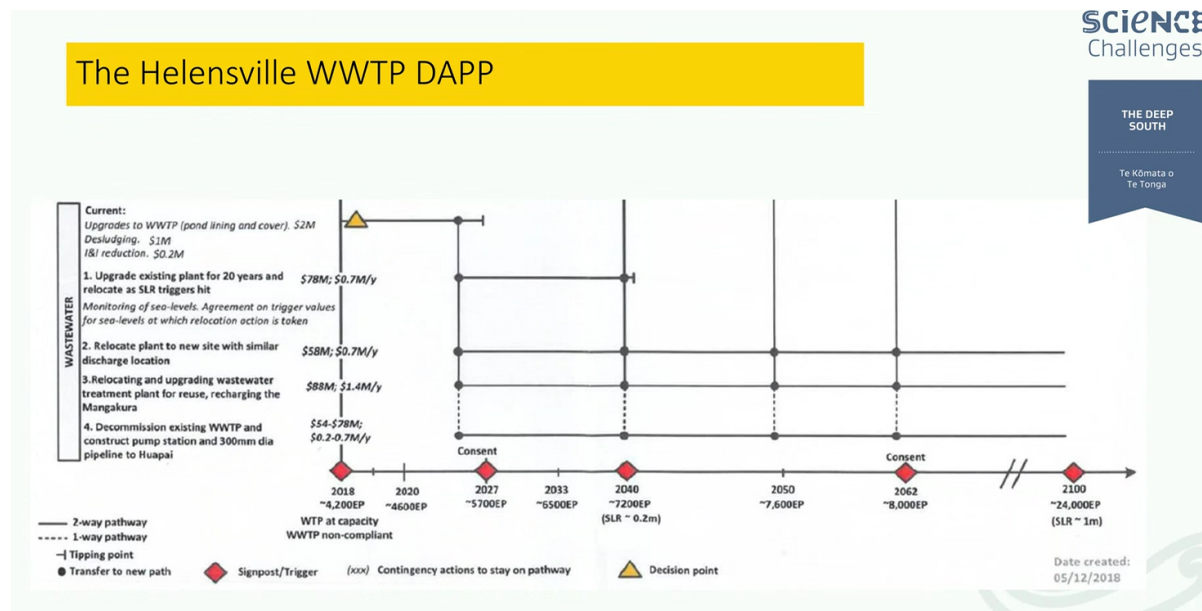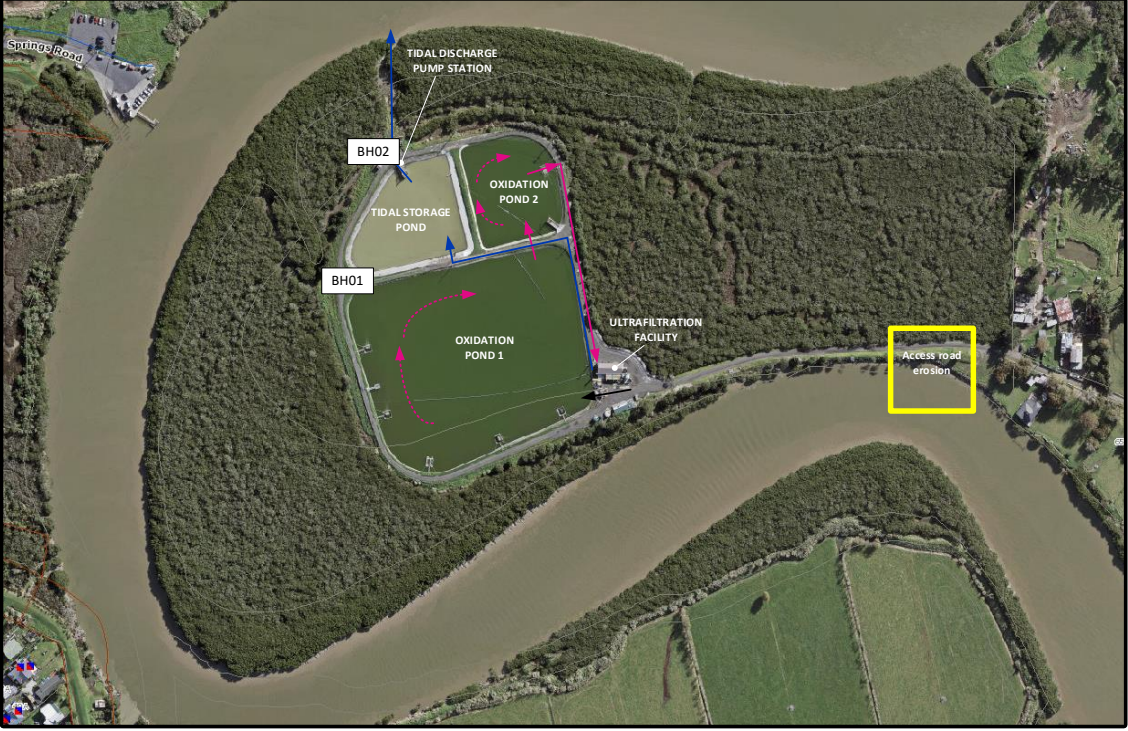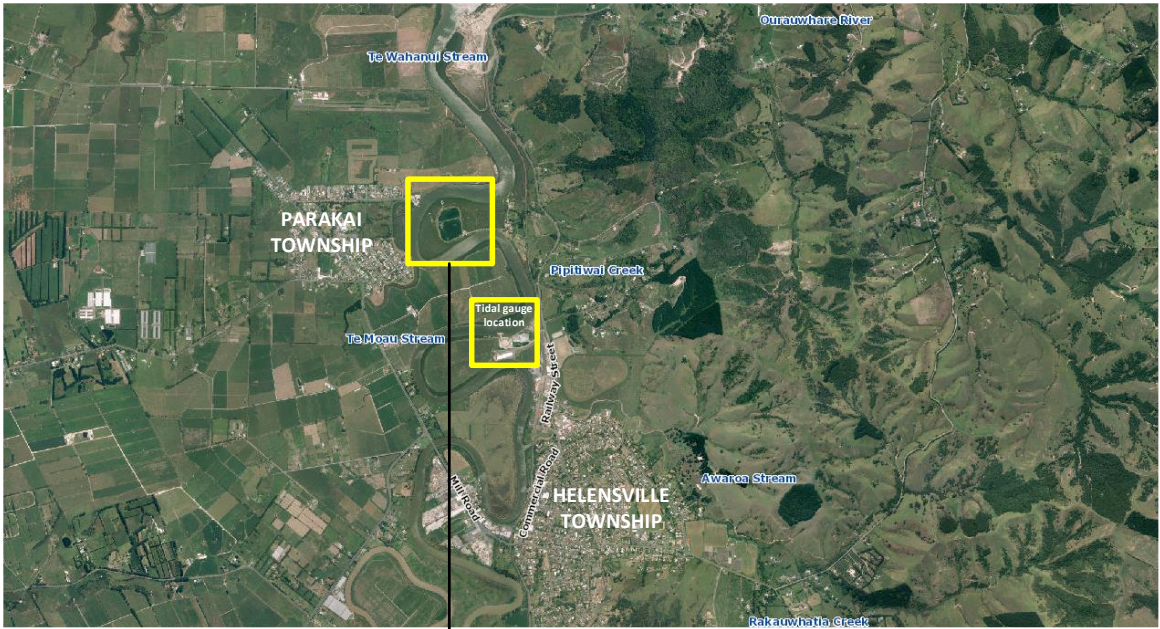

Figure A.1: Dynamic adaptive policy pathways map for the Helensville wastewater treatment plant (Stephens et al., 2021)

PARAKAI TOWNSHIP

Te Wahanui Stream

Ourauwhare River

Te Moau Stream

Pipitiwai Creek

Railway Street

Commercial Road

Mill Road

Tidal gauge location

HELENSVILLE TOWNSHIP

Awaroa Stream

Rakauwhatia Creek

Springs Road

TIDAL DISCHARGE PUMP STATION

BH02

TIDAL STORAGE POND

OXIDATION POND 2

BH01

OXIDATION POND 1

ULTRAFILTRATION FACILITY

Access road erosion

LEGEND:

→ Raw sewage

→ Secondary treated sewage

→ Tertiary filtered effluent

BH02   GW monitoring boreholes
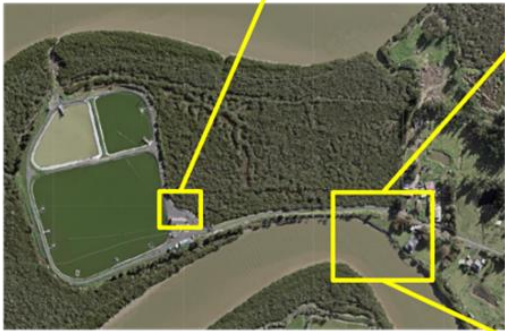
Figure 1: 21st March 2019 Super full moon spring tide (3.8m above MLLW). Access road erosion also observed. This has accelerated (see next figure)

Figure 2: Access road erosion on the 9th September and 3rd October 2019. Approximately 0.5m erosion since the previous picture taken on 21st March 2019.
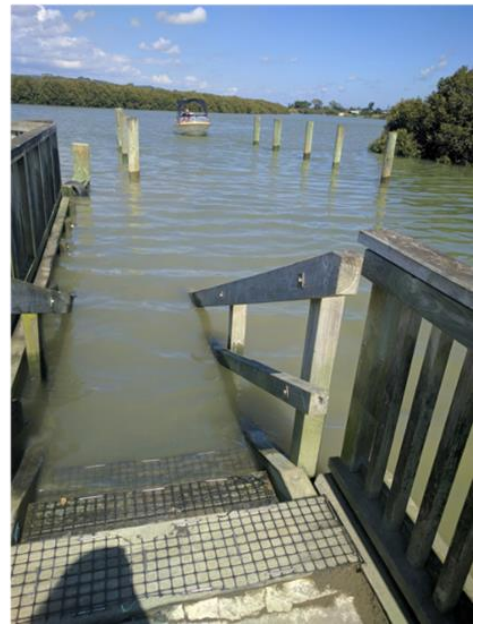
Figure 3: High tide at the boat ramp opposite the Helensville WWTP during the March 2019 super full moon. Photos taken just after peak levels as tide was receding.

Figure 1: 7th July 2017 wet weather event (60mm over 2 days). Pond levels at 1815mm. The pond will overtop the dam embankment into the harbour at 1.85m.

Figure 2: 9th September 2017 wet weather event (125mm between 3rd and 11th Sep). Pond levels at 1660mm. The pond will overtop the dam embankment into the harbour at 1.85m.

DATUM NOTES

1) COORDINATES ARE IN TERMS OF MT EDEN 2000 MERIDIONAL CIRCUIT (EDEN2000).

2) LEVELS ARE IN TERMS OF NZ VERTICAL DATUM 2016 (NZVD2016).

3) COORDINATES AND LEVELS WERE ESTABLISHED AT THIS SITE BY A GNSS STATIC OCCUPATION (3 HOUR EPOCH) PROCESSED VIA LINZ'S POSITIONZ-PP SERVICE.

4) THESE COORDINATE AND LEVEL TERMS DIFFER FROM THOSE ESTABLISHED AT MANGAKURA DAMS 1 & 3 IN 2012, AND AT THE SANDHILLS WEIR IN 2016, BUT ARE BEST PRACTICE OPTION FOR SITE ESTABLISHMENT.

5) RELATIVE LEVELS BETWEEN BM1-5 WERE ESTABLISHED BY PRECISE LEVELLING.

6) TOPOGRAPHIC SURVEY BY GNSS RTK SURVEY.

SURVEY CONTROL MARK COORDINATES AND LEVELS

ID	mN (Eden2000)	mE (Eden2000)	RL (NZVD2016)
BM1	82495.73	37389.11	3.506
BM2	82487.73	37363.01	3.503
BM3	82472.20	37328.79	3.484
BM4	82450.72	37275.87	3.268
BM5	82445.66	37278.06	3.288

GENERAL NOTES

ORTHOPHOTO IMAGERY OBTAINED FROM LINZ DATA SERVICE
AUCKLAND 0.125M URBAN AERIAL PHOTOS (2010-2011)
LICENSE: CREATIVE COMMONS ATTRIBUTION 3.0 NEW ZEALAND
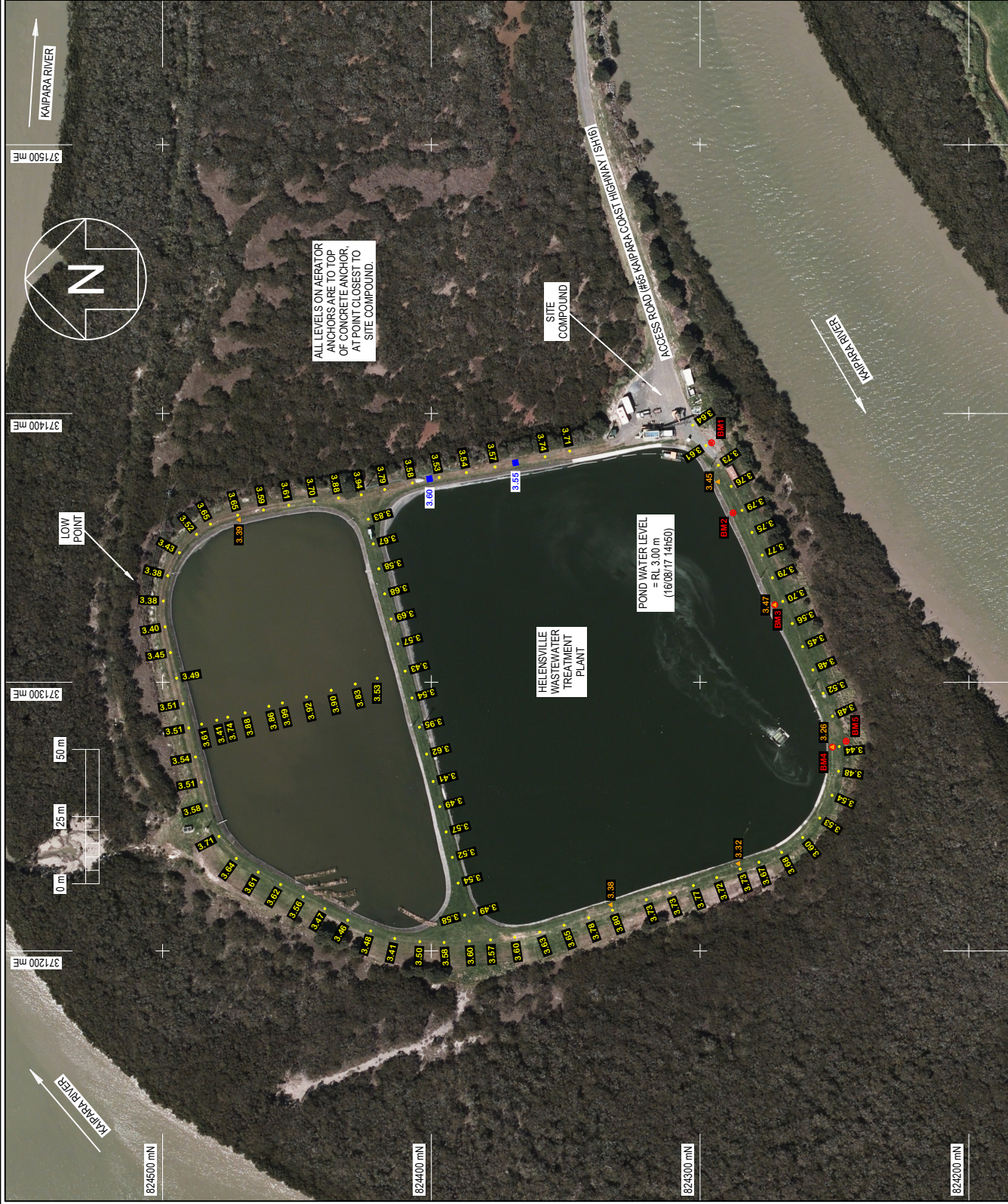LINK: https://data.linz.govt.nz/license/attribution-3-0-new-zealand/

LEGEND

● BM1	SURVEY BENCHMARK (ESTABLISHED BY WATERCARE)
■ 3.60	MANHOLE LID (AND LID LEVEL)
▲ 3.45	AERATOR ANCHOR (AND LEVEL)
• 3.54	SPOT HEIGHT (AND LEVEL)

CLIENT:

Watercare
An Auckland Council Organisation

JOB NO: 17/02	SITE REF: HTP
PLOT NO: 01	VERSION: 1
DRAWN: DS (12D)	
SCALE: 1 : 750 (A1), 1 : 1500 (A3)	
DATE: 01 Sep 2017, 09:28 AM	

ENERGY SURVEYS

Energy Surveys Ltd.
131 Mapara Rd, Acacia Bay, R.D.5., Taupo 3385
P.O.Box 1905, Taupo 3351, New Zealand
Telephone: ++64 7 378 2224
Facsimile: ++64 7 378 2214
Email: surveying@energysurveys.co.nz
Website: www.energysurveys.co.nz

HELENSVILLE WASTEWATER TREATMENT PLANT
CONTROL & TOPOGRAPHIC SURVEY
16 AUG 2017

KAIPARA RIVER

N

ALL LEVELS ON AERATOR ANCHORS ARE TO TOP OF CONCRETE ANCHOR, AT POINT CLOSEST TO SITE COMPOUND.

LOW POINT

SITE COMPOUND

ACCESS ROAD (#65 KAIPARA COAST HIGHWAY / SH16)

POND WATER LEVEL = RL 3.00 m (16/08/17 14h50)

HELENSVILLE WASTEWATER TREATMENT PLANT

KAIPARA RIVER

0 m   25 m   50 m

Appendix B

Groundwater and geology at the WTP site

B.1   Borehole set up

At the case site in Helensville there is data for rainfall, tides, and groundwater levels. The tidal gauge is located closely to the WTP, which can be seen in the bottom yellow box in figure B.1. The top yellow box shows the WTP, where the boreholes are located. These boreholes are labeled as BH01 and BH02 on the right in the figure.
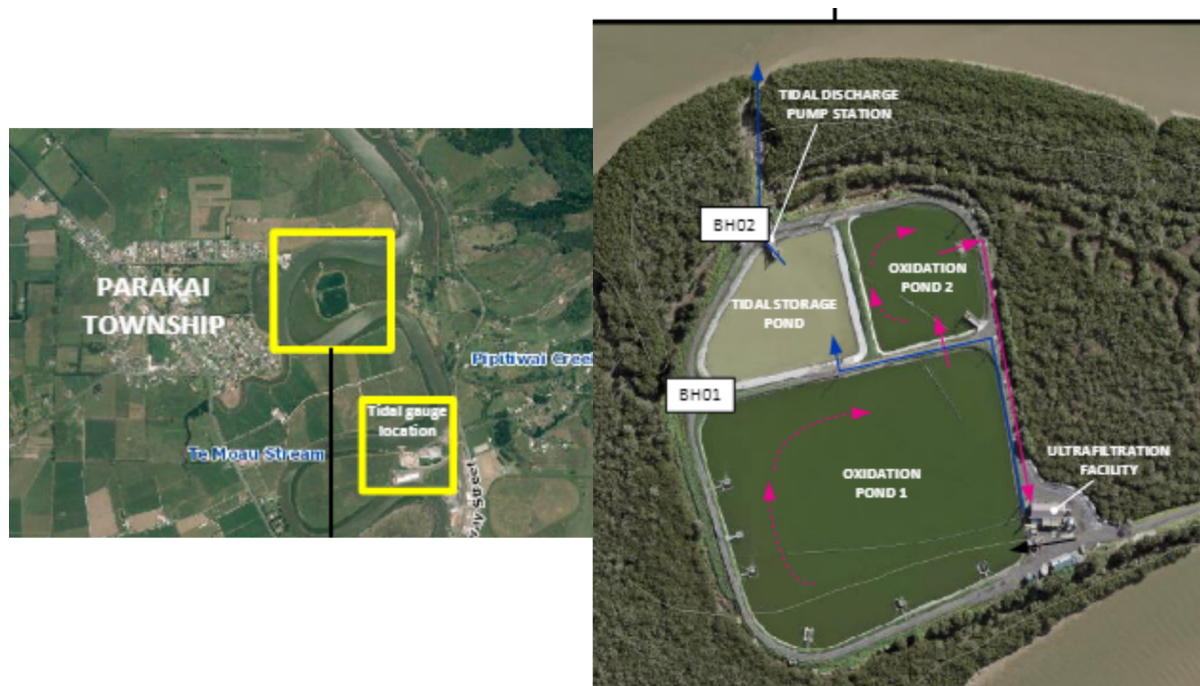

Figure B.1: Locations of WTP and tidal gauge location on the left, and boreholes BH01, BH02 on the right

These two boreholes both have two standpipes within them. One of these standpipes is shallower and one is deeper. The names, tops of the standpipes, their associated boreholes, as well as their measuring depths can be seen in figure B.2.
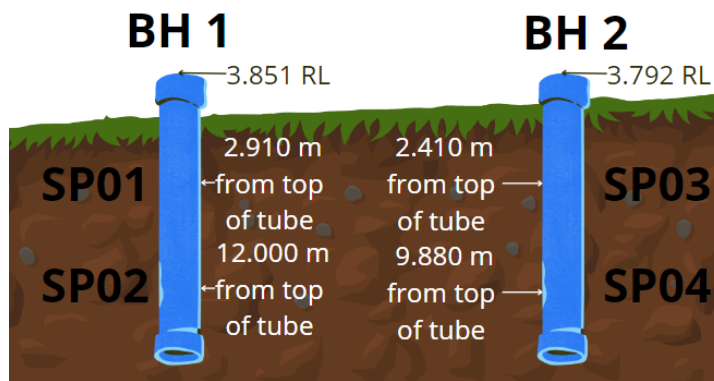
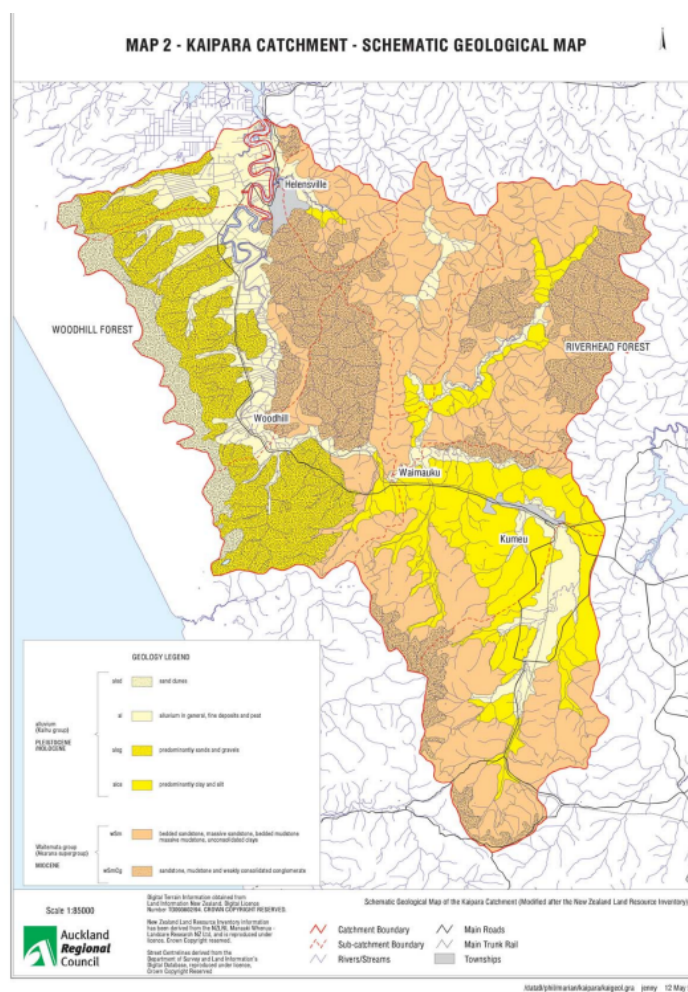Figure B.2: Set up of the boreholes

B.2 Sediment

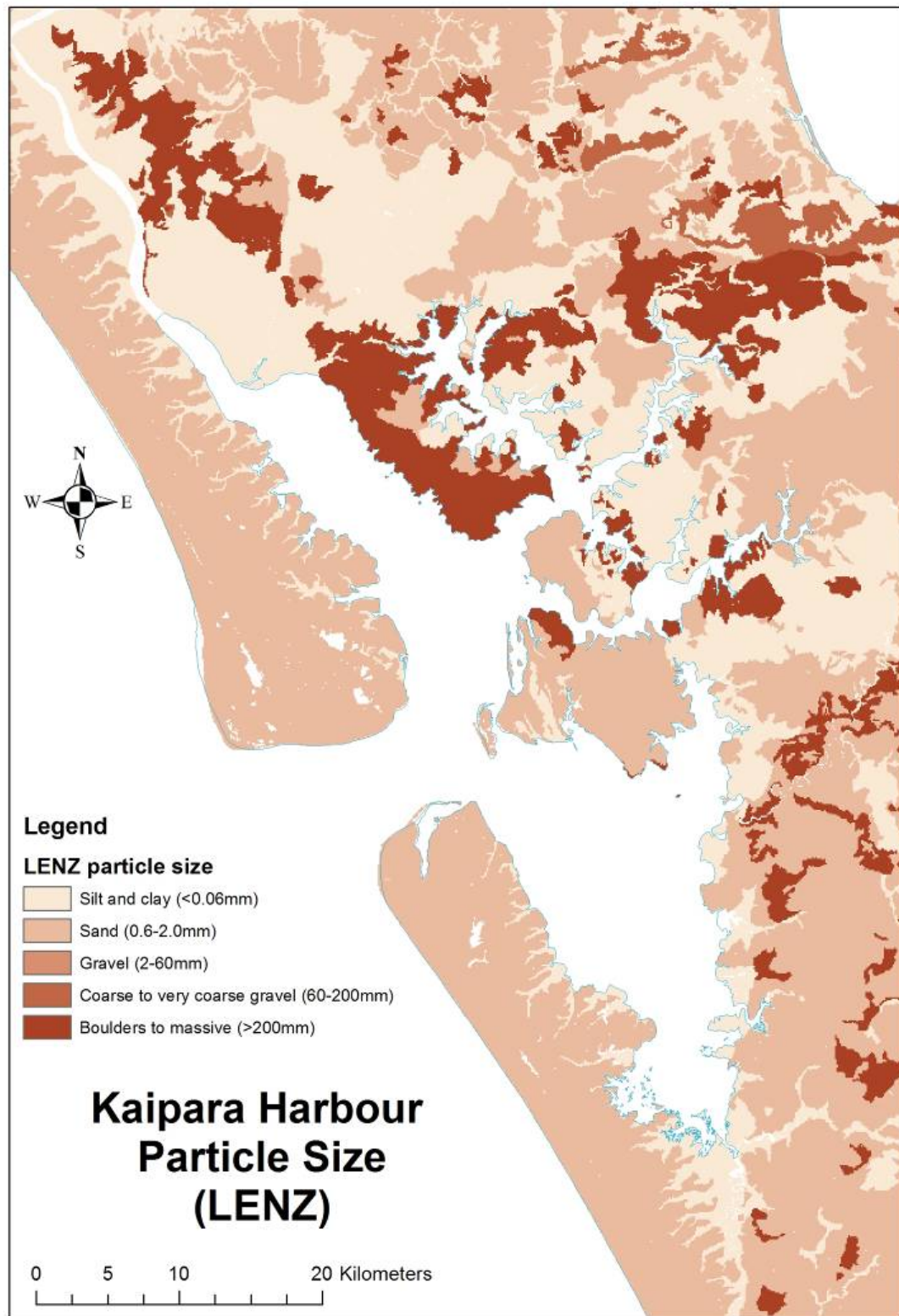Figure B.3: Sediment types in the Kaipara river catchment from (Auckland Regional Council, 2001)

Figure B.4: Sediment sizes from (Haggitt et al., 2008)

B.3   Aquifers

There are three main aquifers in the Kaipara river catchment, which can be seen in figure B.5. The Kaipara Sand and Waitemata Group rocks aquifer have been described in section **??**. Next to this, there is also the small Parakai geothermal aquifer close to the wastewater treatment plant which is mainly used for recreation. The water level here has been decreasing over the past ten years. This aquifer is also very permeable. The water level is kept higher than the surrounding Kaipara dune sands aquifer to avoid the creep of cold water into the geothermal system (Auckland Regional Council, 1993, 2001). Since the water level of the geothermal aquifer follows that of the sand aquifer, the latter is taken as the dominant groundwater source.
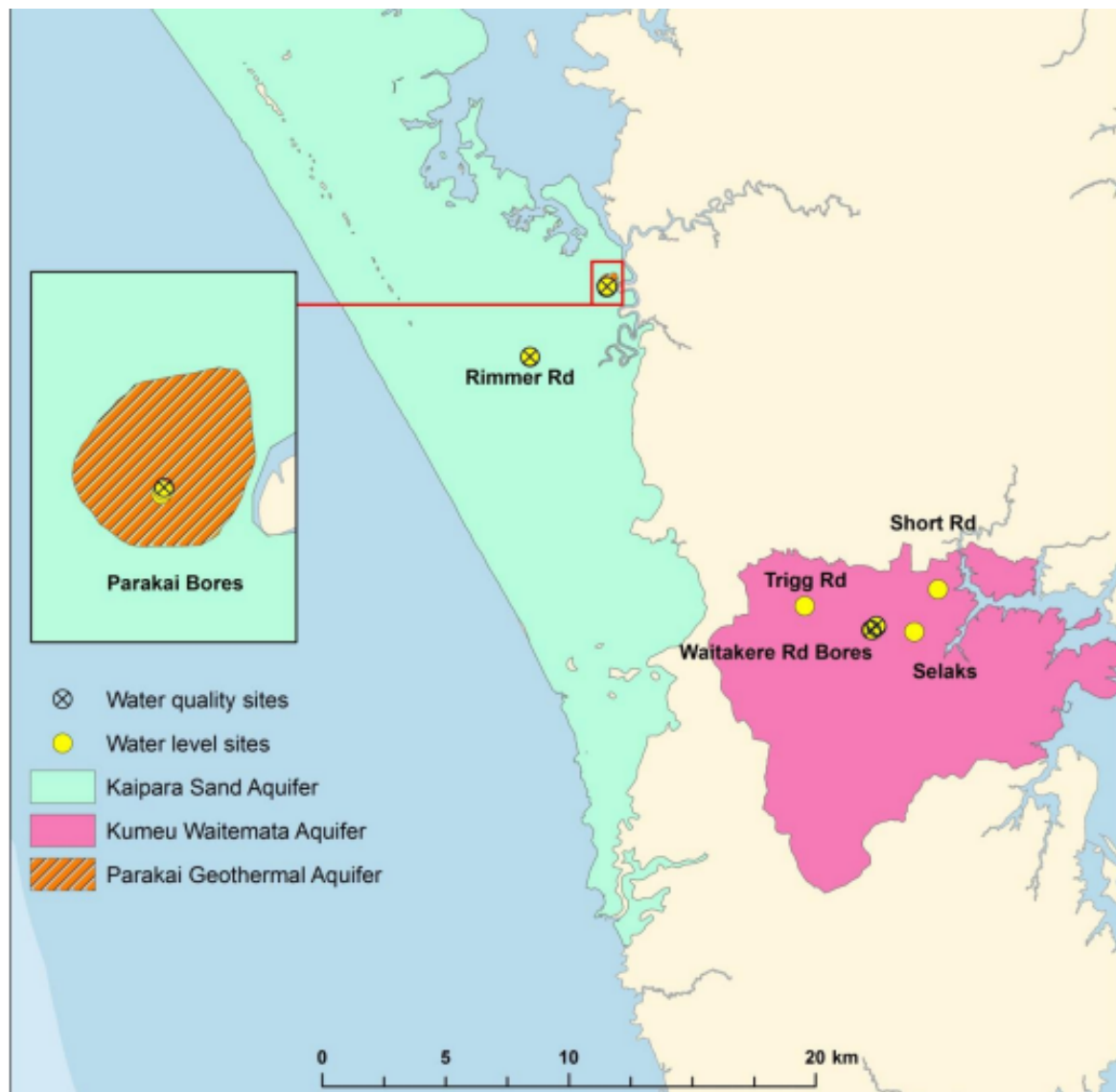

Figure B.5: Locations of different aquifers from (Kalbus et al., 2016)

B.4   Effects of rainfall and tides on groundwater

To assess the effects of rainfall and tides on the groundwater level, they are plotted against each other for a visual inspection and correlations are calculated.

Correlations

The correlations, calculated using Pearson, can be found in table B.1. The shallow standpipes (SP01 and SP03) are strongly correlated with each other, as well as the deeper standpipes (SP02 and SP04) with each other. The standpipes within the same borehole and those of differing measuring levels are also correlated, although this differs. For example, SP03 has its weakest correlation with the deeper standpipe in the same borehole SP04.

Rainfall is correlated with each standpipe, although most strongly with the shallow standpipes. The tides are weakly correlated with the deeper groundwater table, and not at all with the shallow groundwater.

	Tides	SP01	SP02	SP03	SP04	Rainfall
Tides	1.000000	0.026762	0.136657	0.005375	0.164412	0.026215
SP01	0.026762	1.000000	0.401704	0.488035	0.271665	0.520023
SP02	0.136657	0.401704	1.000000	0.445720	0.523834	0.204092
SP03	0.005375	0.488035	0.445720	1.000000	0.360596	0.486681
SP04	0.164412	0.271665	0.523834	0.360596	1.000000	0.139388
Rainfall	0.026215	0.520023	0.204092	0.486681	0.139388	1.000000

Table B.1: Correlations between the standpipes, the rainfall and the tides.

Rainfall

Rainfall data is from the gauge at Mangakura which is in the southeast of the estuary. Using the Pearson correlation method, correlation is strong between the rainfall and the shallow standpipes SP01 and SP03 where the peaks correspond with each other, and in periods with little rain the groundwater table decreases.
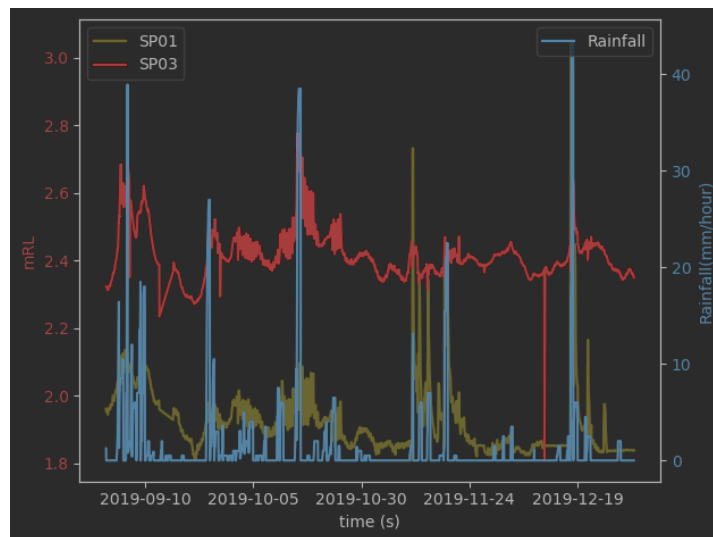

Figure B.6: Borehole vs. rainfall

Tides

From a visual inspection of the tide data plotted against the standpipes, it can be seen that the deep groundwater tables follow the tidal data, while this does not happen with the shallow standpipes.
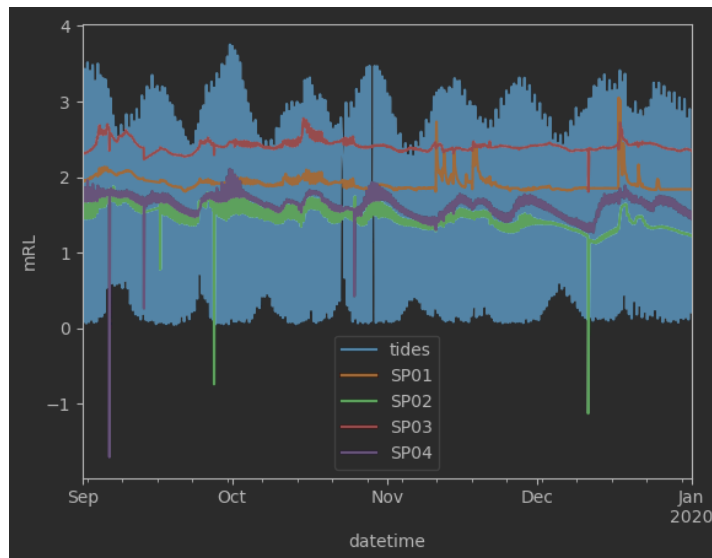
Figure B.7: Boreholes vs. tides

B.5 Conclusions

The groundwater level is affected by rainfall as well as tides. The Kaipara sands aquifer is shallow and quite permeable, although confined in the downstream part of the catchment by a layer of alluvial deposits. Due to these alluvial sediments, the tides have a harder time penetrating. This is not offset by the wastewater treatment plant being at the inner side of the river bend, where coarser material is often deposited. This means that rainfall in the rest of the catchment has a larger effect on the groundwater level than the tides. This can also be seen in the correlations between the standpipes, the tides, and the rainfall which can be found in table B.1.

Appendix C

FLORES model set up

This appendix contains background information on the way FLORES is set up, background on used formulas and a further explanation of the model code and its implementation.

C.1 FLORES input

In order to run FLORES, various inputs are necessary which are described in this section. A flowchart of each necessary file and its name can be found in figure C.1. More information about the input and the calculations done can be found in chapter 3, and on github within the written code.
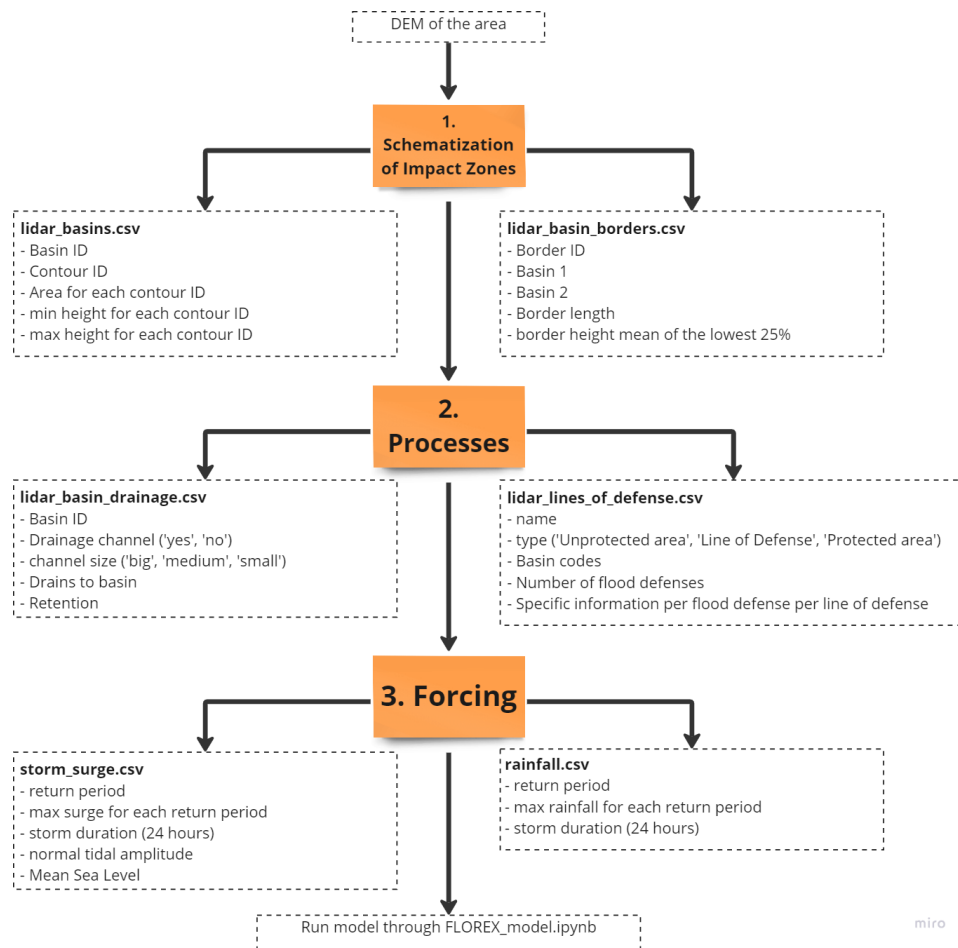
Figure C.1: The various steps in getting from a DEM to setting up the files to run the model

1. Schematization of Impact Zones

Before the DEM of the study area is split up into what is called impact zones (IZ's) in literature, the depressions that are present due to imperfections in the dataset should be filled. This is to keep the downward slope for the flow path. Filling depressions can be done through open source tools such as QGIS using the Wang & Liu algorithm. For this algorithm, a minimum slope is set. Anything under this slope is automatically filled.

After this, a list of neighboring IZ's is made for each IZ, as well as a list of the minimum elevation of their borders. Lastly, a volumetric curve for each IZ is made. For this, the IZ can be divided into contours. Every contour has a certain area, which generates the volume elevation curve.

Information on the contours, their areas, and corresponding basins should be kept in the lidar_basins.csv, while the minimum elevation of each border is kept in the lidar_basin_borders.csv.

2. Processes: drainage and lines of defense

The rest of the schematization falls into two parts: drainage and lines of defense. The drainage is filled in by hand in the lidar_basin_drainage.csv file. For each IZ the existence and size of a drainage channel is filled in, which is either big, medium, or small. Where the IZ drains to is also included. Lastly, the retention is included. As a rule of thumb this can be done by calculating the amount of surface water for said IZ.

Next the lines of defense are schematized. This is done by looking at where the model domain reaches the outside water. Information on potential flood defenses and whether they are land or water based are also put

in by hand in the lidar_lines_of_defense.csv file. Multiple flood defenses can be added to the model.

Lines of defense

FLORES uses a lines of defense concept to separate the open water from the study area. For this concept, multiple lines of defense can be used to separate the area from storm surge. This can be seen in figure 3.6 in chapter 3. The equations below are for cases where no defenses are present, and are taken from (van Berchum, 2019; van Berchum et al., 2018).

Equation 1: broad weir:
This equation is used in the cases where there are no flood defenses present, and the storm surge must flow over land.

$$Q_{bw} = C_{df} \cdot C'_w \cdot \sqrt{g} \cdot L \cdot h^{1.5} \qquad C_{df} = \begin{cases} 1 & \text{for } h2/h1 \leq 0.67 \\ 1 - 27.8(h2/h1 - 0.67)^3 & \text{for } h2/h1 > 0.67 \end{cases}$$

Based on Brunner (2016) and van Berchum et al. (2018).

- C_{df}: the submergence coefficient [-]
- C'_w: the non-dimensional weir coefficient (0.46-0.55)
- h: the upstream water depth [m]
- L: the length of the weir [m]

Equation 2: open channel flow:
This equation is used in cases where there are no flood defenses present, and the storm surge hits an open channel.

$$h_p = h_s - \left(\frac{1}{2} + \frac{c_f \cdot L_C}{R_C} \right) \cdot \frac{|Q_C| \cdot Q_c}{g \cdot A_C^2}$$

Based on De Vries (2014), Stoeten (2013), and van Berchum et al. (2018)

- h_p: the water level [m+MSL] in the protected area.
- h_s: the water level of the storm surge [m+MSL]
- c_f: the friction factor
- L_c: the length of the inlet [m]
- Q_c: the discharge through the inlet [m^3/s]
- R_c: the hydraulic radius [m]
- A_c: the flow area of the channel [m^2]

3. Forcing

The forcing takes two forms, storm-tide and rainfall. For this, two different csv's are added. The first has different return periods for a storm, with accompanying max surge. Additionally, it has the normal tidal amplitude and the mean sea level. The second has different return periods for a storm duration of 24 hours, with their accompanying rain intensity. Both these files start with a return period of 0 years to indicate normal conditions.

C.2   Model python set up

The developed FLORES model was run from a virtual environment. The installed packages for this can be found on the github in the requirements_florex.txt file.

Data

The data necessary to run the model can be put into two categories: data for the schematization and data for the forcing. Due to the simple nature of the model, some information has to be put in by hand such as the size/drainage capacity of channels, capacity of surface water retention, and infiltration.

Github

The github is split up into input files, the model build (.py), and the analysis files (.ipynb). More information on this can be found at https://github.com/xan-source/FLORES_Helensville.git

Appendix D

SFINCS modeling supplementary

This appendix contains background information on the set up of the SFINCS model, the equations used as well as their numerical implementation, and a link as well as an explanation of the github where all the code can be found.

D.1 General process

In general, when using the hydromt-sfincs extension the model can be set up in three main steps. More information on the most recent way this can be done can be found on https://deltares.github.io/hydromt_sfincs/latest/(Eilander, Leijnse, & Winsemius, 2022). First, a data catalog is defined using the necessary data. This helps to increase reproducability. Compared to FLORES, much less pre-processing of the data is required.

Next the model is built. For this, first the grid is defined. This includes active and inactive cells, water level boundary cells, and outflow cells. After adding the roughness data for the active cells, subgrid tables can be made if needed. Next, infiltration data is added and the necessary forcing is set up. Lastly, observation points can be added, as well as features such as dikes or dunes. After this, the files necessary for running the model are saved.

Lastly, the model is run and the results are investigated using post-processing in python.

D.2 Equations used

The equations used in SFINCS are split up into three parts, the momentum equation, the continuity equation, and the boundary conditions used. These are the same for SFINCS-LIE and SFINCS-SSWE, with the exception of the adv_x term in the momentum equation. This is also explained in the numerical implementation later in this appendix.

Momentum equation

$$q_x^{t+\Delta t} = \frac{q_x^t - \left(gh_x^t \frac{\Delta z}{\Delta x} + adv_x - \frac{\tau_{w,x}}{\rho_w}\right)\Delta t}{\left(1 + g\Delta t n^2 q_x^t / h_x^{t\,7/3}\right)}$$

- g: gravitational constant
- n: manning friction coefficient
- q: the flow rate

- h: the average water depth of the two adjacent cells to the h point on the Arakawa C-grid

- Δz: the water level difference between the two adjacent cells of which h is the average

- Δt: the timestep of the model

- ρ_w: the water density

- $\tau_{w,x}$: the wind shear stress

The wind shear stress in the momentum equation is calculated using a secondary formula which is found below

$$\tau_{w,x} = C_d \rho_a u_{w,x} \sqrt{u_{w,x}^2 + u_{w,y}^2}$$

- C_d: wind drag coefficient. This can be self-defined, but the default is the relation by Vatvani et al. (2012)

- ρ_a: the air density

- u_w: the wind speed

Continuity equation

To calculate the water level based on the momentum equation in both directions, the following form of the continuity equation is used for SFINCS (Leijnse et al., 2021).

$$\zeta_{m,n}^{t+\Delta t} = \zeta_{m,n}^t + \left(\frac{\left(q_{x,m-1,n}^{t+\Delta t} - q_{x,m,n}^{t+\Delta t}\right)}{\Delta x} + \frac{\left(q_{y,m,n-1}^{t+\Delta t} - q_{y,m,n}^{t+\Delta t}\right)}{\Delta y} + S_{m,n} \right) \Delta t$$

- ζ: the water level

- Δt: the timestep of the model

- q: the flow rate

- $S_{m,n}$ can be infiltration, precipitation, or a discharge set by the model user

Boundary conditions

Along the open boundaries (mask=2), the water level is forced. This is done by ways of a Riemann type boundary based on work by Dongeren and Svendsen (1997). At this boundary, fluxes are generated for each timestep based on the water levels. The water levels consist of the slowly-varying storm surge and tide, and the rapidly-varying waves. As mentioned before, these fluxes q are located at the velocity points in the Arakawa C-grid explained in the next section. This is done using the following formula from Leijnse et al. (2021):

$$q = h \left(2u^+ - \sqrt{\tfrac{g}{h}} \left(\zeta_i - \zeta_0 \right) + \bar{u} \right) \text{ with } u^+ = \sqrt{g/h} \left(\zeta - \zeta_0 \right)$$

- h: the total water depth at the boundary

- $\bar{u}$: the mean velocity at the boundary

- ζ_i: the water level in the first grid cell with mask 1

- ζ_0: slowly-varying water level (tide + storm surge)

• ζ: rapidly varying water level (waves)

The water level can be forced one of two ways. A model user can input a time-series of the slowly-varying as well as the rapidly-varying water levels. This should be done at the seaward part of the swash zone, where most waves have already broken. The second option is for SFINCS to generate the rapidly-varying water levels based on off-shore wave conditions and bed slope in the surf zone.

In the case of a user-defined input, the water level at every boundary grid cell is calculated based on an interpolation of the weighted average of the two closest inputs (Leijnse, 2023). This can be seen in figure 3.8b

D.3   Numerical implementation

Computational mesh

To calculate the fluxes, water levels and water depths for each gridcell, SFINCS uses the Arakawa C-grid. This is the same computational mesh that is used for Delft-3D. The Arakawa C-grid has a history of being used in coastal modeling, being used in about 85% of shallow water models (De Goede, 2020; Gibson et al., 2002).

The Arakawa C-grid is a staggered grid, and can be seen in figure D.1. The dashed box in this figure shows which variables share the same grid index. The water levels ζ and bed levels b are defined in the center of a cell. The fluxes q and the water depths h are defined in the velocity points, which are perpendicular to the grid cell faces (De Goede, 2020; Leijnse et al., 2021). The benefits of using such a staggered grid are increased robustness, and the easier implementation of the boundary conditions.
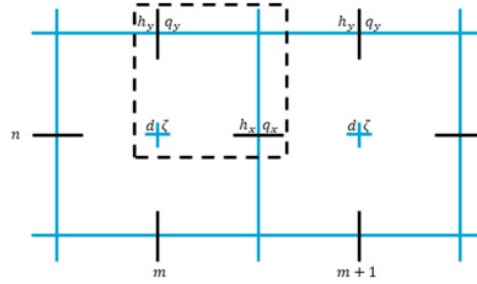

Figure D.1: The Arakawa C-grid used in SFINCS. The staggered grid defines the water levels ζ and bed levels b in the center of a cell, and the fluxes q and water depths h perpendicular to the side of the grid cell. The dashed line shows the variables for one index (m,n) (De Goede, 2020; Leijnse et al., 2021)

Discretized formulas for numerical implementation

The combination of the momentum and continuity equation leads to the discretized formulations for numerical implementation. A smoothing is applied to stabilize the numerical solution when dealing with low friction. For this a user-defined θ is used. The equations below are for SFINCS-SSWE. To get to the equations for SFINCS-LIE, simply take out the advective terms adv_x and adv_y.

$$q_{x,m,n}^{t+\Delta t} = \frac{\left[\theta q_{x,m,n}^t + \frac{1-\theta}{2}\left(q_{x,m+1,n}^t + q_{x,m-1,n}^t\right)\right] - \left(gh_{x,m,n}^t \frac{\left(\zeta_{m+1,n}^t - \zeta_{m,n}^t\right)}{\Delta x} + adv_x - \frac{\tau_{w,x}}{\rho_w}\right)\Delta t}{\left(1 + g\Delta t n^2 q_{x,m,n}^t / h_{x,m,n}^{t\,7/3}\right)}$$

$$q_{y,m,n}^{t+\Delta t} = \frac{\left[\theta q_{y,m,n}^t + \frac{1-\theta}{2}\left(q_{y,m,n+1}^t + q_{y,m,n-1}^t\right)\right] - \left(gh_{y,m,n}^t \frac{\left(\zeta_{m,n+1}^t - \zeta_{m,n}^t\right)}{\Delta y} + adv_y - \frac{\tau_{w,y}}{\rho_w}\right)\Delta t}{\left(1 + g\Delta t n^2 q_{y,m,n}^t / h_{y,m,n}^{t\,7/3}\right)}$$

- θ: a user input used to smooth the fluxes from the previous timestep. The default is 0.9, with a range of 0-1 (de Almeida et al., 2012).

- adv: the advective term of the SWE's. Their calculation can be found in the paper by Leijnse et al. (2021).

D.4 Implementation

Data + software

Data requirements

SFINCS was developed partly with the goal to be able to be implemented in as many cases as possible. To this end, there are many different possibilities with regards to implementations, all with varying inputs. In the figure below all potential standard inputs can be seen, with the minimally required files in green.
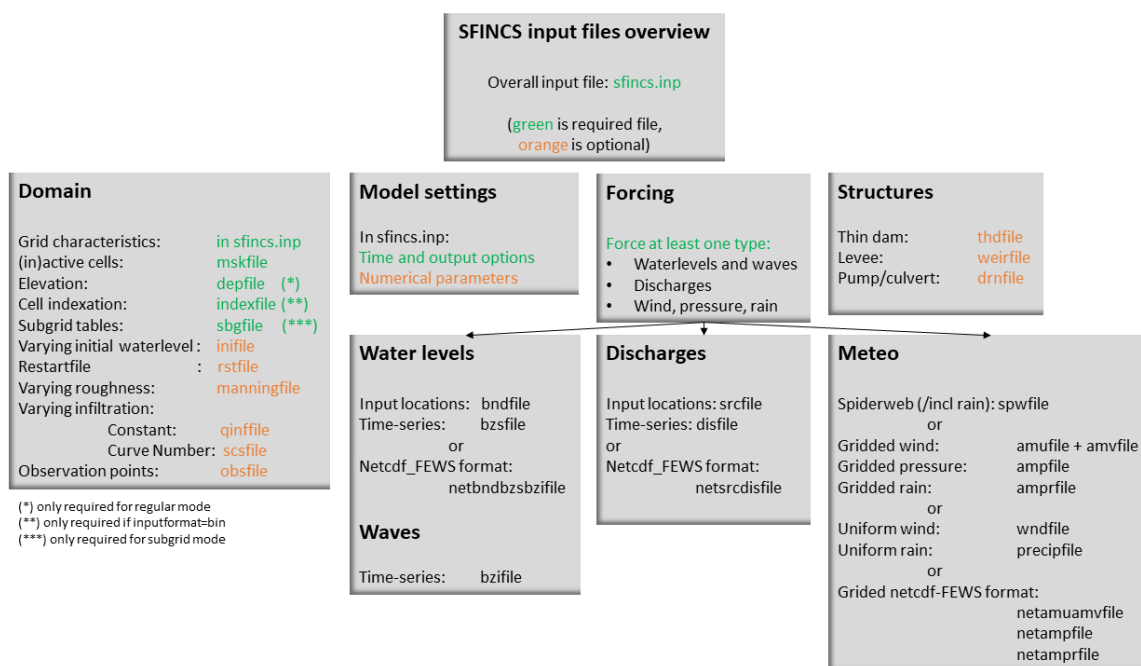
Figure D.2: Overview of possible input files and whether they are required (Leijnse, 2023)

Software requirements

In order to run SFINCS, first the model itself should be installed. For this research the v2.0.2 Blockhaus was used (van Ormondt et al., 2023). This can be downloaded through Deltares. Using an earlier version than this leads to errors with the observation points needed to describe the water level throughout the model's runtime. The SFINCS model itself uses input files that can be generated in a variety of ways (CLI, Delft Dashboard, Matlab using Open Earth Tools, HydroMT-SFINCS). The focus here is on the use of the HydroMT-SFINCS python plug-in, since this allows the model to be set up from a python script, making further analysis easier.

The HydroMT-SFINCS plugin is part of the HydroMT group of tools aimed at automating the process of getting from raw data to a model instance that can be run, and the post-processing afterwards (Eilander, Couasnon, Leijnse, et al., 2022a; Eilander, Leijnse, & Winsemius, 2022). The version used for this research was 0.2.1. This plugin was installed in a clean virtual python environment.

Github

The full list of python packages present in this virtual environment, as well as other information on the modeling set up can be found at https://github.com/xan-source/SFINCS_helensville.git.

Appendix E

Supplementary sensitivity material

This appendix has additional information on the sensitivity analyses done in Section 4.2 from Chapter 4. The set up of the various points for both FLORES and SFINCS can be found in Section **??**.

As a reminder, the graphs in this section show both S1 (first-order sensitivity), and ST (total sensitivity) as well as a confidence bounds which is the white line. First-order sensitivity measures the direct impact of the variable on the model output, while total sensitivity considers both the direct and indirect effects, including potential second order interactions with other parameters. If the results have fully converged, the different ST's should add up to 1.
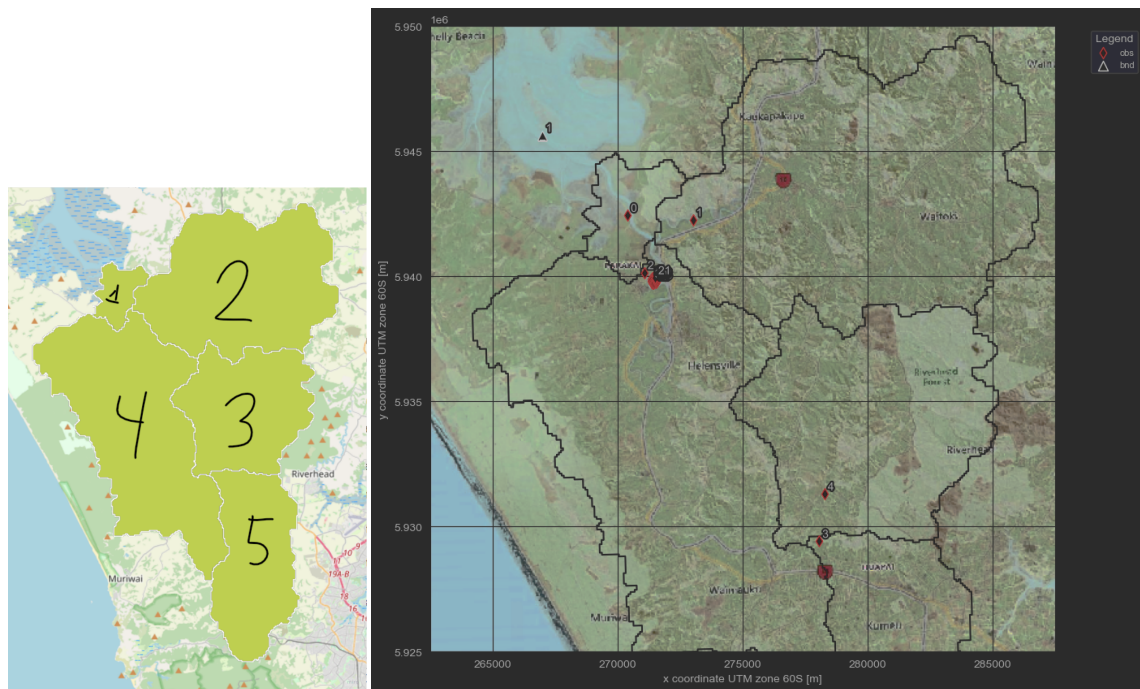
Figure E.1: Locations of observation points for SFINCS compared to FLORES. On the left are the subbasins for the FLORES model, and on the right are the observation points for SFINCS with an overlay of the FLORES subbasins.

E.1   FLORES

The results of the sensitivity analysis for basin 4 can be found in figure 4.5 in section 4.2.
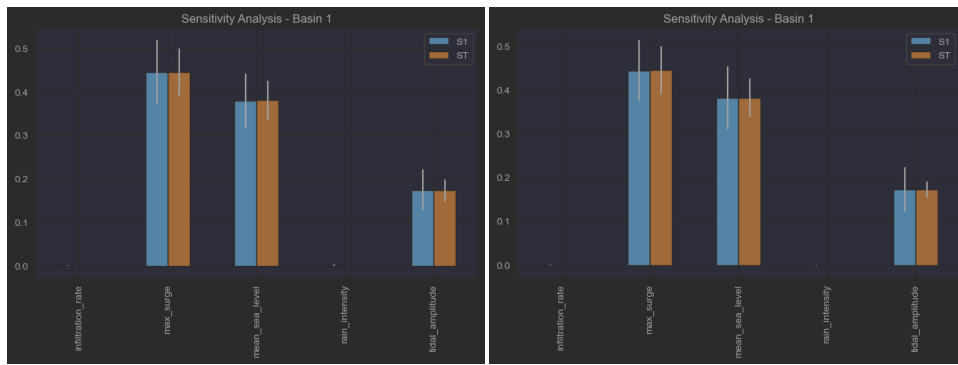
Figure E.2: Sensitivities for output max1. This is the maximum water level in basin 1, using the mean of the lowest 10% and 25% of the border heights respectively.
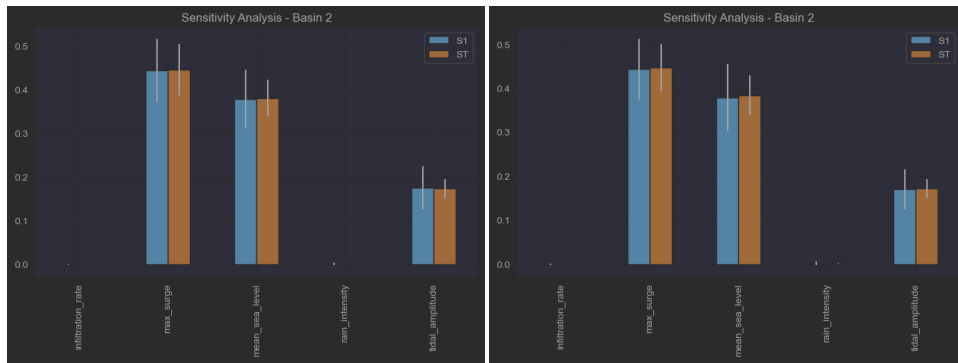

Figure E.3: Sensitivities for output max2. This is the maximum water level in basin 2, using the mean of the lowest 10% and 25% of the border heights respectively.
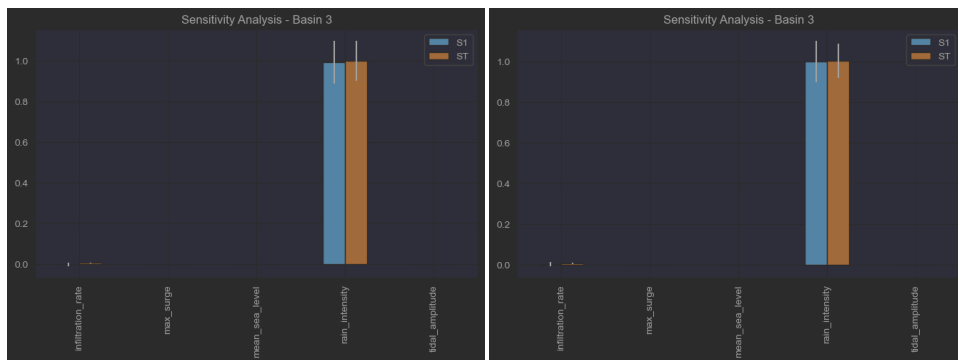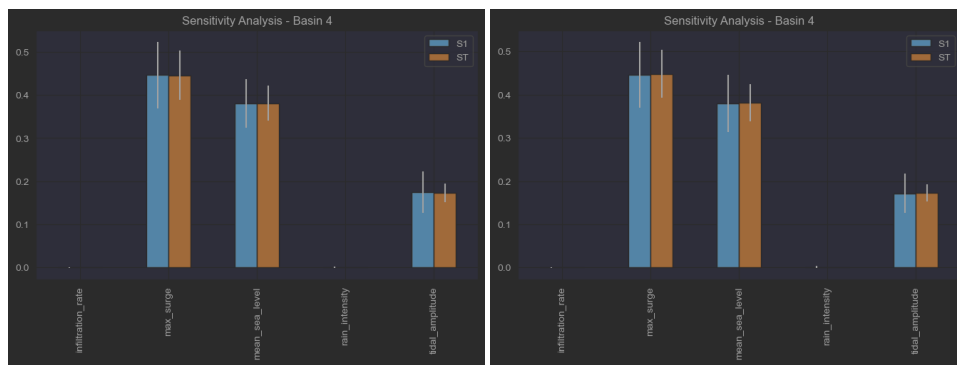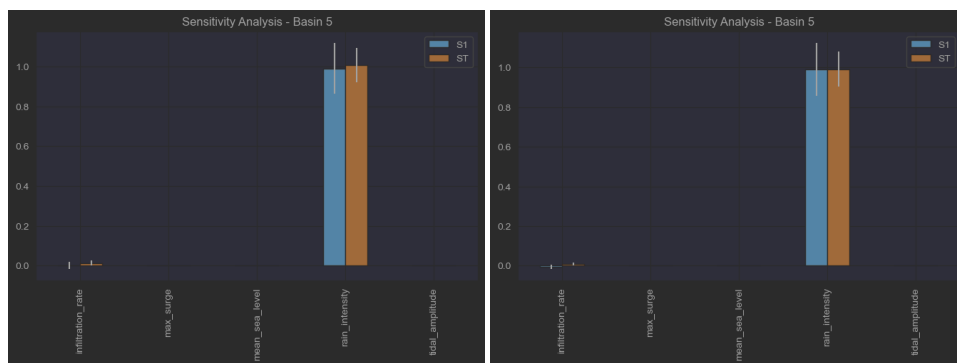

Figure E.4: Sensitivities for output max3. This is the maximum water level in basin 3, using the mean of the lowest 10% and 25% of the border heights respectively.

Figure E.5: Sensitivities for output max4. This is the maximum water level in basin 4, using the mean of the lowest 10% and 25% of the border heights respectively.

Figure E.6: Sensitivities for output max5. This is the maximum water level in basin 5, using the mean of the lowest 10% and 25% of the border heights respectively.

E.2   SFINCS

Similarly to FLORES, the location of the observation points for SFINCS can be found in section 3.4. For the sake of convenience, the observation points can also be found in figure E.7. The results of the two outputs that use the observation points surrounding the wastewater treatment plant pond embankments can be found in figure 4.6 in section 4.2.
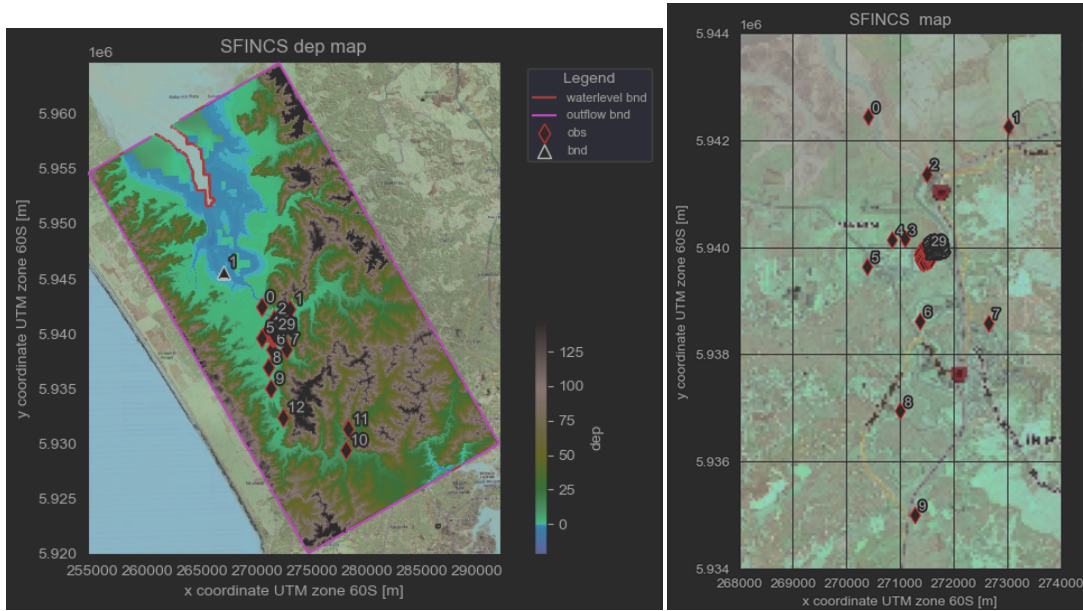
Figure E.7: Reminder of the location of the observation points for SFINCS. On the left the entire basin is visible, and on the right is zoomed in on the observation points close to the WTP for the purpose of visibility.
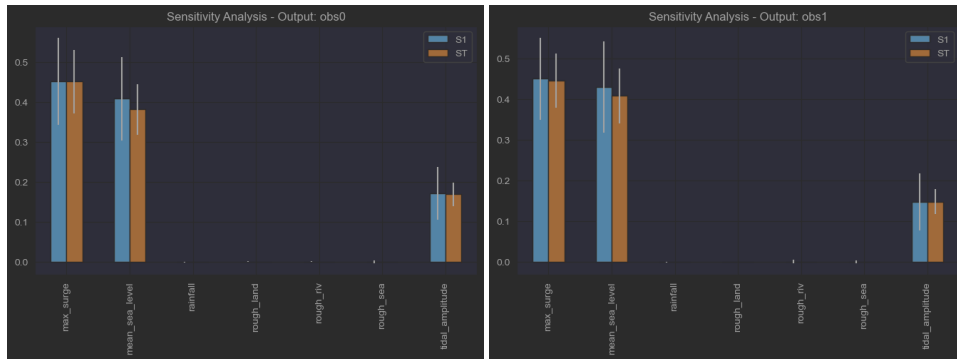
Sensitivities

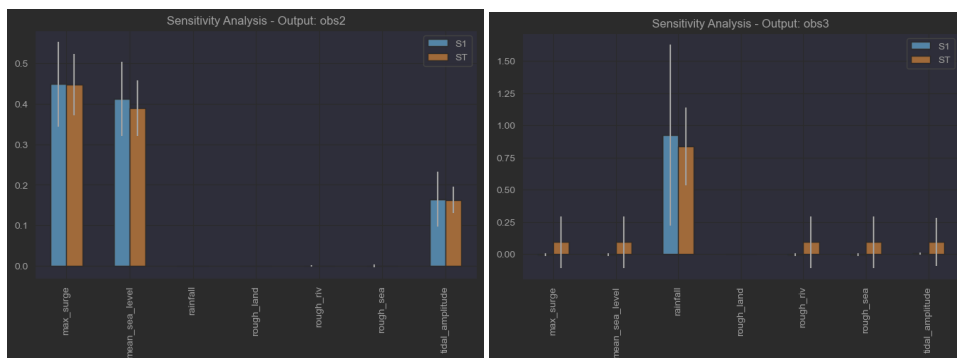Figure E.8: Sensitivities for observation point 0 and 1 respectively.

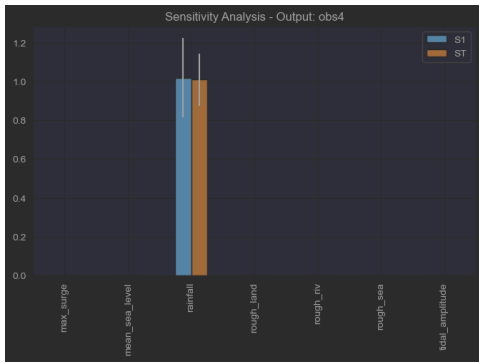Figure E.9: Sensitivities for observation points 2 and 3 respectively.

Figure E.10: Sensitivities for observation point 4